The optimization of southeast Texas extreme rainfall prediction utilizing the Weather Research and Forecast - Environmental Modeling System

---

A Thesis Presented to

the Faculty of the Department of Atmospheric Sciences

University of Houston

In Partial Fulfillment

of the Requirements for the Degree

Master of Science

By

Patrick G. Blood

May 2014

The optimization of southeast Texas extreme rainfall prediction utilizing the Weather Research and Forecast - Environmental Modeling System

---

Patrick G. Blood

APPROVED:

Dr. Bernhard Rappenglueck, Chairman

Dr. Xun Jiang

Mr. Lance Wood, National Weather Service

Dean, College of Natural Sciences and Mathematics

Acknowledgements

First and foremost, I would like to thank the Lord for giving me the required health and strength needed in getting through this journey. I sincerely thank my loving wife, Dr. Lezley Blood and my little buddy, Lucca, for always motivating and supporting me. They are my team and we obtain this graduate degree *together*! I would also like to extend my gratitude to my thesis committee for all of their aid and steady guidance. There is absolutely no way I would have reached my goal of obtaining my M.S. degree at this stage in my life if it wasn't for my family and my "extended" family of friends and colleagues. I understand this is just one completed trek within this larger journey of life but, at this moment, I am very proud of my accomplishment and extremely fortunate and blessed to be surrounded by such a loving and caring supporting cast.

Thank you!

The optimization of southeast Texas extreme rainfall prediction utilizing the Weather Research and Forecast - Environmental Modeling System

---

An Abstract of a Thesis

Presented to

the Faculty of the Department of Atmospheric Sciences

University of Houston

In Partial Fulfillment

of the Requirements for the Degree

Master of Science

By

Patrick G. Blood

May 2014

Abstract

The research focuses on varying multiple initialization datasets, along with planetary boundary layer and microphysical schemes, for a Houston, Texas-centered, local high - resolution Weather Research and Forecast - Environmental Modeling System (WRF - EMS) numerical weather prediction model. Statistical and graphical analyses of WRF - EMS model output and verification will be explored in an attempt to accurately simulate the April 18th, 2009 high rainfall event that adversely-affected the greater Houston metro area. Previous work has shown that high-resolution modeling has historically performed poorly on weakly-forced events (e.g., sea breeze boundary, summer convection) while performing more favorably with stronger-forced convective events (e.g., cold frontal passages, shortwave disturbances). Thus, numerous WRF - EMS model runs have been performed upon this cool season (i.e., stronger synoptically-forced) episode. Numerous WRF - EMS model simulations were run employing differing initial conditions while varying planetary boundary layer and microphysical scheme combinations. The validation of the numerical weather prediction model output will be against quality-controlled Weather Service Doppler radar (WSR-88D) data (i.e., Stage IV radar data). The inclusion of high-resolution land-surface modeling data into the WRF - EMS system will be analyzed to discern this data's overall significance, or consequence, to final WRF - EMS model output. The research goal is to determine if, through iterative computer model simulation, a specific initialization-planetary boundary layer-microphysical scheme combination could more accurately re-create the convective characteristics of a southeastern Texas heavy, or extreme, rainfall event.

Contents

Figures and Tables

1. Introduction

In recent years, within the United States of America, one of the leading weather hazards that has taken the most lives is flooding. Over the past 30 years, non-river flooding or flooding (i.e., flash flooding) caused by excessive precipitation accumulation over relatively-small geographic areas during brief time periods, has caused more fatalities by drowning than any other weather hazard. Since 2002, as documented by the National Weather Service (NWS), an average 52 people have perished in flood-related drowning episodes across the United States (NWS, 2012). Over the past 20 years, in the Texas coastal plains, urban flash flooding within the greater Houston-Galveston area has taken more lives than any other weather hazard. The majority of these fatalities have been drowning in vehicles as a consequence of driving into water of unknown depth. These statistics also hold true for the nation (NWS, 2013 a). The mission of the United States National Weather Service is to protect public life and to mitigate property loss, in tandem with the overall enhancement of the national economy, by the timely and accurate issuance of severe weather watches and warnings. NWS data and products form a national information database and infrastructure that can be used by other governmental agencies, the private sector, the general public, and the global community (NWS, 2013 b). It is in the NWS's best interest to issue lucid, punctual, and precise flood warning products that provide a reasonable public lead preparation time. The positive result is that the affected populous could quickly react and make the necessary decisions needed in avoiding loss of life and injury while minimizing property loss.

Numerical Weather Prediction (NWP) modeling are the main prognostic tools NWS operational meteorologists have at their disposal at attempting to forecast the onset, areal coverage, and intensity of convection. Accurate quantitative precipitation forecasting (QPF) is one of the most desired elements within the general forecasting community (Gaudet and Cotton, 1998). Accurate QPF benefits a large range of national and global interests such as the agricultural and hydrological communities (e.g., farming and water resources), recreational business (e.g., ski resorts), and government warning meteorologists (e.g., public safety). Mesoscale simulation research has shown that, when NWP models are run at relatively high resolutions as low as 10 kilometers (km) x 10 km, they can capture many observed mesoscale storm features. Cold-pool induced meso-highs or meso-lows behind squall lines can be resolved (Zhang, Gao and Parsons, 1988). Precipitation forecasts from the Pennsylvania State University - National Center for Atmospheric Research fifth-generation Mesoscale Model (MM5) over the United States Pacific Northwest during the 1997–99 cool seasons yielded systematic deficiencies within modeled precipitation (Colle, Mass and Westrick, 2000). The MM5 precipitation at 36 km x 36 km (36 km^2), 12 km^2, and 4 km^2 horizontal resolutions were compared with over 250 National Oceanic and Atmospheric Administration (NOAA) cooperative observer, snow telemetry (SNOTEL), avalanche, and NWS sites in order to evaluate the effects of increasing horizontal resolution and to document spatial variations in model skill. The temporal resolution was determinant upon that model's areal resolution and to the type(s) of observation(s) being used in verifying that particular model run. The MM5's runtime was 0 - 48 hours, with a 12 hour spin-up time for the 4 km^2 run as the 15 minute output from the 12 km^2 domain was used to create its separate initial and

boundary conditions beginning at hour 12. Forecast statistics, such as bias, the equitable threat score (ETS), and the root-mean-square (RMS) error score were analyzed during every 6 and 24 hour interval. (Colle et al., 2000) achieved noticeable improvement in bias, ETS, and the RMS error when horizontal resolution increased from 36 km^2 to 12 km^2 resolution; however, going from 12 km^2 to 4 km^2 resolution, improvement in skill were restricted to only the heavy precipitation events; defined as greater than 50.8 millimeters (mm) over a 24 hour period. For light to moderate precipitation events, both the 12 km^2 and 4 km^2 domains had significant over-prediction upon the windward, higher terrain slopes. In contrast, for heavy precipitation events, there was no widespread over-prediction. All resolutions under-predicted lowland and major gap precipitation within the Cascade Mountain range (Colle et al., 2000).

As computer processing becomes more powerful and computing speeds increase, NWP model suites are becoming more precise at predicting future short-term meteorological parameters. The more popular higher resolution NWP model suites currently being utilized by the national meteorological community are, but not limited to, the Weather Research and Forecast (WRF) model developed through the University Corporation for Atmospheric Research (UCAR, 2013 a), the North American Rapid Refresh (RAP) and the National Oceanic and Atmospheric Administration's (NOAA) High-Resolution Rapid Refresh (HRRR) models (NOAA, 2012), the North American Model (NAM) (NOAA/NWS/NCEP), and the NOAA/Storm Prediction Center's (SPC) Short Range Environmental Forecast (SREF) models (NOAA/SPC, 2012).

In years past, NWP model scheme's temporal and spatial scales may not have been resolved to a fine enough scale to accurately determine, or simulate, the correct QPF over a particular area of interest (Hong and Lee, 2009). Current central processing unit speed can still limit the degree of pertinent and valuable information a forecaster requires in properly informing the public about time of onset, location, and rainfall amount for a particular event. Dependent upon the size of convective system and its pertinent initiating elements, research has suggested that higher resolution models have the ability to explicitly resolve convective systems without parameterized convection (Carbone et al., 2002) (Wilson and Roberts, 2002). Increase in computer power has resulted in a decrease of NWP model horizontal grid spacing to less than 5 km^2, thereby allowing explicit resolution of dynamical and thermodynamical processes associated with convective systems and related key terrain features that have direct and significant impact upon precipitation (Xue and Martin, 2006) (Weisman et al., 2007).

The recent development, operational use and increasing finer grid-spacing resolution of the WRF NWP model procures the hypothesis of whether one can accurately simulate a mesoscale extreme weather scenario such as an urban, or more localized, flooding event. Future research is needed to determine if the WRF can ultimately be the best NWP forecasting tool in achieving the mission of saving life and property in high precipitation-leading-to-flooding events. As of 2012, there are two dynamic physical core WRF models; the Advanced Research WRF (ARW) core and the Non-hydrostatic Mesoscale Model (NMM) core. Within these two WRF versions, there are four primary physical parameters that incorporate planetary boundary layer (PBL), microphysical (mp),

convective, and radiation schemes (J. Dudhia, 2012). QPF behavior is driven by numerous meteorological factors; all falling into particular alignment to produce efficient high precipitation processes. The convective and radiative physical processes that occur within our own gulf coast, maritime-influenced PBL, with high consideration given to the land-atmosphere relationship, all play a crucial role in determining and properly analyzing the commencement, duration, and location of an extreme rainfall episode. There has been little to no documented research in utilizing a local WRF model, or adjusting its physical combination schemes, with the primary goal of simulating southeastern Texas heavy rainfall rates. This thesis will be based upon the exploration of the most advanced PBL and microphysical schemes, within a WRF - ARW core, in an attempt to accurately forecast an extreme rainfall event that led to significant flooding within the greater Houston-Galveston, Texas area.

2. Overview of the Weather Research and Forecast - Environmental Modeling System (WRF - EMS)

The Weather Research and Forecast Model - Environmental Modeling System (WRF - EMS) is a non-hydrostatic NWP model that has two basic physical cores; the Advanced Research WRF (ARW) core developed by the National Center of Atmospheric Research (NCAR) (UCAR, 2011 a) and the Non-hydrostatic Mesoscale Model (NMM) core that evolved at the National Center of Environmental Prediction (NCEP) (UCAR, 2013 b).

The WRF - ARW core is based on an Eulerian solver for fully-compressible, non-hydrostatic equations. Computations are made in flux conservative form while using a mass, hydrostatic pressure vertical coordinate. Prognostic variables for this solver are column mass of dry air (mu), horizontal velocities *u* and *v*, vertical velocity *w*, potential temperature (θ), and geopotential height. Non-conserved variables, such as temperature, pressure, and density, are diagnosed from the conserved prognostic variables. The solver uses a third order Runge-Kutta time-integration scheme coupled with a split-explicit second order time integration scheme for acoustic and gravity-wave modes. Fifth order upwind-biased advection operators are used in the fully-conservative flux divergence integration. Second and sixth order schemes are run-time selectable (UCAR, 2007 a). The WRF - NMM dynamic core time stepping consists of the linear multi-step Adams-Bashforth Method for horizontal waves and the Crank-Nicholson scheme for vertical waves. The forward-backward scheme is used for horizontally-propagating fast waves and the implicit scheme is used for vertically-propagating sound waves. Turbulent kinetic energy (TKE) calculations are explicit, iterative, and flux-corrected for every two time steps. The horizontal advection space is energy/enstrophy-conserved, quadratic conservative second-order differential equations. The vertical advection space is a quadratic conservative, second-order, differential equation. TKE advection is conservative upstream, flux-corrected and positive definite. Diffusion is categorized as both lateral and vertical. Lateral diffusion follows the Smagorinsky non-linear approach. PBL and free atmosphere vertical diffusion is handled by the surface layer and the boundary layer parameterization schemes as defined by Janjić (Janjić, 2002) (UCAR, 2013 c).

Within these two cores, four primary physical schemes are employed for either research or operational forecasting. These WRF - EMS physics are categorized under the PBL, microphysical, convective, and radiation schemes. The ARW core package typically runs the Yonsei PBL, Kain - Fritsch (KF) convective scheme (Kain and Fritsch, 1993), and the Dudhia rapid radiation transfer scheme. Vertical interpolation, whether through the now-retired Eta (coordinate) model (Instituto Nacional de Pesquisas Espaciais / Centro de Previsão de Tempo e Estudos Climáticos (INPE/CPTEC), 2006) or through user-defined levels, is performed through the real.exe program. Vertical levels can be user-configured to match the two-dimensional horizontal grid domain. An example of a vertical level set-up is the National Center of Atmospheric Research's (NCAR) real-time spring convection-permitting United States forecasts. This particular run employs defined parameters, or configurable variables within namelist files, that is run over a 1 km^2 to 4 km^2 horizontal domain, out to 3 days. There are 35 vertical levels with a default 50 hectopascal / millibar (hPa / mb) model top (UCAR, 2012).

The NMM core consists of the Mellor-Yamada-Janjic (MYJ) PBL, Betts-Miller-Janjic (BMJ) convective scheme, and the older Geophysics Fluid Dynamics Laboratory (GFDL) radiation scheme. As is the case with the ARW core, there are configurable vertical levels but, when using multiple data sets (i.e., model initiation and lateral boundary condition sets), both data sets will have the same number of vertical levels (UCAR, 2013 c). The WRF - EMS can import data for its initialization from various sources ranging from conventional ground and upper air observations to other gridded numerical weather prediction or reanalysis data. In better understanding land surface processes and these

processes interaction with the overlying atmosphere, the WRF - EMS can be coupled with the Noah Land Surface Model (LSM) (Research Applications Laboratory (RAL), 2013) and the Urban Canopy Model (UCM). The key inputs into the Noah LSM are land-use (vegetation) type, soil texture, slope, and such secondary parameters that are functions of the aforementioned parameters. Examples of secondary parameters would be albedo or the green vegetation fraction. Ultimately, the LSM must provide four quantities to the parent atmospheric model, in this case, the WRF - EMS. These quantities are surface sensible heat, latent heat flux, upward longwave radiation, and (reflected) shortwave radiation (F. Chen, 2007). The Model Evaluation Tools (MET) package for the WRF - EMS is a complimentary software package that allows the user to verify the WRF - EMS's output data. This useful verification tool analyzes the WRF - EMS's gridded output and assigns statistical quantification to this data. The MET verification software applies ensemble and probabilistic verification methods to WRF gridded output data. The MET can assign verification scores that compare temporal and spatial gridded model output data to that of gridded or point-based observations (Developmental Testbed Center (DTC), 2013).

The WRF - EMS model flow chart is for external gridded binary (GRIB) meteorological data to be processed through the WRF - EMS processing system (WPS) file, the wps.exe. Through data assimilation in the WRF - Var, or WRFDA, numerous external data sources (e.g., surface weather observations, satellite, radar, LSM, gridded model) are integrated into the WRF - EMS structure for analysis cycles (Fig. 1). In each analysis cycle, observations of the current, or prior, state of a system are combined with the results from

a pre-determined gridded NWP model (i.e., forecast data) to produce an analysis. This data set is considered as the "best guess" of the current state of the system; the analysis step. The analysis step tries to balance the uncertainty in the data and in the forecast by minimizing a cost function. The cost function sums the squared deviations of the analysis values from the observations, weighted by the accuracy of those observations plus the sum of the squared deviations of the forecast fields, along with the analyzed fields weighted by the accuracy of those in the forecast (MetEd – UCAR, 2009 a). The two types of data assimilation are three-dimensional (3D VAR) and four-dimensional (4D VAR). 3D VAR data assimilation is defined as when only current observations are utilized within the analysis cycle. 4D VAR is an extension of the 3D VAR with the added dimension of time. An example of 4D VAR is when the model is advanced in time and its result becomes the forecast for the next analysis cycle (Schlatter, 2000). Real, ground-truth observational data (e.g., 3D VAR) is imported into the real.exe (REAL) program for future ingestion into the ARW or NMM dynamic core or into the WRF - Var. WRF - Var initialization data is either input (or received as output) by the ARW/NMM dynamic core (i.e., 4D VAR). In each analysis cycle, the WRF pre-processors can generate two large classes of simulations for WRF - EMS model output; ideal.exe or real.exe.

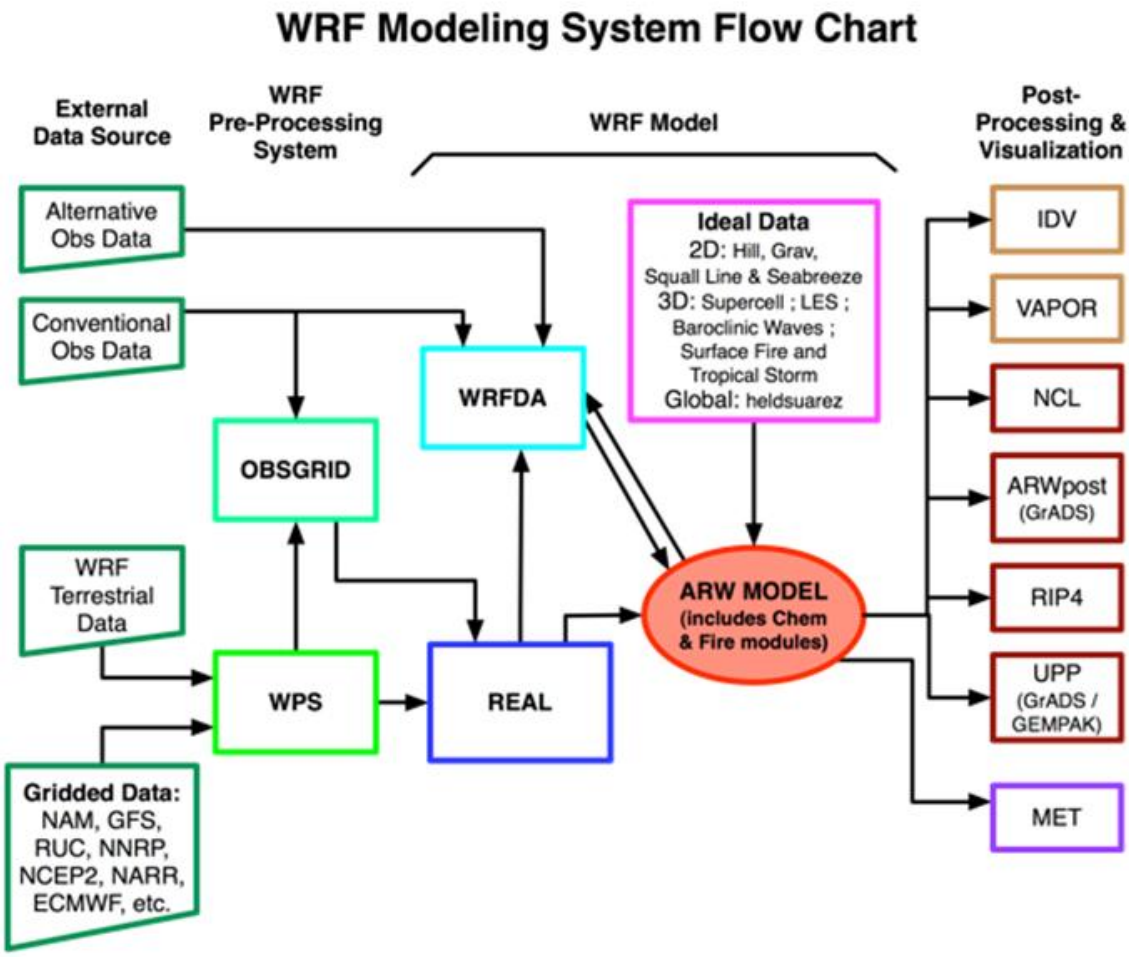

Figure 1: WRF - EMS Model System Flow Chart ((UCAR), 2010)

The WPS is comprised of a set of three programs whose collective role is to prepare the input data to the real.exe program for real-data simulation; *geogrid* defines model domains and interpolates static geographical data to the grids; *ungrib* extracts meteorological fields from the GRIB-formatted files and *metgrid* horizontally interpolates the meteorological fields (i.e., extracted by *ungrib* to those model grids as defined by *geogrid*). The ideal.exe or real.exe file "runs" the model; or executes the procedure(s) required to pass the pre-processed initialization data set (e.g., reanalysis)

into the dynamic core. Within the dynamic ARW or NMM cores, data is then processed through the aforementioned PBL, microphysical, convective, radiation algorithms (UCAR, 2012) (UCAR, 2013 c). The post-processing and visualization of the finalized, executable output files can be accomplished through UNIX-based GrADS or GEMPAK software, or through the Windows-environment Integrated Data Viewer (IDV) from Unidata. Output data files can be statistically-analyzed through the MET package (Developmental Testbed Center (DTC), 2013). The Visualization and Analysis Platform for Ocean, Atmosphere and Solar Researchers (VAPOR), NCAR Command Language (NCL), and the Read/Interpolate/Plot (RIP 4) for FORTRAN users are other data processing tools that are utilized for the visualization of WRF - EMS output data (UCAR, 2012).

The WRF - EMS model can utilize various physical packages that include, but are not limited to, PBL, microphysical, convective, and radiation schemes. The WRF - EMS (version 3.4.1) used in this research will utilize a nested inner grid space of 3 km^2 and allow the model to create its own convection (i.e., explicit convection, cloud updraft structure) within this nested domain. Explicit convection will eliminate the need for a parameterized convective scheme. The model domains were built through the WRF - EMS's Domain Wizard. The Domain Wizard is a systematic, GUI-based software component that allows the user to construct a pre-determined simulation domain. A larger, parent 9 km^2 gridded domain with a smaller, nested 3 km^2 grid space was built through the Domain Wizard and centered over downtown Houston, Texas (Fig. 2). The user executed varying physical package combinations on each domain as each domain is,

in essence, a separate model. Numerous domains can be constructed for future studies and, with the auto_run program, simulation can be more efficiently maximized through pre-scheduled run times.

Figure 2: Parent 9 km^2 outer domain and nested 3 km^2 inner domain

There are three main command functions that make up the WRF - EMS; ems_prep, ems_run, and the auto_run command. The ems_prep command introduces initialization data (e.g., reanalysis) into the WRF - EMS for model initialization. The ems_run

executes the local model. Auto_run is a group of scripts that schedule the execution of the ems_prep and ems_run commands.

The research used the java-based Integrated Data Viewer (IDV) software package from Unidata to view, analyze, and develop graphical model output within a Microsoft Windows environment. Microsoft Excel was used to extract, compile, analyze, and develop graphical output of the MET verification statistics. The research involved executing the WRF - EMS (version 3.4.1 ARW core) numerous times utilizing varying initialization and physical scheme combinations (Fig. 3). 144 planetary boundary layer and microphysical scheme combination WRF - EMS runs were initialized with two global reanalysis datasets and one model forecast initialization dataset. The two reanalysis datasets were the Climate Forecast System Reanalysis (CFSR) and the European Reanalysis (ERA - Interim) with the 12 km^2 resolution North American Model (NAM12) being the third (forecast) initialization dataset. The popular operational NAM12 inherently employs reanalysis functionality that makes it a suitable initialization / boundary layer dataset for which to compare against the other two reanalysis datasets. One of the key benefits of utilizing NAM12 forecast model data is that it allows the forecast to be updated every hour through the first 36 hour period, 3-hourly afterwards. The CFSR and ERA - Interim datasets update every 6 hours, or when their respective models update at the 0600, 1200, 1800, and 0000 UTC hours. Through the WRF's preparation command line structure the user can have the model ingest updated downstream mandatory synoptic hour initialization datasets, 6-hour data for the CFSR and ERA - Interim / 3-hour for the NAM, in updating boundary layer conditions. The

CFSR and ERA - Interim datasets allow the researcher the benefit from that case event's actual downstream data. Hence, access to this periodically updated initialization and boundary layer reanalysis data was very advantageous to this study's simulation.

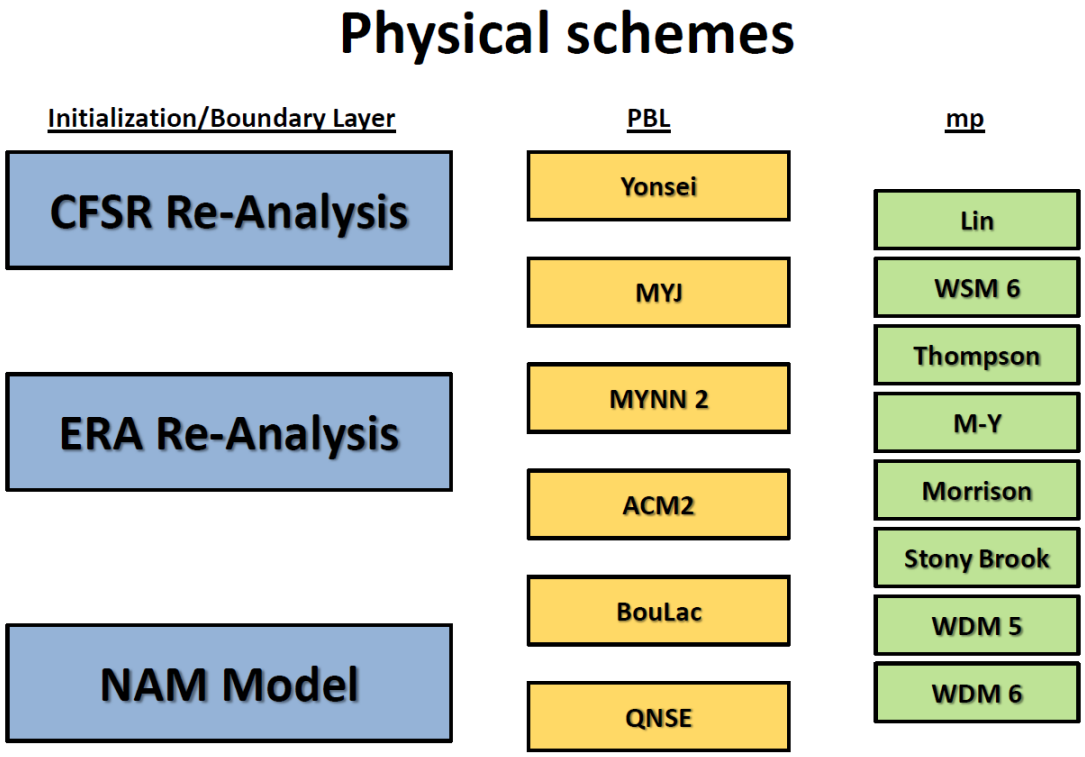

Figure 3: Initialization / PBL / Microphysical (mp) scheme configuration

3. Previous Works

3.1 *Comparison of Impacts of WRF Dynamic Core, Physics Package, and Initial Conditions on Warm Season Rainfall Forecasts* (Gallus and Bresch, 2005)

A series of WRF simulations were performed for 15 August of 2002 rainfall events occurring over the central United States, with an 8 km^2 resolution domain and 60 vertical levels. Four different WRF simulations were integrated over 48 hours, with three-hour lateral boundary conditions updates, where rainfall was averaged over six-hour periods. Observations were taken from 4 km^2 gridded Stage IV multi-sensory data. NCEP Stage IV analysis is a mosaicked national rainfall accumulation product comprised of regional hourly or 6 hourly radar and rain gauge data that is produced and quality controlled by 12 national River Forecast Centers (RFCs).

The goal was to compare the sensitivity of warm season rainfall forecasts with different physics packages and dynamic cores, along with varying initial conditions, within the WRF model. The ARW and NMM dynamic cores were used with the NCAR and NCEP physics packages. The NCAR suite used the Yonsei University (YSU) planetary boundary layer scheme, the Kain - Fritsch (KF) convective scheme, and the Dudhia rapid radiative transfer model radiation scheme. The NCEP package utilized the Betts - Miller - Janjić (BMJ) convective scheme, the Mellor - Yamada - Janjić (MYJ) planetary boundary layer scheme and the Geophysical Fluid Dynamics Laboratory (GFDL) radiation package. In all of the model runs, the other physical schemes (i.e., Noah land surface

model, microphysics) went unchanged. The simulations suggested that the sensitivity of the model to changes in the physical scheme was a direct function of the dynamic core. Similarly, the sensitivity of the dynamic core(s) was a direct function of the physical scheme(s). Generally, the greatest sensitivity was associated with a change in the physics packages within the NMM core while there was less sensitivity (with a physics scheme change) within the ARW core. For light rainfall episodes, the WRF model using the NCAR physics package (i.e., ARW core) was more sensitive to a change in the dynamic core itself than when the WRF model was run with the NCEP physics package (i.e., NMM core). The smaller impact of the NCEP physics was likely due to the broader, smooth rainfall regions produced by the BMJ convective scheme, thus minimizing the correspondence ratio (CR) (Strensrud and Wandishin, 2000). This ratio compared the number of grid points exceeding the 0.01 inch (0.25 mm), 0.25 inch (6.35 mm) and 0.50 inch (12.7 mm) rain thresholds versus those that had at least one grid point exceeding those particular thresholds. For heavier rainfall episodes (greater than 0.50 inches / 12.7 mm), the opposite was true as there was greater sensitivity with the NCEP physical scheme(s). The NCEP physics package led to a much smaller bias when simulating higher rainfall amounts than did the NCAR physics package, thus these particular high rainfall simulations were generally more sensitive to the dynamic core change.

Sensitivity to modeled (e.g., ETA, Rapid Update Cycle (RUC)) initial conditions, with negligible grid spacing and vertical layer change, was generally less substantial than the sensitivity caused by changes to the WRF's dynamic core or physics. For heavier rainfall, the ranking of sensitivity to changes in specific components varied much more over time.

Concerning warm season rainfall, the fine scale structure of rainfall forecasts was more affected by the different physical schemes than by the dynamic core. However, Gallus and Bresch's research showed that the overall domain's areal coverage and volume of rain might have actually been more influenced by the dynamic core than by the physical scheme(s).

3.2 ***On the Impact of WRF Model Vertical Grid Resolution on Midwest Summer Rainfall Forecasts*** (Aligo, Gallus and Segal, 2008)

A refined vertical grid resolution (VGR) should conceptually improve the prediction of convection-related, microphysical and boundary layer processes, which in turn should improve rainfall forecasts. (Aligo, Gallus, & Segal, 2008) performed 68 WRF ARW core model exploratory sensitivity simulations, using the North American Regional Reanalysis (NARR) for the initial and lateral boundary conditions in convection-permitting runs, to determine the impact of the VGR on the forecast skill of Midwestern United States summer rainfall.

The variance of a refined VGR did not necessarily result in a consistent improvement in quantitative precipitation forecasts (QPF). When the VGR was refined in a case study of averaged microphysical schemes, there were lower ETS and higher bias values as rainfall was over-predicted for half of the rainfall thresholds. Simulations were averaged over "strongly-forced" warm season convective cases, or those cases that displayed (non) linear bowing, parallel, leading, or trailing stratiform convective characteristics, at least

20 m/s 500 hPa winds, and/or near-surface cross-frontal horizontal temperature gradients of at least 7° C over 100 km. When the number of vertical levels was increased, ETS values worsened for all rainfall thresholds while many biases increased, indicating a further over-prediction of rainfall. There was a systematic increase in bias with a VGR increase, which was suggested to be related to grid cell saturation occurring more frequently in the finer VGR runs. Within these finer VGR runs, enhanced upward motion(s), occurring in tandem with higher relative humidity 'prior' to convective initiation, might indicate that these enhanced upward motion(s) might have led to the frequent grid cell saturation. Qualitatively, varying the VGR resulted in noticeable 18 hour accumulated rainfall differences (> 25 mm) over widespread areas among different microphysical schemes and cases. Most of the rainfall differences were due to local shifts in rainfall centers; some areas of rainfall were completely removed and/or created.

There was skill improvement for all rainfall thresholds when vertical resolution was increased above the melting level. This was possibly related to the better resolution of sub-freezing microphysical processes. Skill also improved over most rainfall thresholds when above-freezing layer (e.g., warm cloud layer and/or processes) with increased VGR. Improved lower QPF skill (< 12.7 mm) was attributed to better-resolved surface turbulent momentum and thermal fluxes. This study showed that a more-refined VGR resulted in QPF improvement within weakly-forced cases. Vertical motions in these weakly-forced situations are mainly governed by thermodynamic forcing; or are more sensitive to vertical temperature and moisture profiles. Application of the factor separation method (Stein & Alpert, 1993) suggested that a more-refined VGR frequently

had a counter-intuitively negative impact on skill through boundary layer and warm cloud processes interacting with microphysical processes above the melting level. In relation to the non-linear interaction (synergy) between the above and below melting layer physical processes, 70% of the higher level (62 level) WRF runs displayed negative synergy while 28% had positive synergy. These findings suggested that the majority of these higher VGR runs displayed degraded ETS while only a third provided positive results. It should be noted that that, for higher rain amounts of between 12.7 and 19.0 mm (0.25 in, 0.75 in), there were improved 62 VGR level QPF skill scores, or increased positive synergy.

In conclusion, QPF skill can be sensitive to the VGR and, at least on a case-by-case basis, there may only be limited skill by refining the number of vertical levels, especially if the initial conditions (IC) and lateral boundary conditions (LBC) are on a relatively-coarse vertical grid. In this study, the ICs and LBCs were from the NARR, which provides 29 data levels. Conceptually, increasing the number of model levels from 31 to 62 should have better resolved the simulated vertical processes, but this increasing VGR did not provide any additional IC or LBC refinement. Significant modulation should occur with horizontal grid resolution of higher VGR upon forecasted rainfall due to IC/LBC error and incomplete model physics formulation. It was noted that future work could focus on a detailed evaluation of specific cloud microphysical or boundary layer processes affected by VGR modification(s). Carrying out full-seasonal sensitivity simulations, while utilizing a more-refined VGR, would provide further insight into this study's QPF evaluations.

3.3 ***The Impact of Different WRF Model Physical Parameterizations and Their Interactions on Warm Season MCS Rainfall*** (Jankov et al., 2005)

In recent years, a mixed-physics ensemble approach has been investigated as a method to better predict mesoscale convective system (MCS) rainfall. The main goal of the study was to note and quantify general trends in the impact of various physical schemes and their interactions upon warm season MCS rainfall forecasts. Knowledge of how different physical schemes, or their combinations, influence rainfall forecasts may be of major importance in designing and interpreting mixed-physics ensembles.

A matrix of 18 WRF model configurations using different physical scheme combinations was run with 12 km^2 grid spacing for eight International H2O Project (IHOP) MCS cases. Each case utilized three convection schemes; the KF, the BMJ, and the use of no convective scheme (NC), Three microphysical schemes; NCEP - 5 microphysics (MPN), (Lin, 1983) microphysics (MPL), and Ferrier microphysics (MPF), while two PBL schemes; the Medium Range Forecast (MRF) and older WRF - NMM (ETA), were used. All runs were initialized with a diabatic Local Analysis and Prediction System (LAPS) hot start initialization (Jian, Shieh and McGinley, 2003).

In the majority of the cases, MCSs dominated the rainfall field and were captured in the interior of the domain. An analysis of ETS and bias indicated that no single model configuration was clearly better than the rest. The best configuration varied in both time and rainfall threshold(s). Objective testing of sensitivity to physical scheme changes was

performed by evaluating correspondence ratio and squared correlation coefficient values. Both objective measures were computed for sets of two model runs in which two of three model physical schemes were held fixed and the third varied (e.g., the PBL and the convective schemes were fixed while the microphysical scheme varied). Both the correspondence ratio and the correlation coefficient indicated that the highest sensitivity was in the choice of convective scheme. Less sensitivity occurred with varied PBL schemes with the least sensitivity associated with microphysics scheme change. The correspondence ratio for light rainfall indicated that sensitivity was highest during the first 6 hours. During heavier rainfall events, the correspondence ratio was highest during the latter forecast times.

Additional testing of rain rate and volume sensitivity to changes in the physics was performed using the factor separation method (Stein and Alpert, 1993). This method was used to quantify the impacts of the variation of two different physical schemes as compared to a "control run". The KF, MRF, and the MPN physical schemes were chosen to match the real-time model configuration used by NOAA's Forecast System Laboratory (FSL) during the IHOP experiment and for their interaction, or synergy, upon simulated rainfall. Statistical significance of the obtained results was tested by following are-sampling method suggested by (Hamill, 1999). A change from the KF to NC significantly increased system rain rate. A change from KF to BMJ significantly increased the areal coverage of lighter rainfall while lowering system rain rates, though not significantly, in relation to the KF runs. In general, changes in convective schemes were found to have the largest impact on rain rates when the KF was replaced with the NC, no matter the

microphysical nor PBL scheme. Regarding rain volume, the microphysical scheme choice exerted the largest impact in the NC runs with the least impact with the BMJ runs. The impact of synergy between different physical schemes, although occasionally of comparable magnitude to the impacts from only changing one scheme compared to a control run, varied greatly among cases and over time, and was typically not statistically significant. One exception was for the interaction of the ETA with the MPL, or the MPF, which significantly reduced the rain volume increase that had been previously noted for the heavier threshold MPN microphysics scheme. These results suggest that most of the significant trends noted for a switch in one physical process scheme (e.g., increase in rain rate when KF is switched to NC) remain consistent even when other physical process schemes were altered. A switch from the MPN to either the MPL, or the MPF, increased rain volume markedly no matter the convective nor PBL scheme. A switch from KF to BMJ decreased rain volume, especially for heavier rainfall amounts, regardless of the microphysics and PBL scheme. Averaged skill scores over all eight cases for the 18 configurations indicated that not one configuration was obviously best at all times and/or thresholds. The greatest forecast variability was discovered with changes in the convective scheme, although notable impacts also occurred from changes in the microphysics and PBL schemes. Specifically, convective scheme changes notably affected average rain rate forecast numbers. Total rain volume forecasts were influenced by the microphysics and the convective schemes.

In conclusion, this study's results implied that, if an ensemble designed for MCS rainfall prediction lacks sufficient spread, model runs with different convective schemes should

be included as an efficient way to increase spread. If rain volume is a desired quantity (e.g., for hydrological purposes), model runs with the MPL and the MPF microphysical schemes may require different bias correction, or weighting, in an ensemble compared to runs using the MPN. Future work will focus on more detailed case analyses in order to relate the explicit interaction of physics schemes to the larger-scale environment. (Jankov et al., 2005) state that detailed case analyses, along with the general findings of this study, will be used to design and interpret future mixed-physics ensemble results.

4. Project Description

The thesis research primarily focused on varying a WRF - EMS's multiple PBL and microphysical schemes in an attempt to accurately simulate a historically high rainfall event that had adversely impacted southeastern Texas. An adverse Houston - Galveston regionally high rainfall event that created (flash) flooding is defined as an event that has either (a) caused loss of life and/or (b) created significant economic loss. The study will mainly focus on a cool seasonal case event (e.g., October - April) where prominent synoptic and/or mesoscale forcing existed. Historically, higher resolution modeling has been largely unsuccessful at attempting to forecast the initialization and evolution of warm season, weakly-forced convection (e.g., sea breeze) (Case et al., 2011). The reasoning behind these unsuccessful attempts could be that sub-scale convective physical processes have yet to be fully-resolved by current NWP modeling, or even completely understood, theoretically, within the meteorological community. This research, as well as

near term research studies, will have a higher probability of successfully simulating convection within more strongly-forced environments (e.g., cool season) versus weakly-forced regimes (e.g., warm season). It was advantageous to employ a larger scale (spectral) model data set to the regional outer domain (e.g., 9 km^2 parent domain) as there will be a higher probability that a stronger-forced environment will be better resolved by spectral modeling. Thus, focusing on stronger-forced convective regimes will likely provide a more successful attempt at studying the correlation between a combination of selectable physical scheme parameters and the improvement of resolving the temporal and areal behavior of intense convection. The study will research one cool season high rainfall event that ultimately produced flooding. The case study event that will be intensively researched within this paper will be the April 18th, 2009 Houston metro area extreme rain/flooding event. Using the scientific method and validating NWP model output against ground-truth observations (e.g., quality-controlled radar data), 144 WRF - EMS simulations will be run that will employ three initialization datasets while varying six PBL and eight microphysical scheme combinations. Inherently, within the WRF - EMS system, there are various surface layer physical parameters and LSM datasets that will be associated with particular PBL schemes. The research goal is to determine if high-resolution computer model simulation can accurately re-create the convective characteristics of a regional, historically high rainfall event.

If these WRF simulations are structured in the aforementioned manner, then will this output have the ability to forecast the magnitude, or scope, of a high rainfall event's temporal and spatial behavior?

4.1 **Verification Methodology**

A verification software package, the Meteorological Evaluation Tool (MET) package, will be employed to analyze the WRF - EMS model output data. The main strength of this highly-configurable package is that, through a variety of statistical methods, it aids in the verification of model output data. The MET software is designed to provide a variety of verification techniques. For example, the MET package can provide standard verification scores that compare gridded model data output to both gridded and point-based "ground truth" observations through both time and space. Spatial verification methods compare gridded model data to gridded observations using neighborhood, object-based, and intensity-scale decomposition approaches. The MET software can also utilize ensemble and probabilistic verification methods that correlate gridded model data to point-based, or gridded, observations. This research will utilize the MET software to verify, through grid-based verification, quantitative rainfall against Stage IV radar data.

5. Initialization Data

5.1 **Initialization Datasets**

Model runs were initialized with either reanalysis or model data. Unlike previous versions of the WRF - EMS, the WRF - EMS version 3.4 has the ability to ingest reanalysis data from the University Collaboration of Atmospheric Research's (UCAR)

data servers. NCEP literature defines meteorological reanalysis data as "a data assimilation project which aims to assimilate historical observational data spanning an extended period, using a single consistent assimilation or *analysis* scheme throughout" (Kalnay et al., 1996). While numerical models are used to predict future states of the atmosphere, they are based on how the climate system evolves from an initial state. This initial state provided as model input must consist of data that ranges over a field of predictable meteorological fields; the fields that will ultimately determine the model's future evolution. Gridded meteorological parameters required by the model, with the initialization data, must be valid at a single point-in-time that corresponds to the present, or the recent past. Issues that arise from using available observation, or real world, data within modeling domains are as follows; observational data usually does not include all of the model's prognostic fields and may include additional fields, have different spatial distribution from the forecast model grid, may be valid over a range of times rather than a single time, and quality can suffer due to observational error. Thus, meteorological reanalysis data assimilation is used to produce an *analysis* of the initial state. This is the statistical "best fit" of the numerical model to the available data, taking into account error in both data sets. In essence, reanalysis data is quality-controlled observational data that is continually feed into a model whereas, at every time step, the model's "first guess" is "compared" to observational data at each defined grid point. Bias (e.g., error) is then worked into the next time step between the prognostication's "guess" and observation comparison. This study will be performed on an historical event and utilizing reanalysis data will allow the research the benefit of time. In lieu of one, initial observational data ingest at forecast hour 0 (e.g., NAM, GFS), observational data was continually ingested

into the core analysis model (i.e., nudging) to ensure better down-the-line local model forecast initialization and downstream input (output).

The two reanalysis data sets that were involved in this study were the Climate Forecast System Reanalysis (CFSR) and the European Reanalysis (ERA - Interim) datasets. The CFSR utilizes the operational GFS model and the Noah Land surface model (LSM). The ERA - Interim is so named "interim "as it is was originally planned as a provisionary reanalysis in preparation for the next-generation extended reanalysis that would eventually replace the previous ERA - 40 reanalysis. The ERA - Interim runs a 2006 version of the European Center for Medium Range Weather Forecasting (ECMWF) integrated forecast model. Both reanalysis datasets go back to the year 1979 and continue to run real time through the present (Overview of current atmospheric reanalyses, 2014).

5.1.1 **Climate Forecast System Reanalysis (CFSR)**

The reanalysis CFSR dataset is a global, high-resolution, coupled atmosphere-ocean-land surface-sea ice domain system that has a near 38 km^2 horizontal resolution, or T382 model spectrum resolution, with 64 vertical levels. CFSR is designed to provide the best estimate of the state of these coupled domains over the years ranging from 1979 to 2010. The key strengths of the CFSR is that this finer resolution reanalysis involves the coupling of the atmosphere and ocean during the generation of a 6 hour guess field, an interactive sea-ice model, and it provides advanced assimilation of satellite radiances. Other strengths of this relatively un-tested global data set are that it accounts for CO_2 and

other trace gases, aerosols, and solar variation (Climate Forecast System Reanalysis (CFSR), 2013).

In the study, *An Assessment of the Surface Climate in the NCEP Climate Forecast System Reanalysis*, the CFSR data set was compared to observational estimates and the three reanalysis datasets; the NCEP/NCAR reanalysis (R1), the NCEP/DOE reanalysis (R2), and the ERA40 produced by the ECMWF (Wanqiu et al., 2011). The study discovered that the CFSR had more accurate time-mean precipitation distribution over various regions, compared to the three previous reanalysis datasets and this lead to a better representation of freshwater flux (i.e., evaporation minus precipitation). CFSR displayed improvement over the inter-annual variability in relation to precipitation correlation with Indian Ocean and western Pacific observations. The CFSR's inter-annual variability and long-term trend of 2 meter (m) temperatures were found to be superior to the R1 and R2 reanalysis datasets. The study did find that the CFSR tended to overestimate downward solar radiation flux over the tropical Western Hemisphere oceans and this was consistent with less cloudiness and resultant higher sea surface temperature. The CFSR's evaporative latent heat flux also appears to be larger than (estimated) global observation. There were identified inconsistencies, or noted long-term variation error, in the dramatic change of variables during the years between 1998 and 2001 and this was possibly attributed to changes in assimilated satellite observation. Other issues involved inconsistent soil moisture values and sea ice extent that may have future impacts on the application of the CFSR for climate diagnoses and prediction (Wanqui, Pingping and Soo-Hyun, 2010).

5.1.2 **European Reanalysis (ERA- Interim)**

The ERA - Interim spectral resolution is T255 (i.e., ~80 km^2 horizontal resolution) and there are 60 vertical levels (Overview of current atmopsheric anaylses, 2014) (ERA-Interim, 2008). The ERA - Interim reanalysis is produced with a sequential data assimilation scheme, advancing forward in time using 12-hour analysis cycles. In each cycle, available observations are combined with prior information from a forecast model (e.g., ECMWF operational forecast model) to estimate the evolving state of the global atmosphere and its underlying surface. This involves computing a 12-hour 4D Var analysis of the basic upper-air atmospheric fields of temperature, wind, humidity, ozone, and pressure. A key feature of 4D Var is the flow-dependent influence of observations that results from using a forecast model to constrain the analysis (Thépaut et al., 1996). The ability of the data assimilation system to exploit physical information implicit in the model equations can be very beneficial, especially where observations are sparse. (Whitaker, Compo and Thépaut, 2009) have shown that 4D Var outperforms 3D Var in such situations, and that it is capable of producing accurate analyses of the large-scale tropospheric circulation based only on observations of surface pressure. The ERA - Interim's version of 4D Var updates a set of parameter estimates that define bias corrections needed for the majority of satellite-based radiance observations. A following analysis occurs of near-surface parameters such as 2 meter temperature and humidity, soil moisture and temperature, snow, and ocean waves. These analyses are then used to initialize a short-range model forecast, which provides the prior state estimates needed for the next analysis cycle.

The forecast model has a crucial role in the data assimilation process. Use of the model equations makes it possible to extrapolate information from locally observed parameters to unobserved parameters in a physically meaningful way, and to also carry this information forward in time. As time evolves, the skill and accuracy of the forecast model determines how well the assimilated information can be retained. More accurate model forecasts translate to smaller adjustments needed to maintain consistency with the observations. While producing a forecast, the model estimates a wide variety of physical parameters such as precipitation, turbulent fluxes, radiation fields, cloud properties, soil moisture, etc. Even if not directly observed, these are constrained by the observations used to initialize the forecast. The accuracy of these model-generated estimates naturally depends on the quality of the model physics as well as that of the analysis.

The data assimilation produces a coherent record of the global atmospheric evolution constrained by the observations available during the period of reanalysis. The ERA - Interim archive currently contains 6-hour gridded estimates of three-dimensional (3D) meteorological variables, and 3-hour estimates of a large number of surface parameters and other two-dimensional (2D) fields, for all dates from January 1, 1989 (Dee, 2011). The research's statistical scoring concluded that the better initialization dataset was the CFSR reanalysis. The most plausible reasoning for this is that the CFSR reanalysis dataset, when compared to the ERA - Interim dataset, has higher overall resolution. The CFSR's horizontal resolution is nearly twice that of the ERA-Interim's; 38 km^2 versus 80 km^2, respectively. The CFSR also uses more vertical levels; 64 vertical level resolution versus 60 vertical levels in the ERA - Interim. Another reason could be that the

operational GFS model was a better "first guess" performer than the ECMWF during this particular case study. More accurate prognostication within the reanalysis would allow for lower downstream (e.g., every 6 hours) error during the 4D VAR data assimilation process, thus resulting in cleaner future data ingestion that more closely matched observation data.

6. Synoptic Review of April 18th, 2009

The synoptic scenario of the April 18th, 2009 high rainfall event was of a 1200 UTC 558 decameter (dam) 500 millibar (mb) closed-off upper low centered over the 5 corners region of the Texas and Oklahoma panhandles, northeastern New Mexico, southeastern Colorado, and southwestern Nebraska. This vertically-stacked low was observed across all mandatory pressure level surfaces. The broadening upper low transitioned eastward into the southern plains through 0000 UTC, April 19th, 2009. Downstream of this 500 mb low, the upper wind pattern became diffluent over southeastern Oklahoma and northeastern Texas. At 300 mb, or at the jet stream level, it was noted that there was enhanced diffluence associated with a split flow pattern over southeastern Texas; a 39 m/s (75 knot) upper Sabine River Valley south-southwest wind existed just north of a more west-southwest lower Sabine River Valley 33 m/s (65 knot) wind. Mid-level diffulence within a very moist environment was also evident at the 700 mb level as moderate 13 - 15 m/s (25 - 30 knot) morning winds advected a 6 degree Celsius (°C) dew

point southern Rio Grande Valley air mass into eastern Texas. The 850 mb pressure surface indicated relatively high mid-level moisture as 10 °C to 15 °C dew point air was advected northward from extreme northeastern Mexico into southeastern Texas. 1200 UTC local area soundings depicted a saturated column from the surface to around a height of 1000 meters (m). In comparing the upper air constant pressure surface 850 mb chart to the Corpus Christi, Texas upper air sounding, it was observed that the column was becoming more saturated through a higher altitude, or up through 1,500 m, during the mid to late morning hours.

By 1800 UTC, surface observations were becoming supportive of a high rainfall event. For example, a moderate southeastern 13 - 15 m/s (25 - 30 knot) onshore flow advected in approximately 21 °C dew point moist gulf air into a warm inland 21 °C air mass; a near zero (0.5 °C) surface dew point depression was observed along the upper Texas coastline through the 1200 UTC - 2100 UTC 9 hour period. Of note, a zero dew point depression, 19 °C over 19 °C, at 0000 UTC in Galveston was within on-going precipitation. A very significant feature for meso-scale precipitation focus was an observed 1800 UTC low-level convergence zone created by the formation of a Harris County-centered surface trough. Radar imagery depicted the development of a meso-low that ultimately enhanced the low-level inflow of extremely moisture rich air into the system (i.e., cluster of thunderstorms) during the period of highest observed rainfall (rates) across southeastern Harris and northern Galveston counties.

6.1 **Rainfall Behavior**

In relation to rainfall rates, the April 18th, 2009 heavy rain event was unprecedented in the region's plus-100 years of modern observing history. This event recorded the highest one hour rainfall of 175.26 millimeters (mm) (6.9 inches) in Texas history (Fig. 4, 5). This was recorded at the A100 Clear Creek and Bay Area Boulevard Harris County Flood Control District (HCFCD) - maintained rain gauge. (Fig. 6) This hourly rainfall exceeded the previous record 172.72 mm (6.8 inches) amount recorded in the June 2007 Marble Falls, Texas high rainfall summer event, as well as the 160.02 mm (6.3 inches) hourly amount observed during June 2001's Tropical Storm Allison that impacted the Houston, Texas area. All three of these events are considered 1-in-500 year events by flood plain statistical standards. Three-hour and six-hour rates were 233.68 mm/3 hours (9.2 inches/3 hours) and 251.46 mm/6 hours (9.9 inches/6 hours) and both are 1-in-500 year occurrences. The 12-hour and 24-hour (1 day) rates were 254.00 mm/12 hours (10 inches/12 hours) and 279.40 mm/1 day (11 inches/1 day), 1-in-50 year and 1-in-25 year occurrences, respectively. The smaller temporal scale unprecedented copious rainfall rates were very impressive, as well. Examples of this were the 18.03 mm per minute rate (0.71 inches/1 minute rate) at the Willow Spring - Fairmont Parkway gauge, the 15 minute rate of 61.98 mm (2.44 inches/15 minute rate) at the Clear Creek – I - 45 gauge (Fig. 7) and the 30 minute rate of 107.19 mm (4.22 inches/30 minute rate) at the Clear Creek - Bay Area Blvd gauge. For reference, the United States national record for a one minute rainfall rate is 31.24 mm/1 minute (1.23 inches/1 minute) in Unionville, Maryland.

The precipitation was measured with a tipping bucket mechanism that has inherent error within convective rainfall scenarios. Research has proven that there is 10% to 20% error due to the inability of the tipping bucket mechanism to catch up within intense rainfall, rain spillage, and rain loss due to wind capture. If rain gauge tipping bucket error is considered, then it is reasonable to assume that an additional 10% to 20% more rain fell during this episode. Placing this in perspective means that the Clear Lake area could have easily experienced over 203.2 mm (8 inches) per hour rainfall rates that Saturday afternoon! Probabilistically, this event could be a "once in a lifetime" event, as the one and three hour rainfall rates both have a 0.2% chance of annual re-occurrence, while the six hour rates equate to a 1% annual chance of reoccurrence.

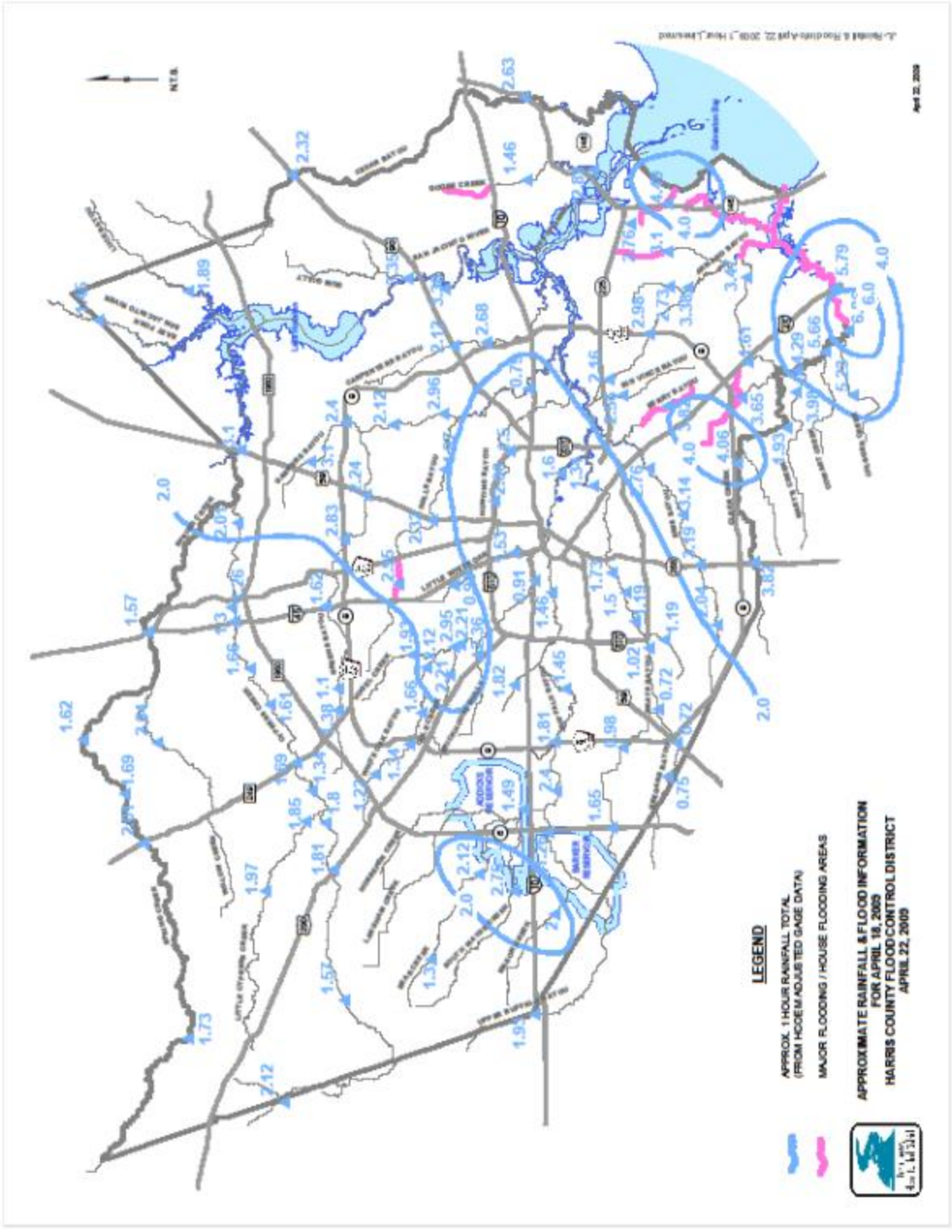

Figure 4: 1 hour maximum rain gauge observations (inches) with major flooded areas (HCFCD, 2010)

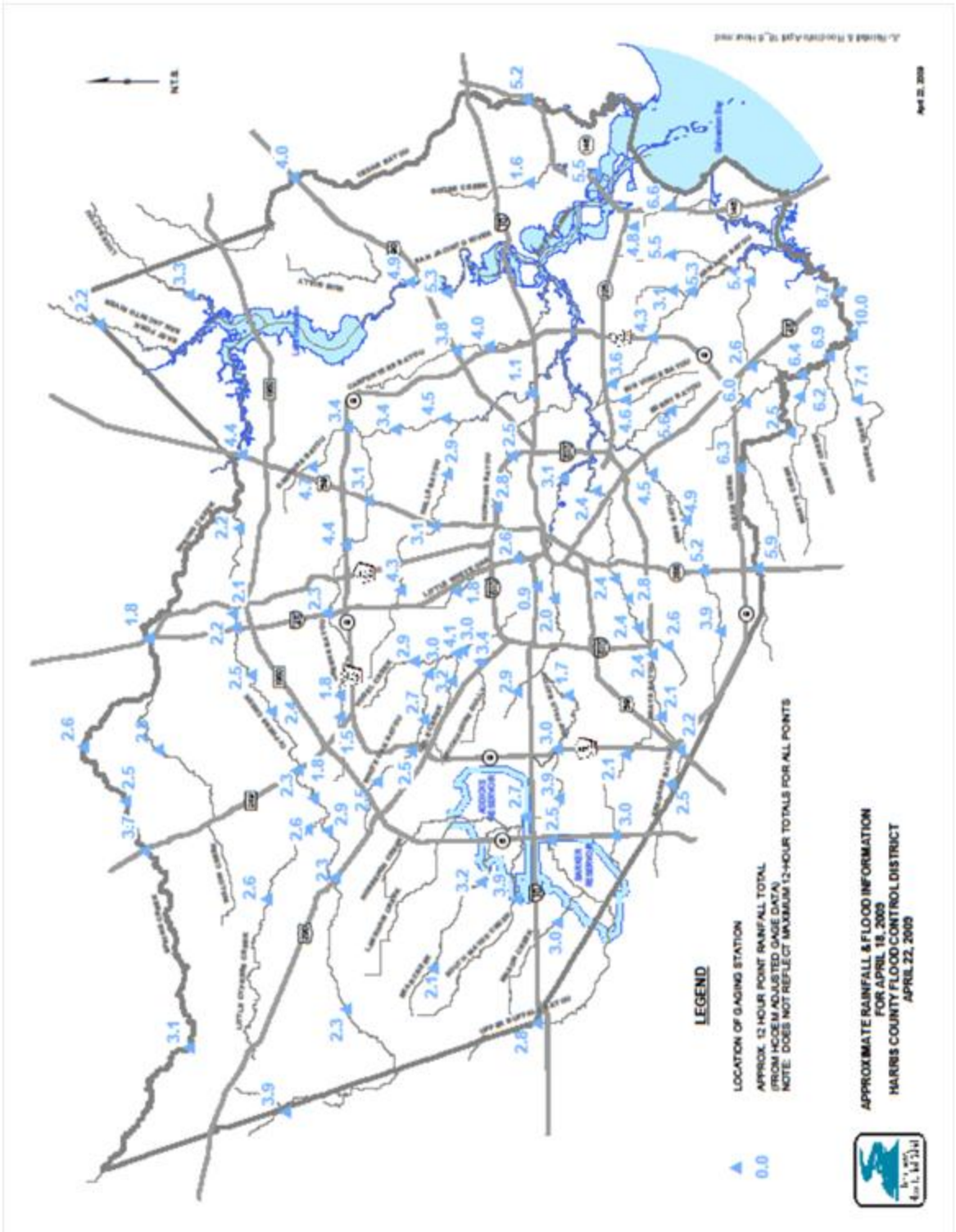

Figure 5: 12 hour maximum rain gauge observations (inches) (HCFCD, 2010)

Figure 6: 15 minute and 1 hour Clear Creek / Bay Area rain gauge data (HCFCD, 2009)

Figure 7: 15 minute and 1 hour Clear Creek / I-45 rain gauge data (HCFCD, 2009)

6.2 **Storm Data**

Harris County storm data reported homes were flooded, numerous roadways were underwater and there was bayou flooding from the localized 203 to 254 mm (8 to 10 inch) rain totals that had fallen across the county. In the northern part of Harris County, five children, all under the age of 7, drowned in a vehicle that drove into a flooded drainage ditch. There was wind damage to homes and uprooted trees reported in the town of Seabrook, Texas. In northern Galveston County, there were 300 flooded homes in League City, Texas. High water rescues were required in the town of Dickinson, Texas. Strong thunderstorm winds caused the downing of large trees in the Clear Lake Shores area. An EF0 tornado touched down a few miles southeast of Hitchcock, Texas that damaged several homes along its path. In Fort Bend County, numerous roadways were flooded in and around Missouri City, Texas. In Wharton County, trees and power lines were reported downed by storm winds in New Taiton, Texas (NWS, 2009).

7. The Planetary Boundary Layer (PBL)

The WRF - EMS is a widely utilized NWP model within the atmospheric science community for the purpose of meteorological research and prognostication. Since L.F. Richardson first attempted NWP in 1922, advancement in weather forecasting has only improved with the continued development and subsequent evolution of computing power.

Although modern-era models are operating with unprecedented finer grid resolutions, many crucial physical atmospheric processes are still not completely resolved and must still be parameterized. These processes include, but are not limited to, the diurnal evolution of the PBL, the microphysics of cloud formation and precipitation, the transfer of surface heat, moisture, and momentum into the atmosphere, and heat exchange between the atmosphere and terrestrial associated with shortwave and longwave radiation. The formation, structure and maintenance of the PBL are critical to the prediction of meteorological elements (e.g., temperature, wind, precipitation). An accurate depiction of the PBL through NWP simulation demands that the handling of turbulent motion/mixing of heat, momentum, and moisture be realistically-resolved through parameterization (Xie et al., 2012).

Over the past three or four decades, considerable progress has been made in the development and improvement of PBL parameterization within atmospheric modeling. In the WRF - EMS, PBL processes can be parameterized either through local closure (e.g., K-theory) or non-local closure schemes. The difficulty in accurately simulating PBL evolution lies within the inability to properly resolve the convective boundary layer sub-scale eddies and large asymmetrical thermals. K-theory is limited to simulating turbulent mixing within adjacent layers symmetrically, thus mixing is not appropriately reproduced. To better produce turbulent mixing within the PBL various non-local closure models have been developed to overcome the shortcomings of K-theory. Non-local schemes can employ parameterized adjustment terms that represent large scale buoyant plume motion (i.e., cloud updrafts, thermals) or can explicitly treat upward or

downward heat/momentum/moisture transport through conserved atmospheric scalars. The importance of PBL parameterization through such methods as vertical mixing formulation and use of the critical Richardson number to determine boundary/mixing layer height have been emphasized as a couple of the most important factors in improving weather prediction models. PBL parameterizations within large scale NWP modeling are mainly divided into either first order or one-and-a-half order total kinetic energy (TKE) closure schemes (Xie et al., 2012). Research has shown that the simulated mean boundary layer structure is not very sensitive to the order of closure while turbulent structure is better represented, or more sensitive within weak wind regimes, through TKE closure schemes. There has been little research in comparing the typical characteristics of one scheme to another in both stable and unstable boundary layer regimes. Each PBL within the WRF - EMS is tied to a particular surface layer scheme although few studies have been conducted that link a surface layer's contribution to respective PBL behavior. The physical effects of land surface elements are significant, such as over highly urbanized areas, and the understanding of the non-local scheme's ability to blend turbulent mixing characteristics close, or far away, from the surface can ultimately affect heat, momentum and moisture transport.

7.1 **Yonsei University PBL scheme**

This first-order non-local scheme, with a counter gradient term in the eddy-diffusion equation, was developed by Yonsei University in South Korea (Hu, Nielsen-Gammon and Zhang, 2010). The Yonsei University scheme (YSU) parameterizes the distribution

of heat, moisture, and momentum in the part of the atmosphere directly influenced by the earth's surface, or the PBL. It determines the vertical extent and intensity of mixing based upon the stability of the lowest model layer that is approximately 20 meters thick (Hong, Noh and Dudhia, 2006). The YSU scheme is modified in WRF (ver. 2.0) from the (Hong et al., 2006) formulation by increasing the critical bulk Richardson number from zero to 0.25 over land, thereby enhancing mixing in the stable boundary layer (Hong and Kim, 2008).

The advantages to the YSU scheme, in relation to the previous Medium Range Forecast (MRF) PBL scheme, is that its explicit solutions increase boundary layer mixing within thermally-induced free convection regimes while decreasing mixing in mechanically-induced forced convection regimes (Pagowski, 2004). The YSU scheme also does a better job at reproducing convective inhibition than did the older MRF PBL scheme. It does perform well in the vicinity of frontal boundaries. The downstream boundary layer remains less-diluted by cloud entrainment, thus leaving more available “fuel”, or larger regions of Convective Available Potential Energy (CAPE), for imminent stronger convection within the frontogenesis zone (Hong et al., 2006).

7.2 **Mellor - Yamada - Janjić PBL scheme**

The Mellor - Yamada - Janjić PBL scheme (MYJ) is a second-order, single point locally-closed scheme at which diffusion rates per layer are determined by the wind, moisture, and temperature conditions at a particular layer's top and bottom interface. In 2011,

NCEP introduced the NMM-B (Non-hydrostatic Multiscale Meteorological model) that is based on the Arakawa B-grid (Barcelona Supercomputing Center, 2013). The Arakawa B-grid is a "staggered" grid system that separates the evaluation of the two sets of quantities; one might evaluate velocities at the grid center and masses at grid corners (Arakawa and Lamb, 1977). In equations that describe turbulence, there is a closure problem as the number of unknowns is larger the number of equations. These unknown turbulence terms are parameterized as a function of known quantities at the same point (Stull, 1988). Local closure is employed as diffusion rates in each NMM-B model layer are determined by the wind, moisture, and temperature conditions at that particular layer's top and bottom interfaces (Mellor and Yamada, 1974) (Janjić, 2002). The MYJ scheme is a surface layer scheme based on similarity theory (Monin and Obukhov, 1954). The Monin - Obukhov similarity theory is based upon the relationship that describes the vertical behavior of non-dimensional mean flow and turbulence properties within the atmospheric surface layer (i.e., defined as the lowest 10% of the atmospheric PBL) as a function of the Monin - Obukhov key parameters. The Monin - Obukhov similarity hypothesis states that surface layer quantities, when properly non-dimensionalized, become universal functions of the quotient z/L, where z is the height above ground (in meters) and L is the Obukhov length (Air Pollution Training Institute, 2000). The unit-less Obukhov length is a fundamental scaling quantity in surface layer theory that measures the relative importance of mechanical and thermal forcing upon atmospheric turbulence. Or, in other words, the Monin - Obukhov length is a rough measure of the height at which turbulence is generated more by buoyancy than by wind shear (Stull, 1988).

The MYJ scheme also includes parameterizations of water and land viscous sub-layers. Over land, viscous sub-layer effects are taken into account through variable roughness heights with respect to temperature and humidity. The more-shallow convective mixed layer (e.g., cool and moist boundary layer) produced by the MYJ PBL scheme assumes that no mixing occurs with air above the PBL, while air within the PBL is mixed intensely amongst adjacent layers. This results in excessive low-level moisture as evapotranspiration adds moisture while ample dry air is entrained into the PBL from the upper layers (Hu, Nielsen-Gammon and Zhang, 2010). MYJ requires a prediction equation and parameterization for the TKE sources and sinks for each model layer. TKE is defined as the mean kinetic energy per unit mass associated with turbulent flow eddies. The prediction of TKE provides a better emulation of atmospheric mixing, but these prognostications can prove to be very complex. The complexities arise when sub-grid scale eddies are created as a result of the effects of vertical wind shear and buoyancy (MetEd – UCAR, 2011).

7.3 **Mellor - Yamada - Nakanishi - Niino PBL scheme**

The Mellor - Yamada - Nakanishi - Niino PBL scheme (MYNN) has been recently implemented into the WRF - ARW. It is a TKE-based local mixing scheme similar to the MYJ PBL scheme. The main features of this scheme include an option to run a 2.5 to 3.0 closure level (e.g., MYNN 2.5) and it is tuned to a database of large eddy simulations (LES) in order to overcome the typical biases associated with other Mellor - Yamada schemes (Nakanishi and Niino, 2006). These biases involve insufficient growth of the

convective boundary layer and the underestimation of TKE. Liquid water potential temperatures and total water content are used as thermodynamic variables. The MYNN employs more elaborate mixing length formulations to flexibly change behavior, or enhance mixing, across slightly more stable conditions. Recent changes to the scheme include the adjustment of closure constants to aid in the suppression of negative TKE values while removing the critical Richardson Number (Nakanishi and Niino, 2009). There have also been other modifications to closure constants and mixing length formulae (e.g., surface layer, buoyancy length) to help in the compensation of overly-diffusive behavior (Olson and Brown, 2012).

7.4 **Asymmetric Convective Model PBL scheme**

The Asymmetric Convective Model version 2 PBL (ACM2) is an evolved version of the earlier ACM1 PBL. The ACM2 explicitly treats the upward and downward transport of conserved atmospheric scalars with local eddy diffusion through a combination of both local and non-local closure methods (Pleim, 2007). The design of this model is based upon Blackadar's scheme (Blackadar, 1976), but takes into account the important fact that, in the convective boundary layer (CBL), the vertical transport is asymmetric (Wyngaard and Brost, 1984). Upward plumes are rather fast and narrow, transporting mass more rapidly out of the surface layer into subsequent upper layers, while downward streams are wide and slow. Accordingly, upward stream transport (e.g., updrafts) is simulated as non-local while downward stream transport (e.g., downdrafts) is local.

One drawback is that, since this method mixes the same amount of mass to every vertical layer in the boundary layer, it has the potential to remove too much mass out of the surface layer too quickly (Tonnesen et al., 1998). The concept of this model is that buoyant plumbs (i.e., cloud updrafts, thermals) rise from the surface layer and transfer the air's thermal, moisture and momentum properties directly into all above layers. Downward mixing occurs only between adjacent layers in the form of a slow subsidence, or a sedimentation process. Unlike the YSU that uses the parameterized adjustment term γ_c, ACM2's explicit treatment of non-local fluxes is expected to properly simulate a wider array of more applicable quantities, such as humidity and wind, in addition to the heat components. For any scalar quantity, C_i, the ACM2 governing equation is:

$$\delta C_i / \delta t = f_{convection}\, Mu\, C_i - f_{convection}\, Md_i\, C_i + f_{convection}\, Md_i\, C_{i+1}\, \Delta z_{i+1} / \Delta z_i + \delta/\delta z\, [K_c\, (1 - f_{convection})\, \delta C_i / \delta z]$$

where Mu is the non-local upward convective mixing rate, Md_i is the downward mixing rate from layer i to $i - 1$, $Md_i\, C_{i+1}\, \Delta z_{i+1} / \Delta z_i$ is the asymmetric downward flux from the adjacent upper layer, $\delta/\delta z\, [K_c\, (1 - f_{convection})\, \delta C_i / \delta z]$ is the local upward eddy diffusion term. C_i represents the scalar at the lowest model layer and Δz_i is the thickness of layer i, $f_{convection}$ is the key parameter that controls the contribution of non-local mixing versus that of local mixing and is defined as:

$$f_{convection} = [1 + k^{-2/3} / 0.1a\, (-h/L)^{-1/3}]^{-1}$$

where a is a constant set 7.2, *k* is the von Karman constant whose value is 0.4, *h* is PBL height and *L* is the Monin-Obukhov length scale.

The non-local mass exchange in the ACM2 PBL is a physical representation of upward transport by detraining convective plumes that can apply to any quantity (Xie et al., 2012).

7.5 **PBL mathematics & physics**

Sub-grid turbulent fluxes within PBL parameterization are handled through parameterization using the prognostic mean variables C, *u*, *v*, θ, and *q* within vertical diffusion equations. A simple relation to for vertical diffusion can be expressed as:

$$\delta C/\delta t = -\delta/\delta z\ (\overline{w`c`}) = \delta/\delta z\ [K_c\ (\delta C/\delta z)]$$

where K_c is the eddy diffusivity coefficient for the mean variable C, the heat/momentum variable (Shin and Hong, 2011).

The YSU PBL is a first-order non-local closure scheme as it does not require any additional prognostic equations to express the effects of turbulence on the mean variables. In other words, a non-local closure method alone explicitly treats the upward and downward transport of conserved atmospheric scalars (e.g., heat, momentum). This scheme is based on the K profile in the determining the diffusivity, K_c , within the

boundary layer while K_c is a function of local wind shear and the local Richardson number within the free atmosphere. Within the mixed layer, following the "non-local K" approach and adding the non-local gradient adjustment term γ_c to express turbulent diffusion, the YSU is characterized as:

$$\delta C/\delta t = \delta/\delta z \, [K_c \, (\delta C/\delta z - \gamma_c) - (\overline{w`c`})_h \, (z/h)^3]$$

where C represents the heat or momentum variable, K_c is the eddy diffusivity coefficient, γ_c is a correction to the local gradient that incorporates the contribution of large scale eddies to the total flux, and $(\overline{w`c`})_h$ is the flux at the inversion layer. One critical revision within the YSU's PBL scheme, and that set it apart from its parent MRF PBL scheme, was to its vertical diffusion package; the inclusion of a asymptotic entrainment flux term at the inversion layer - $(\overline{w`c`})_h \, (z/h)^3$ that explicitly treats the entrainment process (Xie et al., 2012).

The YSU PBL scheme has been found to increase boundary layer mixing in a thermally-induced free convection regime and to reduce it within mechanically-induced forced convection regimes. This yields a more realistic PBL structure than predicted with its predecessor, the MRF PBL scheme. Local closure schemes (e.g., TKE closure, one-and-one-half order closure), are employed within the MYJ, QNSE, MYNN2, and BouLac PBLs. These PBL schemes estimate the turbulent fluxes at each grid point from the mean values of atmospheric variables, or their gradients, at a particular grid point. In other words, local closure schemes only allow for vertical mixing within the boundary layer to

occur between neighboring grid boxes. These schemes require one additional prognostic equation of the TKE, *e*. These schemes are called turbulent kinetic energy (TKE) closure schemes because they derive their eddy diffusion coefficients from prognostic TKE equations. The governing equations for the TKE local closure schemes are:

$$\delta e/\delta t = -1/\rho\ \delta/\delta Z\ \rho\overline{w'e'} - \overline{u'w'}\ \delta U/\delta Z - \overline{v'w'}\ \delta V/\delta Z + \beta\overline{w'\theta'} - \varepsilon$$

$$\overline{w'u'} = -K_m\ \delta U / \delta Z$$

$$\overline{w'v'} = -K_m\ \delta V / \delta Z$$

$$\overline{w'e'} = -K_e\ \delta e / \delta Z$$

$$\overline{w'\theta'} = -K_h\ \delta\theta / \delta Z$$

where *e* is the turbulent kinetic energy, β is the buoyancy coefficient, ε denotes TKE dissipation by molecular processes, ($-\overline{u'w'}\ \delta U/\delta Z - \overline{v'w'}\ \delta V/\delta Z$) describes the production of TKE due to shear, and the $\beta\overline{w'\theta'}$ term is TKE production due to buoyancy.

Diffusivity in the MYJ, QNSE, and BouLac PBL schemes is commonly expressed as:

$$K_c = l\sqrt{e}\ S_c$$

where l is the mixing length and S_c is the proportional coefficient. All three PBL schemes differ on how they handle l and S_c (Shin and Hong, 2011).

The surface layer schemes compute frictional velocities u^* and exchange coefficients for the computation of surface heat/moisture fluxes created by land surface models and surface stress within the PBL schemes. There are limitations to the allowable combinations between PBL schemes and surface layer schemes. The MYJ PBL is a one-dimensional 1.5 order, level 2.5 TKE local closure scheme. The MYJ has the tendency to simulate a cooler and more moist boundary layer that limits the depth of the convective mixing layer (Hu, Nielsen-Gammon and Zhang, 2010).

The Quasi-Normal Scale Elimination (QNSE) PBL is local TKE closure scheme that uses modern QNSE theory for the handling of small scale eddy viscosity and eddy diffusivity variables. The QNSE theory treats turbulence and the resulting waves as one entity to better resolve the effect of internal waves. This theory has been suggested to better improve turbulence representation within the WRF (Sukoriansky, Galperin and Perov, 2006).

The more recently developed Mellor - Yamada - Nakanishi - Niino (MYNN) PBL for WRF - ARW core is a TKE-based local mixing scheme. The main feature of this scheme is the option to run it at a level 2.5 or level 3.0 closure. This research ran the MYNN scheme with the 2.5 closure scheme. The MYNN is tuned to a database of Large Eddy Simulations (LES). This LES relation aids in overcoming the typical lower level cooler and more moist biases associated with other Mellor - Yamada-type schemes, or for the insufficient growth of the convective boundary layer and subsequent TKE

underestimation. The MYNN updates its stability functions that allow for more mixing within slightly stable conditions (Nakanishi and Niino, 2009).

The Bougeault and Lacarrere (BouLac) PBL is a local TKE closure scheme developed at the University of South Florida and is designed specifically for use with the Noah LSM and the multi-layer urban canopy model (UCM) (Bougeault and P., 1989).

7.6 **Surface layer schemes**

Surface layer schemes in the WRF handle the surface layer physics that are typically observed within the lower 10% of the atmospheric boundary layer (i.e., lowest atmospheric layer most influenced by the Earth's surface). WRF's surface layer schemes calculate heat, moisture and momentum fluxes between the surface skin, or lowest layer of air in contact with the surface, and the reference model level (e.g., 2 m or 10 m). Surface layer schemes work in tandem with their respective PBL schemes to calculate the roughness length (Z_o) and friction velocity (u^*) as a function of land-use type. Monin - Obukhov similarity theory, or the relationship describing the vertical behavior of non-dimensionalized mean flow and turbulence properties within the atmospheric surface layer, are inherently linked with the YSU, MYJ, QNSE, MYNN, and BouLac PBLs. (Shin and Hong, 2011) Each PBL is assigned it's unique surface layer scheme (e.g., MYJ Monin - Obukhov similarity theory, QNSE Monin - Obukhov similarity theory) to work in accordance within that PBL's algorithms. The ACM2 PBL is linked to the Pleim - Xiu (EPA) surface layer scheme. The Pleim - Xiu (EPA) surface layer scheme has been

associated with earlier versions of the WRF and is primarily utilized within air quality studies (Gilliam, Pliem and Xiu, 2007).

7.7 **Noah land surface model (LSM)**

The land surface physics scheme that was utilized in all of this research's WRF -EMS runs was the Noah Land Surface model (LSM). This LSM uses soil temperature and soil moisture at depths of 10, 30, 60, and 100 cm, fractional snow cover, and frozen soil physics (Chen and Dudhia, 2001). The Noah LSM provides the essential quantities of surface sensible and latent heat and moisture flux, along with upward-directed shortwave and longwave radiation, to the WRF's assigned PBL scheme. The Noah LSM scheme diagnoses skin temperature and surface longwave radiative emissivity as well as shortwave radiative (reflected) surface albedo. Vegetation transpiration and potential evaporation, if near a sufficient water source, are both parameterized within this LSM. Through such satellite-derived measures as the Normalized Difference Vegetation Index (NDVI) the effects of vegetation are included within the LSM to aid in the seasonal calculation of the green vegetation index, or the amount of photosynthetic-active healthy, green vegetation. Other parameters include the green vegetation fraction that partitions direct, bare soil evaporation from canopy transpiration and canopy (frictional) resistance (F. Chen, 2007) (Chen and Dudhia, 2001).

The coupling of the Noah LSM and the single layer Urban Canopy Model (UCM) was used in conjunction with the MYJ and BouLac PBL schemes. The UCM is used to better

represent the physical processes that are involved in the exchange of heat, water vapor, and momentum within the urban environment. While the Noah LSM handles natural surfaces, the single-layer UCM parameterizes man-made surfaces. This includes the shadowing effects of buildings, shortwave and longwave radiation reflection, canopy layer wind profiles and multi-layer heat transfer equations for roof, wall and roadway surfaces (Kusaka and Kimura, 2004).

8. Microphysical Schemes

The WRF's microphysical schemes are responsible in resolving such cloud-scale physical processes as cloud formation and evolution (e.g., updraft and downdraft structure) as well as warm/cold precipitation generation and the subsequent downstream sustainability of existing hydrometeors (i.e., sedimentation). The handling of the vertical transport of various atmospheric hydro/frozen species due to sedimentation, or the tendency for suspended hydrometeors to "fall out", is a key aspect to modeling atmospheric microphysical (cloud) scale processes (Morrison, 2011). It has important implications in the timing and amount of accumulated ground-level precipitation along with the vertical distribution of hydrometeors within the resident, or regional, atmosphere.

The microphysical schemes utilized within this research are classified as bulk schemes. These parameter manipulation-friendly bulk schemes are favored as they require fewer prognostic variables with easier integration that make for a more computational cost-

effective scheme. The basic concept of bulk parameterization is to relate surface layer fluxes (i.e., bulk transfer coefficients of wind, temperature, moisture) at particular heights to logarithmic profiles of particle quantities. Bulk schemes assume some functional form for hydrometeor particle size distribution (e.g., gamma function) and prognose one or two mathematical moments of these particle size distributions. In traditional bulk schemes, sedimentation is calculated using a characteristic moment-weighted fall speed for each forecasted bulk quantity. One or more hydrometeor bulk quantities (e.g., cloud water, rain, snow, etc…) and a characteristic moment-weighted velocity is used to calculate the sedimentation of each quantity. The particle size distribution for each category, or species, is generally assumed to follow some analytic basis function. Exponential size distributions are assumed to be in the gamma form of:

$$N' = N_0 e^{-\lambda D}$$

where D is the particle diameter and N_0 and λ are the intercept and slope parameters, respectively. Hydrometeor quantity, ψ, follows the conservation equation:

$$\delta(\rho\psi)/\delta t = -\delta(v\rho\psi)/\delta z = -\delta[(w - V)\rho\psi]/\delta z$$

where ρ is air density, t is time, z is height, $v = w - V$ is the velocity (positive in the upward direction), w is the vertical air motion, and V is the hydrometeor fall speed due to the gravitation force.

The definition of a mathematic *moment* is the quantitative measure of the shape of a set of points or, in microphysical schemes, species (e.g., ice crystals, rain, graupel, etc...). A *single moment* is defined as the arithmetic mean about a distribution of a points/species (Fig. 8). A *double moment* is the variance within a group of species, or that species' standard deviation (Morrison, 2011) (Milbrandt and Yau, 2005).

The WRF's prognostication of precipitation uses a two-step, time-splitting approach for solving the time-dependent advection and sedimentation equations. In the two-step time-splitting approach, prognostic quantities of rain, snow, hail, etc… are initially updated after advection, followed by sedimentation calculation using these aforementioned forecasted quantities. This method has been utilized in a high number of microphysical schemes due to its simplicity, low computational cost, and other desirable characteristics such as monotonicity and positive definiteness, although the method is diffusive in relation to other higher-order methods. Sedimentation has traditionally been considered a component of microphysical schemes since particle fall speeds are calculated by the scheme and are ultimately used for the calculation of several other microphysical processes. The calculation of sedimentation and particle fall speeds is usually contained within the microphysical code and therefore separated from the advection code. This has made for easier WRF model implementation in giving the end-user a higher number of microphysical schemes for which to choose (Morrison, 2011).

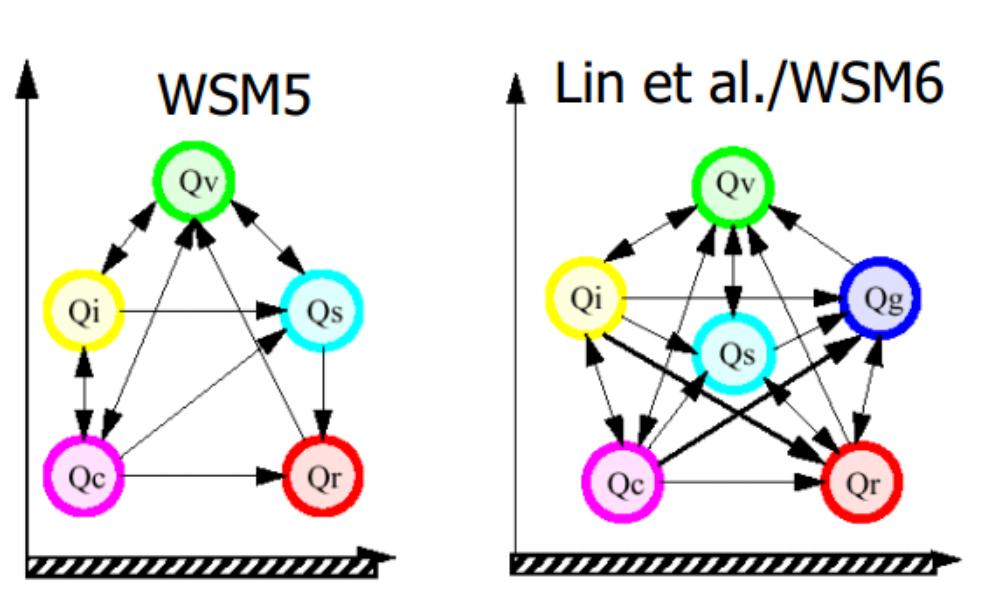

Figure 8: WRF single moment 5-Class and Lin / WRF single moment 6-Class microphysical scheme's species mixing ratio (Q) relationships (UCAR, 2012)

8.1 **Microphysical scheme descriptions**

There were eight microphysical schemes employed in this research (Fig. 9). A brief description of each scheme is as follows:

8.1.1 **(Purdue) Lin**

Originated from the Purdue cloud model, the Lin microphysics scheme offers six classes of hydrometeors; water vapor, cloud water, rain, ice, snow and graupel. Ice sedimentation and time-split fall terms, along with saturation adjustment following (Tao et al., 1989), are included within this relatively-sophisticated scheme (Lin, Farley and Orville, 1983).

8.1.2 **WRF Single Moment 6-Class**

The WRF Single-Moment 6-Class (WSM6) is a single moment six-class microphysical scheme that includes the graupel species. This scheme employs ice number concentration with an improved snow and graupel fall speed algorithms with semi-Lagrangian fall terms. Semi-Lagrangian schemes or terms use the Eulerian framework (i.e., observing the parcel from a fixed point), but the discrete equations are from a Lagrangian perspective (i.e., following the air parcel). The fall speeds of both snow and graupel, within either the sedimentation or accretion processes, are assigned the same fall speed, but the speed is weighted based upon that particle's mixing ratio(s) (Hong, Dudhia and Chen, 2004).

8.1.3 **Thompson**

This revised version of the Reisner2 scheme is a six-class microphysical scheme that includes graupel. A double moment scheme that predicts both the ice and rain number concentration and utilizes time-split fall terms. This newer scheme is more advanced with the handling of snow size distribution. Snow size distribution is dependent upon ice water content and temperature and is represented as a sum of exponential and gamma distributions. Unlike other bulk schemes that assume a spherical snow shape with constant density, snow within the new Thompson scheme takes on a non-spherical shape with a bulk density that varies inversely with diameter as has been discovered in real world observation (Thompson et al., 2008).

8.1.4 **Milbrandt - Yau**

The Milbrandt - Yau (Mil - Yau) is a sophisticated double moment, seven-class microphysical scheme that separates graupel and hail. There is a prognostication of number concentration for all six water and ice species with a total of 13 variables (e.g., six species mass, six species number concentration plus a water vapor species) and time-split fall terms. This scheme is unique in that it does not treat the spectral shape parameter of a particle, α, as a constant. A diagnostic equation is used for the spectral shape parameter based upon a gamma distribution of the mean particle size for hydrometeor sedimentation in narrowing the size spectra (Milbrandt and Yau, 2005).

8.1.5 **Morrison**

The Morrison is a double moment, six-class microphysical scheme that uses time-split fall terms. Along with the prediction of species mass mixing ratios, this cloud-resolving scheme also predicts the number concentrations for both ice and water particles. This double moment prediction of both mixing ratio and number concentration is advantageous for the evolution of precipitation processes as it allows for a more robust treatment of all particle size distributions (Morrison, Thompson and Tatarskii, 2009).

8.1.6 **Stonybrook-Lin**

The SB - Lin microphysical scheme is a five-class scheme that includes riming intensity to account for mixed phase processes and temperature-dependent ice characteristics. A continuous spectrum, from pristine ice crystals to heavily rimed particles and graupel, the SB - Lin only uses one prognostic variable (i.e., precipitating ice) rather than two separate variables for snow and graupel. This method nearly halves the number of parameterized processes, as compared to other six class schemes, thus making it more computationally-efficient (Lin and Colle, 2011).

8.1.7 **WRF Double Moment 5-Class**

The WRF Double Moment five-class (WDM5) microphysical scheme that differentiates it from the WSM5 by utilizing a double moment for warm rain processes. Mass mixing ratio and number concentration are calculated for cloud condensation nuclei (CCN), cloud, and rain particles (Lim and Hong, 2010).

8.1.8 **WRF Double Moment 6-Class**

The WRF Double Moment six-class **(**WDM6) is based upon the WSM6 as it provides a prognostication for 13 different mass mixing ratio and number concentration variables; water vapor, cloud, rain, ice, snow, and graupel particles along with the CCN number concentration variable. The main strength of this scheme is its ability to allow flexibility

in varying rain drop size distribution by predicting cloud and rain number concentrations, coupled with explicit CCN distribution, at reasonable computational cost (Lim and Hong, 2010).

Microphysical Scheme	Mass (kg/kg)	Number (#/kg)
Lin	Qv Qc Qr Qi Qs Qg	
WSM 6	Qv Qc Qr Qi Qs Qg	
Thompson	Qv Qc Qr Qi Qs Qg	Ni Nr
Milbrandt-Yau	Qv Qc Qr Qi Qs Qg Qh	Nc Nr Ni Ns Ng Nh
Morrison	Qv Qc Qr Qi Qs Qg	Nr Ni Ns Ng
Stonybrook	Qc Qr Qi Qs Qg	
WDM5	Qv Qc Qr Qi Qs	Nn Nc Nr
WDM6	Qv Qc Qr Qi Qs Qg	Nn Nc Nr

Microphysical Schemes with their mass and number variables

Figure 9: Microphysical schemes

9. Radiation

9.1 **Dudhia shortwave radiation scheme**

This NCAR radiation scheme runs in ten minute intervals (UCAR, 2012). Only the downward fluxes of Rayleigh scattering, reflection, and absorption characteristics of a cloudless (i.e., clear sky) model atmosphere, with respect to shortwave radiation, are determined within this scheme. Scattering and water vapor absorption are both assumed to be independent of wavelength. Total downward radiative flux equals the clear sky effects upon downward radiative flux out of a layer toward the surface in tandem with cloud albedo and absorption properties. Upward reflected shortwave radiation from the surface and cloud cover is essentially ignored with the assumption that this radiation has escaped to space. Although the Dudhia shortwave scheme only utilizes one large shortwave spectral band in its calculation of radiative transfer, this scheme is requested more frequently so it is more adequate for short-range forecasts. The shortwave scheme also accounts for water vapor absorption over the full solar spectrum throughout a particular layer (J. Dudhia, 1989). Solar radiation absorption calculations in the model atmosphere are based upon the Lacis and Hansen water vapor formula (Lacis and Hansen, 1974 a). This method is described for rapidly computing the amount of solar energy absorbed at the earth's surface and within the atmosphere as a function of altitude. This method’s parametric calculation accounts for absorption variance due to the amount of clouds and cloud type, the amount of water vapor in each layer and the albedo of the earth's surface. The formula calculates a particular layer’s water vapor path, the total

amount of water vapor present in the column measured by a microwave radiometer (U. S. Dept. of Energy, 2013), while adjusting for the solar zenith angle and solar beam length throughout the layer (Lacis and Hansen, 1974 b).

9.2 **Rapid Radiation Transfer Method (RRTM) longwave radiation scheme**

Longwave radiative processes are calculated using correlated k-distribution method from wavelengths ranging from 3.33 μm to 1 mm. The variation of absorption coefficients in the vertical must be remedied as they significantly vary over temperature and pressure surfaces. The correlated k-distribution's approach to this problem is to correlate different absorption line profiles with one another. The method takes thorough line-by-line calculations over 16 longwave band intervals and calculates the probability distribution of absorption coefficients within those intervals (Fu and Liou, 1992) (Mlawer et al., 1997). Absorption coefficients, as a function of temperature and pressure, are maintained for each band for both lower and upper atmosphere over 59 pressure levels, from 1050 hPa (mb) to 0.01 hPa (mb). The longwave radiative transfer routine takes into account the effect of overlapping absorption lines for multiple absorbing gases by adjusting the absorption coefficient by a factor that takes into account the amount and strength of each absorber (MetEd, 2012 a). A probability distribution is used to determine each layer's temperature change with the longwave radiative processes ultimately determining a layer's temperature (pressure), and amount of longwave absorber(s). The amount of longwave absorbers in each layer, such as greenhouse gases and clouds, is calculated every three hours. Longwave radiation leaving the surface, based on skin temperature, is

calculated in three minute time steps. The RRTM calculates cloud optical depth while its parameterization methods uses pre-set tables in accurately representing the longwave radiative effects of ozone (O_3), carbon dioxide (CO_2), water vapor (H_2O), chlorofluorocarbons (CFCs), carbon tetrachloride (CCl_4), methane (CH_4), and nitrous oxide (N_2O) (Mlawer et al., 1997).

10. Verification Results

10.1 **Description of the parameterized temporal, rainfall accumulation, areal verification domain categories**

In handling the hypothesis of whether the 3 km^2 WRF - EMS could affectively resolve an extreme rainfall event, five parameters were set up within the MET software. The research method of the verification process was to not only vary the rainfall accumulation quantities, but to also vary the temporal and spatial elements. Understanding the current limitations of the WRF - EMS system and its associated physical schemes made it clear that, if verification parameters were set too low, the majority of model output would be of no value to this particular study. The numerous complexities of the ever-evolving PBL and microphysical schemes within numerical weather prediction of any resolution stress the modern inability to successfully re-produce skillful output (e.g., scores) for extreme, or rare, events. Hence, this research wanted to vary the verification scoring parameters to

better comprehend which physical scheme modeled output would better display correlation with observed rainfall accumulation.

The research goal was to observe what initialization datasets and physical scheme WRF - EMS model output would best resolve a regional high rainfall event. The case study produced extreme values of greater than 150 mm per hour rates, but the majority of the higher hourly rates ranged from 50 mm to 100 mm over Harris and Galveston counties. Most of the rain fell within a 6 hour period, from around 1800 UTC through 2400 UTC on the 18th of April, 2009 over Harris and Galveston counties. In capturing the most pertinent rain accumulation in the regional surface rain gauge network and local radar observation, this study wanted to verify three quantitative rain measures; 25 mm, 50 mm, and 100 mm accumulation. The researcher wanted to set hourly, three hourly, and six hourly parameters. The reasoning for this was that the WRF - EMS output was verified against quality-controlled Stage IV hourly and six hourly radar-derived rainfall accumulation data. The six-hourly parameter was included to capture a realistic, full duration high rainfall event. The desire to accurately depict the geographic coverage of the most intense rain allowed for three areal coverage domains; county, city, and town scale. Setting these areal coverage parameters through the MET software afforded a 17 x 17 grid that translated to a 48 km x 48 km (2,304 km^2) geographic area that could roughly be equated to a typical southeastern Texas county. The other two spatial parameters of 9 x 9 (24 km^2) and 3 x 3 (6 km^2) grid spacing translated to regional city (e.g., Houston in Harris County) and town (e.g., League City in Galveston County) geographical

interpretations, respectively. These areal parameters were a logical fit for the WRF - EMS's 9 km^2 parent, with a nested 3 km^2, domain set-up.

The research employed the five parameterized verification domains as follows; 1 hour / 50 mm / 24 km^2, 3 hour / 25mm / 6 km^2, 3 hour / 100 mm / 24 km^2, 6 hour / 100 mm / 24 km^2, and 6 hour / 100 mm / 48 km^2.

Statistical Score Definitions (Verification)

Forecast	Observed *Yes* = 1	Observed *No* = 0	Total
f = 1 **Yes**	n_{11} **Hit**	n_{10} **False Alarm**	$n_{11} + n_{10}$ **Forecast Yes**
f = 0 **No**	n_{01} **Miss**	n_{00} **Correct Negative**	$n_{01} + n_{00}$ **Forecast No**
Total	$n_{11} + n_{01}$ **Observed Yes**	$n_{10} + n_{00}$ **Observed No**	$n_{11} + n_{10} + n_{01} + n_{00}$

Figure 10: Verification chart

10.2 **Frequency Bias (FB)**

Frequency Bias is the dichotomous forecast measurement of the ratio of the frequency of forecast events ($\boldsymbol{n_{11} + n_{10}}$) to the frequency of observed events ($\boldsymbol{n_{11} + n_{01}}$) (Fig. 10). Frequency Bias indicated whether model output had a tendency to over or under, forecast the defined rain accumulation over a particular temporal and spatial parameter. A perfect

value is 1. Values less than 1 were an under-forecast while values greater than 1 were an over-forecast. MET verification software defines Frequency Bias as:

$$n_{11} + n_{10} / n_{11} + n_{01} = n_1 + n_1$$

10.3 **Critical Success Index (CSI)**

The Critical Success Index measures the fraction of the number of times the event was correctly forecast ($n_{11)}$ to the number of times it was either correctly forecast or it occurred without being forecast $(n_{11} + n_{10} + n_{01})$ (Fig. 10). This index is a measure of accuracy when correct negatives have been removed from consideration. The Critical Success Index is only concerned with the forecasts that "count". This index is sensitive to hits and penalizes both misses and false alarms. The Critical Success Index score depends on the climatological frequency of events (i.e., poorer scores for rarer events) since some hits can occur purely due to random chance. The Critical Success Index ranges from 0 to 1, with 1 being the perfect score. MET verification software defines the Critical Success Index as:

$$n_{11} / n_{11} + n_{10} + n_{01}$$

10.4 **Heidke Skill Score (HSS)**

The Heidke Skill Score measures the fraction of correct forecasts after eliminating those forecasts that would have been correct purely due to random chance. A generalized skill score where the score in the numerator is the number of correct forecasts minus the correct forecast due to pure random chance **($n_{11} + n_{00} - C$)** while the denominator is the total observed/forecasted events (**T**) minus the correct forecast due to pure random chance (**C**). The Heidke Skill Score ranges from minus infinity (-∞) to 1, with 1 being the perfect score. MET verification software defines the Heidke Skill Score as:

$$n_{11} + n_{00} - C / T - C$$

where, $C = (n_{11} + n_{10})(n_{11} + n_{01}) + (n_{01} + n_{00})(n_{10} + n_{00}) / T$

The five 108 temporal/rainfall/spatial statistical parameterized verification domain categories, with 324 statistics (1,620 total) of FB, CSI, and HSS PBL - microphysical relationship statistics (i.e., scores), utilizing the CFSR and ERA reanalysis initialization datasets, are discussed in the following chapter; **Chapter 11. Results and Discussion**.

11. Results and Discussion

11.1 **Climate Forecast System Re-Analysis (CFSR) initialization**

The best bias and maximum (i.e., highest) accuracy score results will be discussed and analyzed within each parameterized verification domain.

It must be noted that the maximum score(s) did not always correspond to the overall better performer(s). Typically, the highest scoring PBL - microphysical (mp) schemes did correspond to those PBL - microphysical scheme combinations that consistently performed the best across space and time. With that being said, this research did have certain scenarios occur in which the maximum accuracy score did not necessarily correspond to the overall better PBL - microphysical scheme performer(s). Unfortunately, it was physically impossible to plot thousands of PBL - microphysical scheme combination data points within one table or into one graph. Thus, this dilemma was handled through discussion within my individual parameterized verification domain categories.

CFSR											
		1 hr / 50 mm / 24 km^2		3 hr / 25 mm / 6 km^2		3 hr / 100 mm / 24 km^2		6 hr / 100 mm / 24 km^2		6 hr / 100 mm /48 km^2	
PBL	mp	CSI	HSS	CSI	HSS	CSI	HSS	CSI	HSS	CSI	HSS
ACM2	Lin	0.159	0.188	0.339	0.357	0.127	0.157	0.217	n/a	0.386	0.283
	WDM5	0.068	0.076	0.315	0.347	0.000	-0.013	0.143	0.211	0.237	0.296
	Mil - Yau	**0.265**	**0.405**	**0.397**	**0.452**	**0.155**	**0.236**	**0.227**	n/a	**0.457**	**0.501**
Bou - Lac	Lin	0.090	0.115	0.201	0.098	0.073	0.063	0.164	0.245	0.231	0.174
	WDM5	**0.131**	**0.161**	**0.410**	**0.434**	**0.118**	**0.147**	**0.279**	**0.386**	**0.308**	**0.353**
	Mil - Yau	0.032	0.005	0.173	0.138	0.022	0.000	0.236	0.358	0.230	0.274
MYNN	Lin	0.062	0.022	0.200	0.085	0.000	-0.015	0.136	0.202	0.186	0.168
	WDM5	**0.088**	**0.129**	**0.431**	**0.456**	**0.099**	**0.166**	0.201	0.257	**0.284**	0.281
	Mil - Yau	0.026	0.013	0.233	0.258	0.000	0.000	**0.255**	**0.395**	0.188	**0.292**

Table 1: Maximum accuracy scores over the five verification domains (CFSR)

The best one hour 50 mm 24 km^2 FB (i.e., bias) statistics were with the MYJ - Lin PBL - microphysical combination. The MYJ - Lin achieved the best bias scoring with a 28% top ranking occurrence across all PBL - microphysical combinations and displayed improvement with time. The ACM2 - Mil - Yau combination exhibited the maximum accuracy with a 0.265 Critical Success Index (CSI) score and a 0.405 Heidke Skill Score (HSS) (Table 1). The WDM5 microphysics, when associated with either the MYNN or the BouLac PBL scheme, scored maximum accuracy scores. This microphysical scheme scored the relatively highest scores within the BouLac PBL with a 0.131 CSI score and a 0.161 HSS (Table 1). The PBL - microphysical scheme combination that was most successful at resolving an hourly rainfall amount of 50 mm over a city scale was the ACM2 - Mil - Yau relationship. The ACM2 - Mil - Yau scored the highest with an 80% chance of being the maximum scoring combination. While the MYJ - Thompson (e.g., 66% first place occurrence), and the YSU - WDM6 or QNSE - Thompson (e.g., 58% first place occurrence) PBL - microphysical combination schemes were better performers at resolving hourly 50 mm rainfall over a city scale, the maximum accuracy scores belong to the ACM2 - Mil - Yau and the MYJ - Thompson relationships (Fig. 11, 12).

It was determined that the better performing PBL and microphysical combinations inherently utilized the more complex physics within their respective schemes. The ACM2 PBL benefits from the asymmetric method of better simulating cumulonimbus updraft and downdraft structure. The BouLac PBL algorithm's benefit from their ability to ingest higher-resolution urban canopy data. Ultimately, this attribute better handled the land use

data idiosyncrasies of resolving heat and moisture transport into the evolving-convective mixing layer across an urban landscape versus that of a non-urban environment. The MYNN's primary strength was its ability to better close off (i.e., resolve) highly erratic sub-grid eddy behavior within its more-advanced 2.5 order differential mathematical array structure. The Lin and the WDM5 microphysical scheme strengths are their ability to attempt to model the existence of graupel within a storm cloud. The Mil - Yau is the most advanced microphysical scheme employed within this research. The Mil - Yau is a double moment scheme that can prognosticate the relative amount and number of the hail and graupel species. More complex microphysical cloud schemes that employ more species and higher moment mathematics, when in association with the above PBL schemes, were more successful at better resolving rainfall within the pre-determined domains of this research.

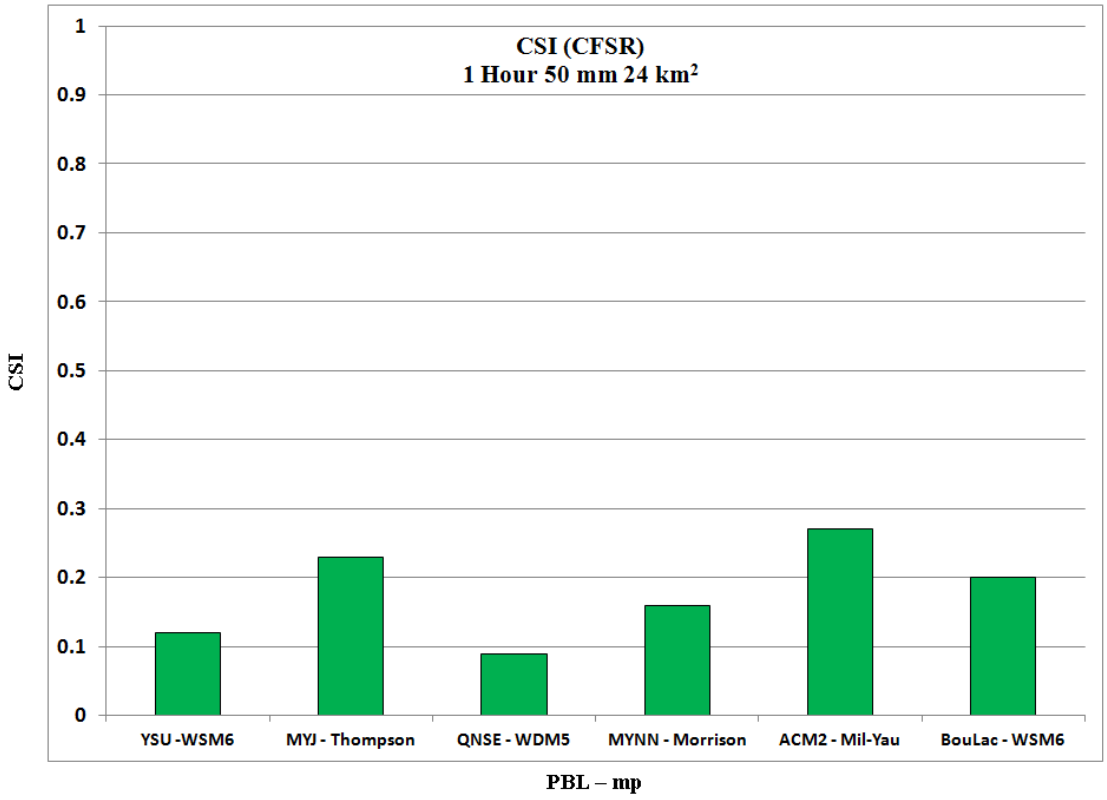

Figure 11: Maximum 1 Hr 50 mm 24 km^2 PBL - mp Critical Success Index (CSI) scores

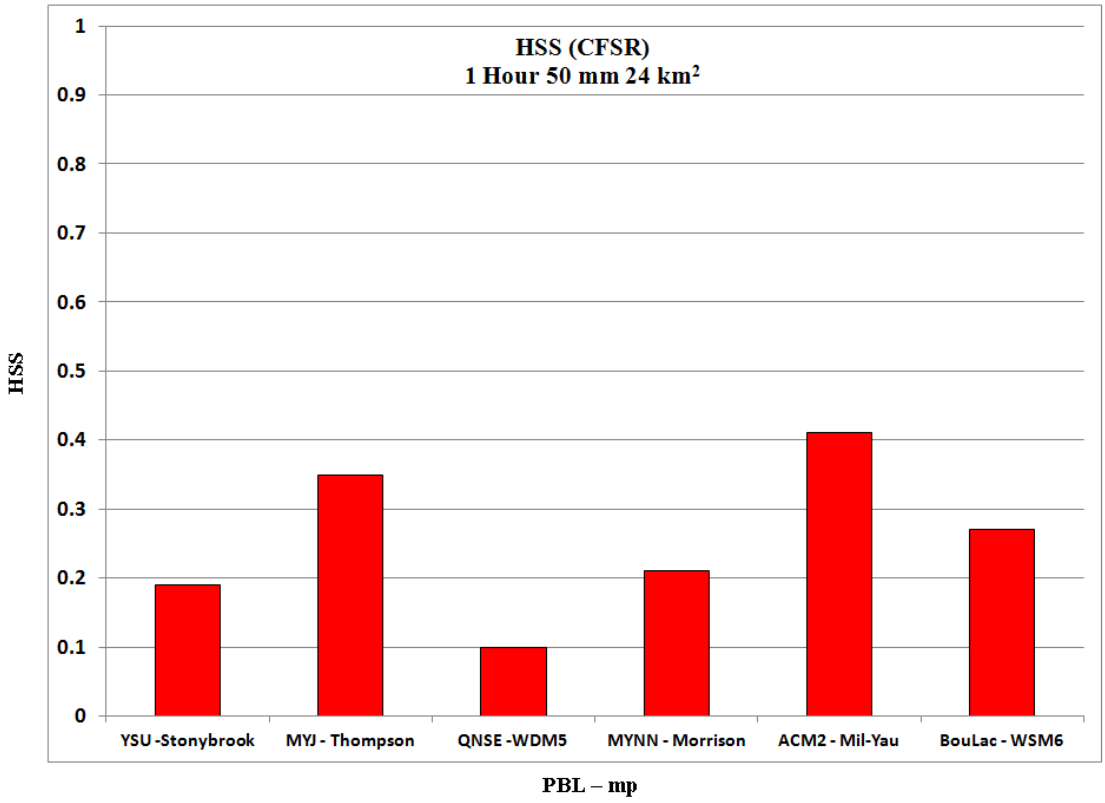

Figure 12: Maximum 1 Hr 50 mm 24 km^2 PBL - mp Heidke Skill Score (HSS)

Higher scores for the three hourly 25 mm rainfall accumulations over an area approximately the size of a typical U. S. town, or suburb, again favored the more advanced PBL and microphysical scheme combinations. One of the few combinations that scored a perfect bias score of 1 within the study was the MYJ - WDM6 at 2300 UTC. Although the MYJ has been known to under forecast PBL height, the associated microphysical scheme of the WDM6 is one of the more advanced microphysical schemes within this study. The WDM6 is a double moment, 6 - class scheme that has the ability to forecast the existence and amount of graupel within a cumulonimbus cloud. The WDM6 also has the unique ability to prognosticate the number of cloud condensation nuclei

(CCN). These attributes are the main reasons this microphysical scheme, even when coupled with the historically cooler and more moist MYJ PBL, remained one of the top performers of this research. Strong PBL - microphysical scheme combination performers, with respect to maximum accuracy scores, were the ACM2 - Mil - Yau, the BouLac and MYNN when in association with the WSM5. These combinations scored above a 0.397 within this particular domain (Table 1); relatively consistently higher accuracy scores that were discovered within the verification. The Lin and WDM6 microphysical schemes successfully forecasted the event in time (e.g., typically greater than 0.75 bias) (Fig. 13). Generally, between the hours of 2000 UTC and 2100 UTC, the WDM6 microphysics scheme was a top ranked performer across all PBLs, with the exception of the MYNN and the ACM2 PBLs, while the WSM6 scheme was a solid performer. The WDM5 was ranked number one 8 out of 10 times while it also improved with time across all PBLs, with the exception of the ACM2 PBL, in the CSI results (Fig. 14). A strong CSI performer was the Thompson microphysical scheme as it ranked number two nearly three quarters of the time (i.e., 73% occurrence). The best HSS performer was the WDM5 scheme. The WDM5 was ranked number one across all PBLs, with the exception of the ACM2, and improved with time (Fig. 15). Although not a consistent top scorer, the Morrison microphysical scheme performed admirably with relatively higher HSSs. Between the hours of 1900 UTC and 2000 UTC; the Thompson scheme dominated the rankings across all PBLs, with the lone exception being the ACM2 PBL. The favored PBL and microphysical relationships, or those combinations that consistently ranked number one, were the BouLac - WDM5 (e.g., 100% occurrence), the ACM2 - Mil - Yau (e.g., 83% occurrence) and the MYJ - WDM5 (e.g., 75% occurrence). It was again

determined that the better performing PBL and microphysical combinations within this verification domain inherently utilized the more complex physics within their respective schemes. The better performing combinations, such as the ACM2 - Mil-Yau and the BouLac or MYNN with the WRF microphysical double moment schemes (e.g., WDM5, WDM6), repeatedly scored higher when forecasting three hourly 25 mm rainfall amounts over a town or suburb geographical scale (Table 1).

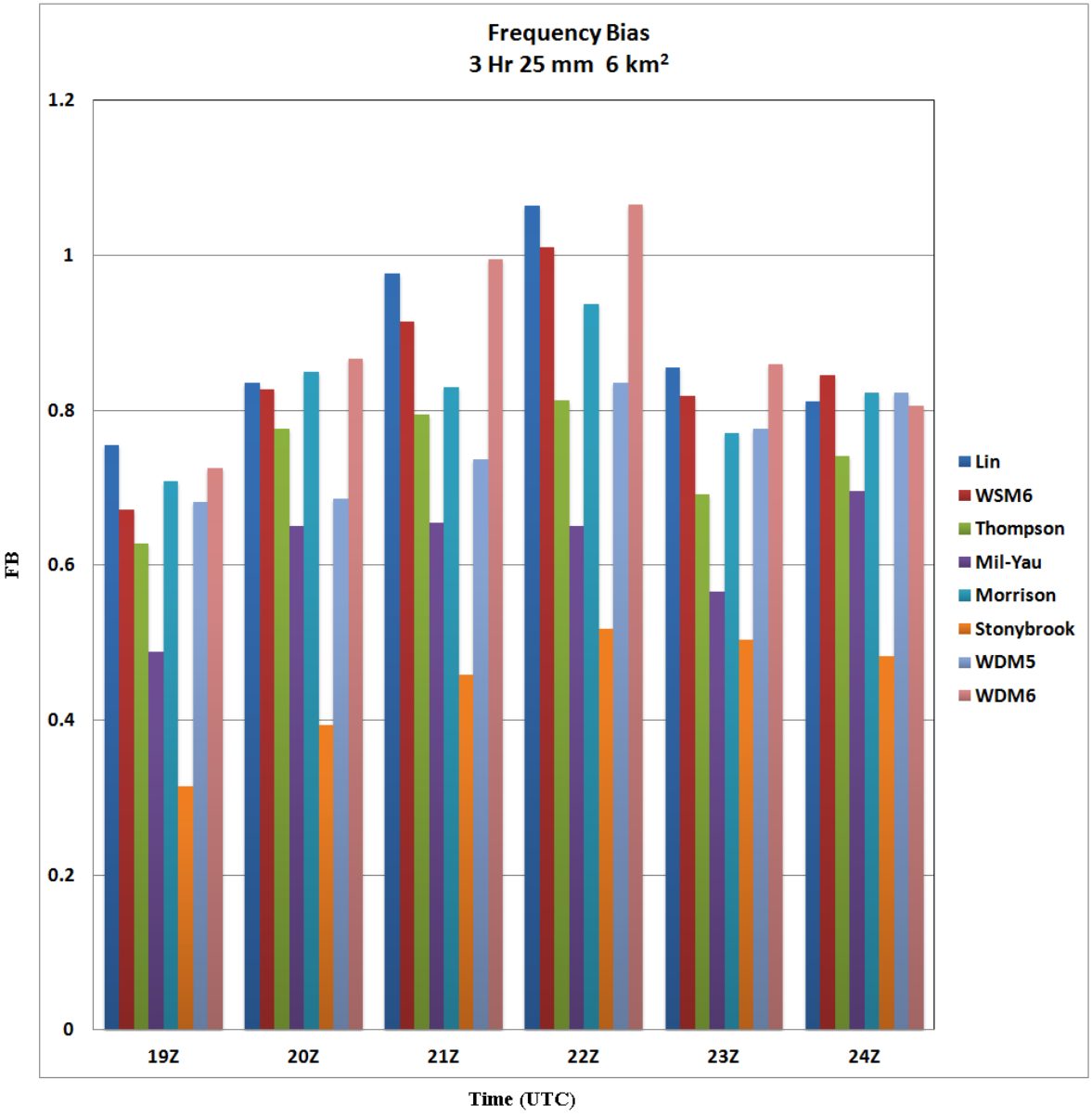

Figure 13: ACM2 PBL - mp frequency bias (FB)

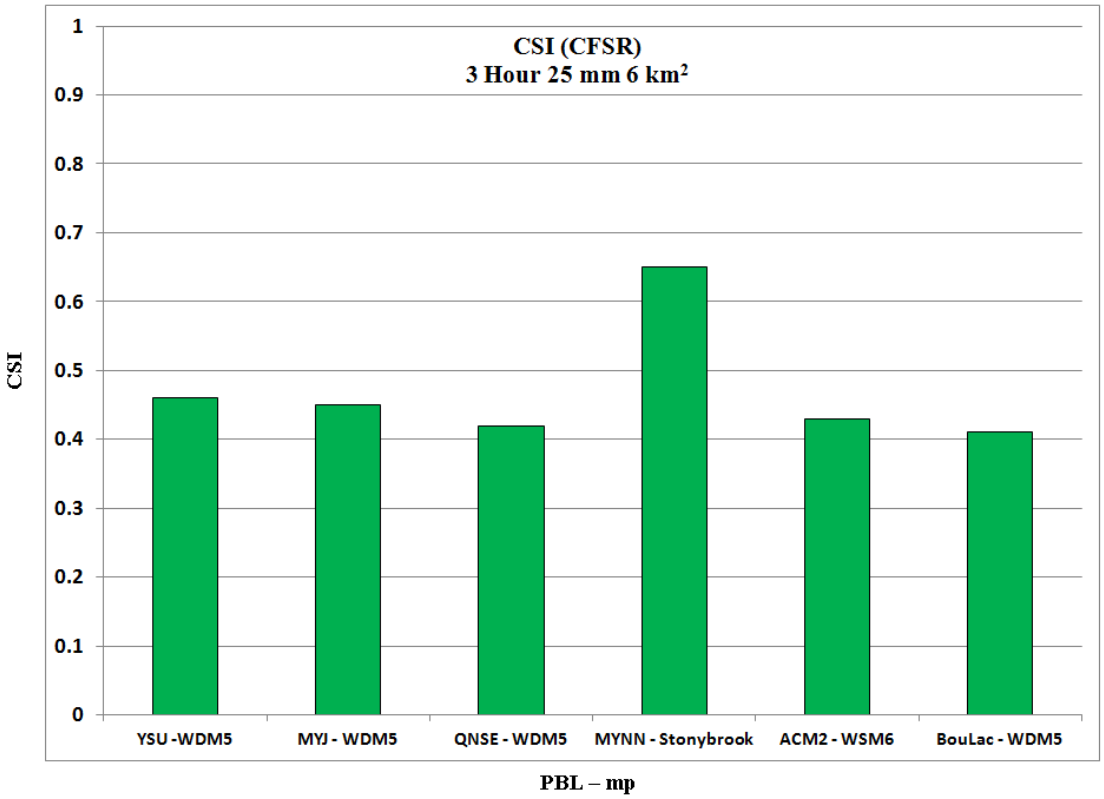

Figure 14: Maximum 3 Hr 25 mm 6 km^2 PBL - mp CSI

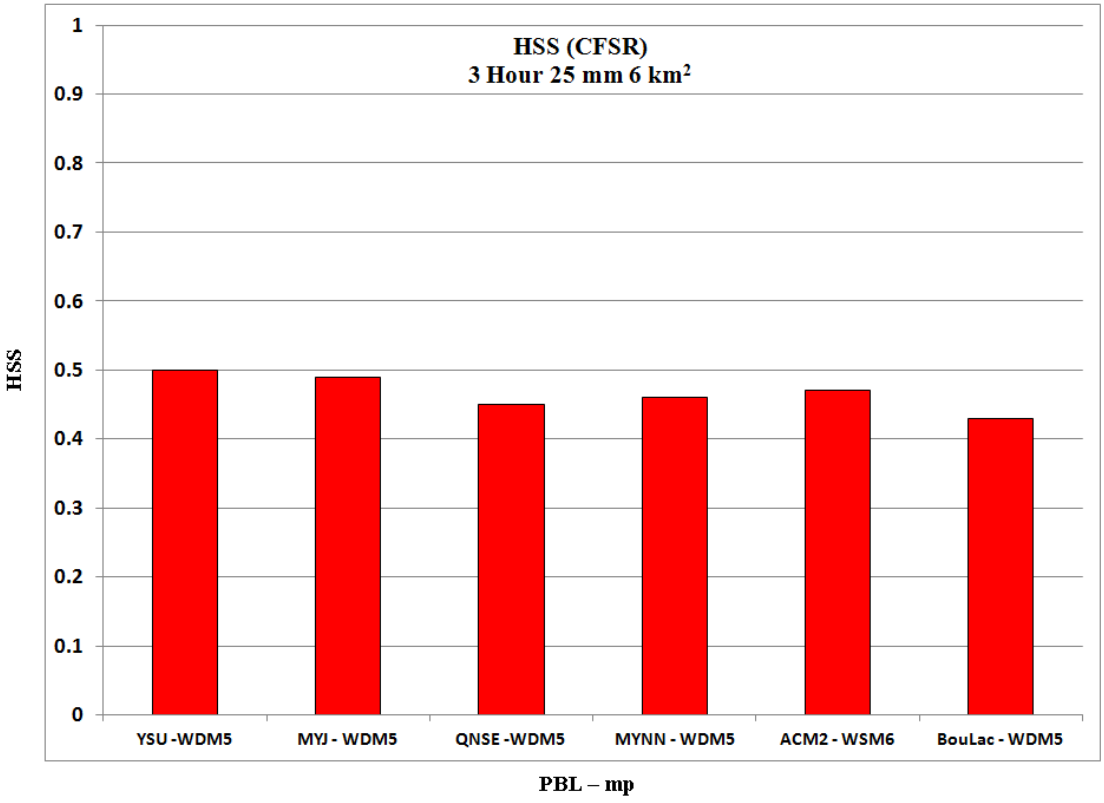

Figure 15: Maximum 3 Hr 25 mm 6 km^2 PBL - mp HSS

When determining which microphysical scheme best simulated three-hour 100 mm rainfall accumulation over an area approximately the size of a large U.S. city, the Lin microphysical scheme consistently scored highest across all PBLs, with the exception of the ACM2 where the WSM6 was favored. Even though there was gross over-forecasting early in the event and when the ACM2 - WDM6 combination scored highest, the ACM2 - Lin / WSM6 combinations consistently attained the highest bias scores from 2000 through 2400 UTC (Fig. 16). Although not usually within the maximum scoring category, this study proved that the Thompson and WDM6 microphysical schemes were also strong indicators of forecasting the occurrence of high rainfall of 100 mm within

three hours over a city-sized domain. The Thompson did well as it is a double moment 6 - class scheme that forecasts the existence of graupel particles. The WDM5 scored the highest CSI scores with a 31% first place occurrence while the Lin and Mil - Yau microphysical scheme combinations out-performed most of the other combinations the majority of the time (Fig. 17). Microphysical schemes that performed consistently better, or those that recorded the maximum HSS, were the WDM5 and the Mil - Yau microphysical schemes (Table 1) (Fig. 18). The favored PBL and microphysics "power" relationship was the MYNN - WDM5 whose scores ranked number one across the board. The ACM2 - Mil - Yau and the BouLac - WDM5 PBL - microphysical scheme combinations were strong second and third place performers, respectively (Fig. 17, 18).

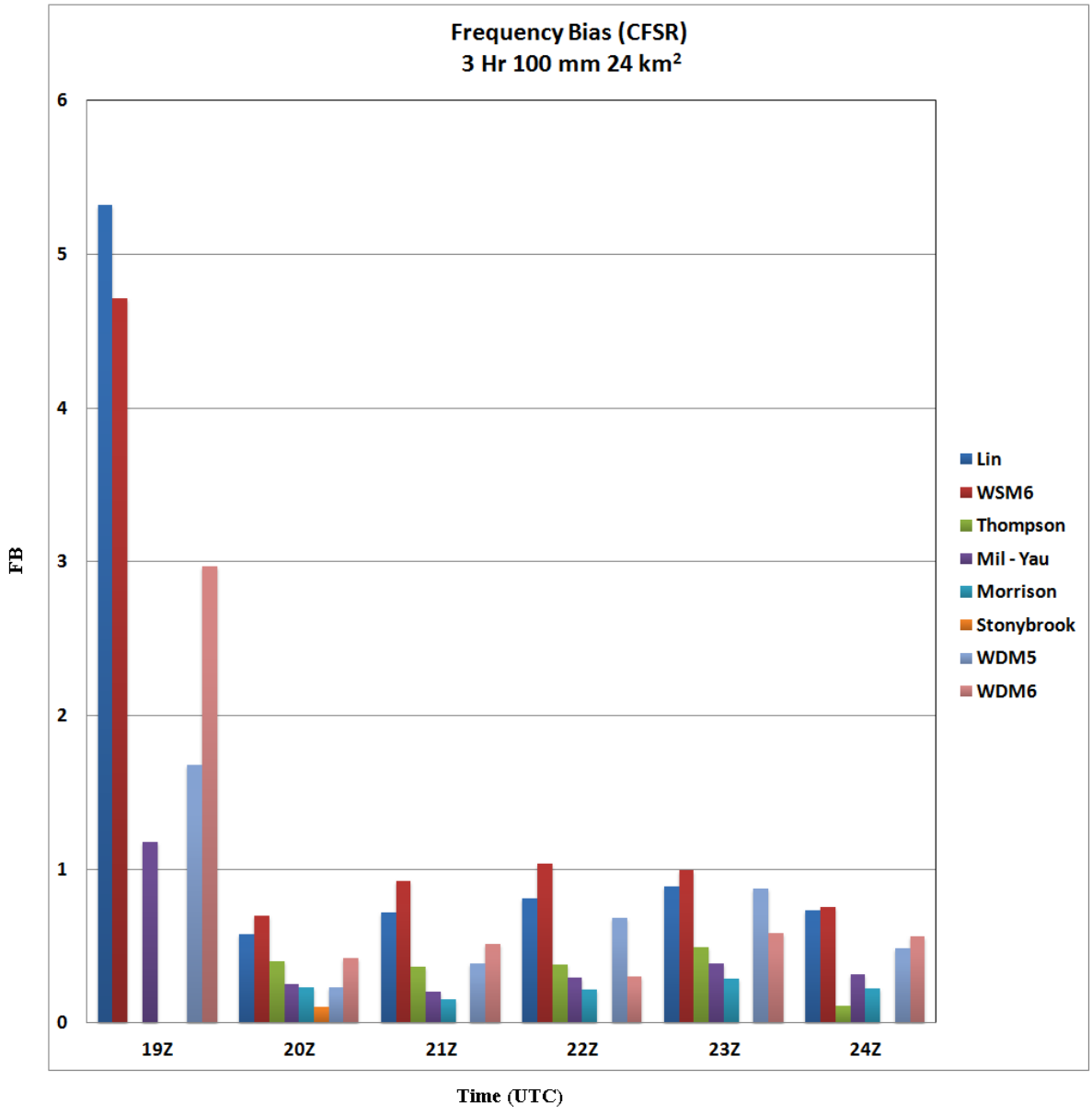

Figure 16: ACM2 PBL - mp FB

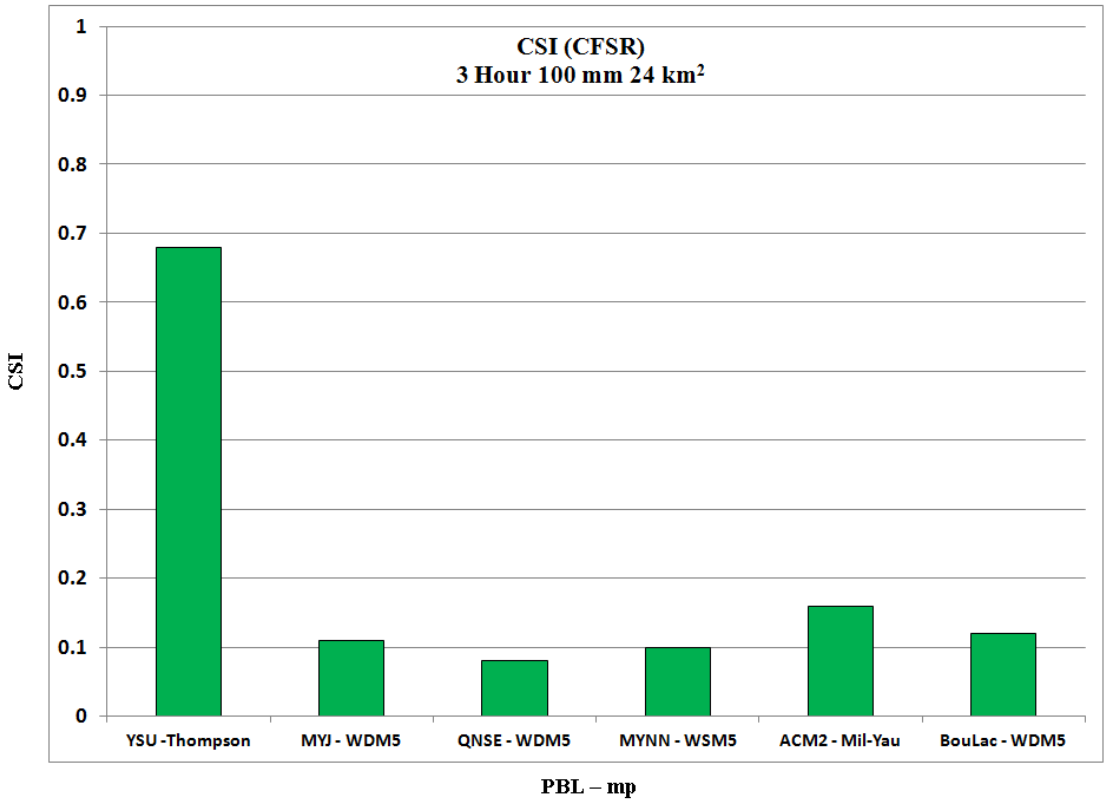

Figure 17: Maximum 3 Hr 100 mm 24 km^2 PBL - mp CSI scores

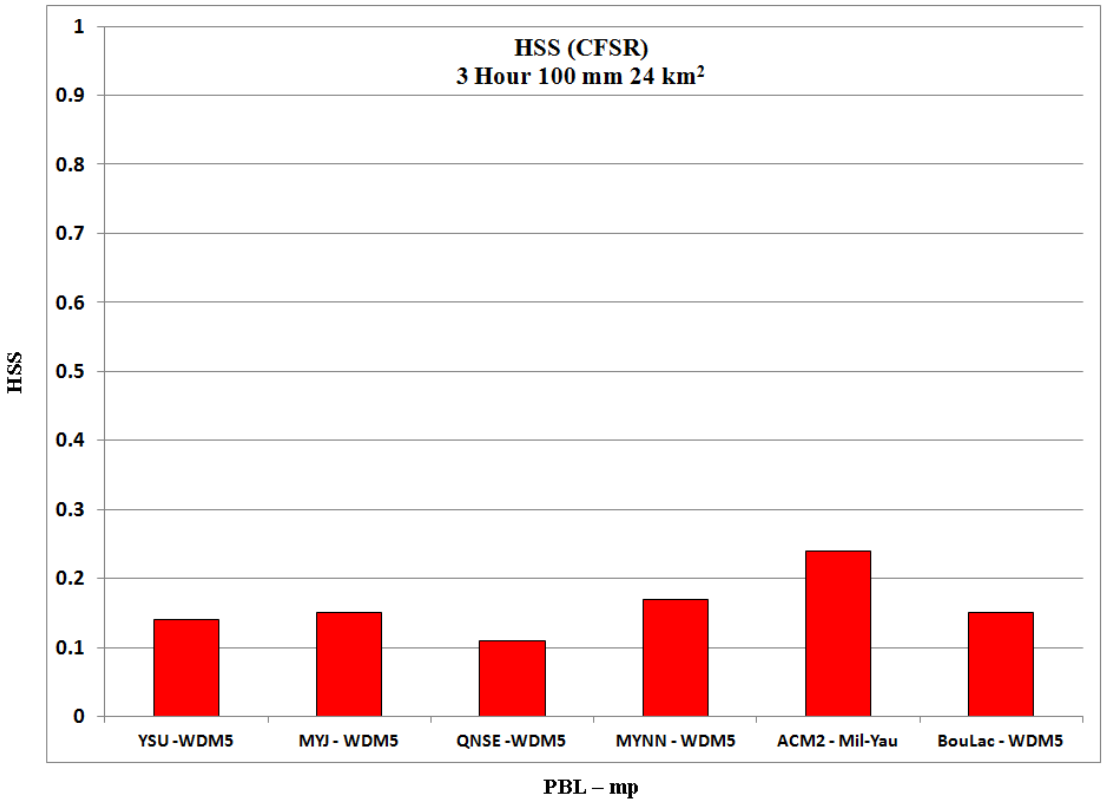

Figure 18: Maximum 3 Hr 100 mm 24 km^2 PBL - mp HSS

The Lin microphysical scheme was the best indicator, in relation to bias, of forecasting the occurrence of six-hour 100 mm over a city scale with a 56% top ranking occurrence across all PBL schemes (Fig. 19). The exceptions to this rule were the WSM6 or Morrison microphysical schemes that were both linked the ACM2 PBL. In terms of bias, the Thompson and WDM6 microphysical schemes were generally strong. The best early-in-time (i.e., 1900 – 2100 UTC) performer was the Thompson microphysical scheme. The Lin microphysical scheme was the better late period (2200 – 2400 UTC) performer. The overall better accuracy scores were typically associated with the Thompson or the WDM5 microphysical schemes with a 25% number one ranking occurrence (Fig. 20).

The Lin or Mil - Yau microphysical schemes scored the maximum CSI scores (Fig. 21). Early period strength belonged to the Thompson microphysics with late period maximum scoring favoring the Lin microphysics scheme. The WDM5 microphysics ranked the highest within the HSS with a 25% first place occurrence but, overall, the ACM2 - Mil-Yau relationship dominated the category in relation to top three (re)occurrences. There was ample variance amongst PBL - microphysical combinations with relation to the highest HSS, but the Lin and the Mil - Yau microphysics favored the more advanced PBL schemes (Fig 22). The maximum PBL - microphysical combination accuracy scores were in good correlation with those better PBL - microphysical combination performers over time and space. The BouLac - WDM5 and MYNN - Mil - Yau combinations were evidence to this fact (Table 1). The PBL- microphysical relationships that most frequently achieved the maximum accuracy scores, across all possible 48 PBL - microphysical combinations, were the ACM2 - Mil - Yau and the MYNN - WDM5 relationships. An example of the highest accuracy score(s) not necessarily correlating with the overall better performer(s) is shown within the QNSE PBL (Fig 20). The Thompson microphysics performed better over time while the Lin microphysics achieved the maximum HSS, 0.471, at 2000 UTC.

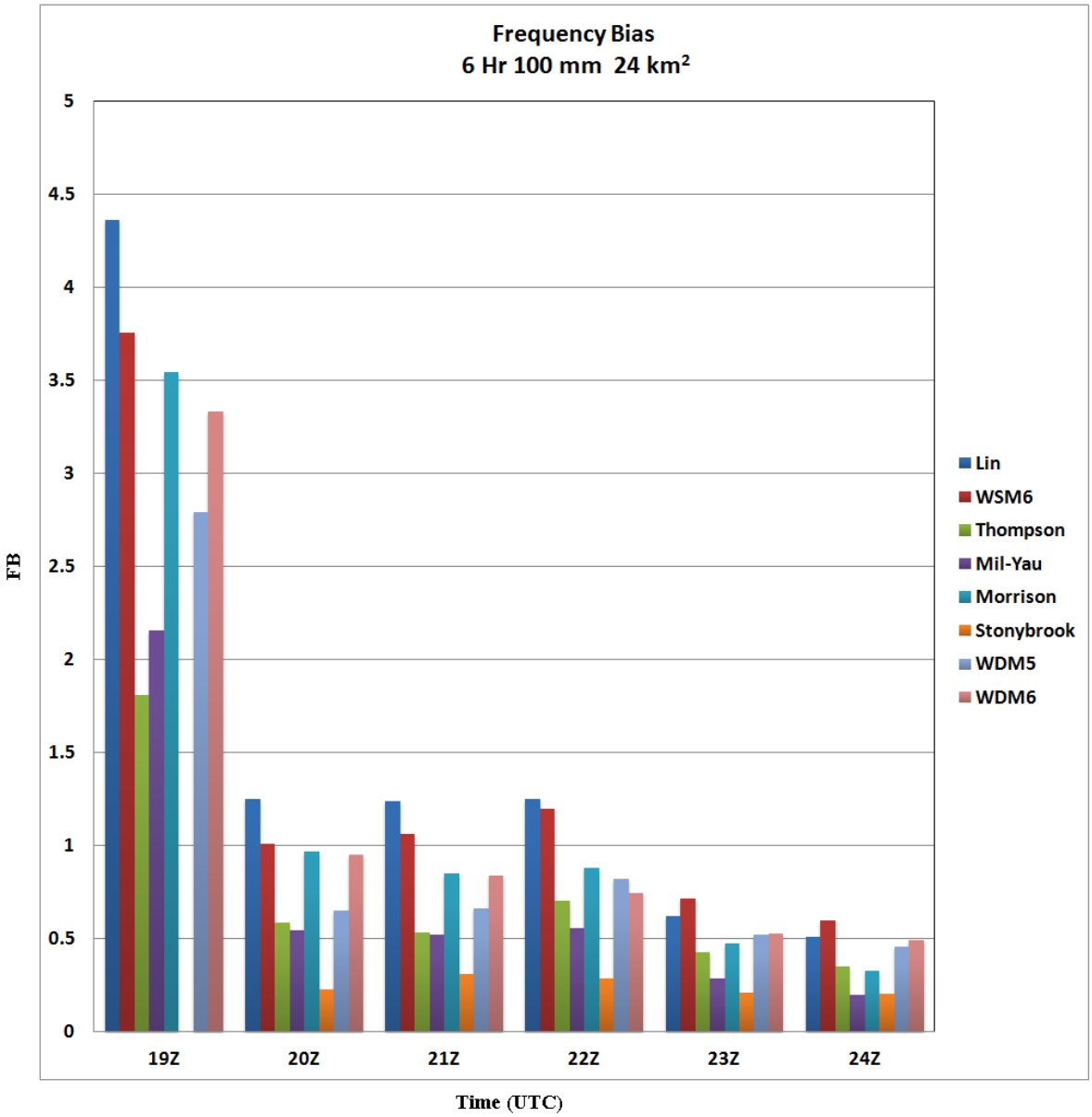

Figure 19: YSU PBL - mp FB

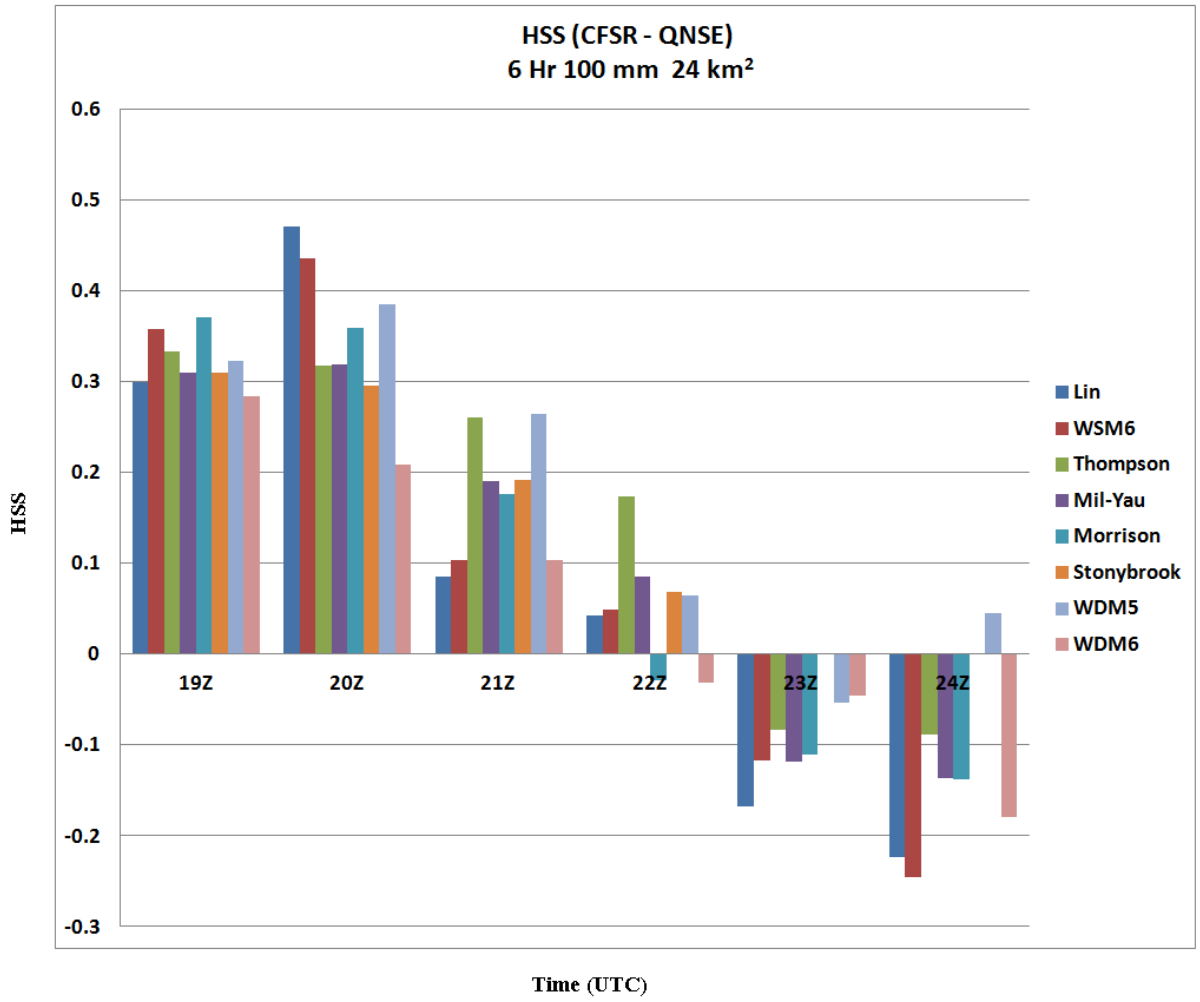

Figure 20: QNSE PBL - mp HSS

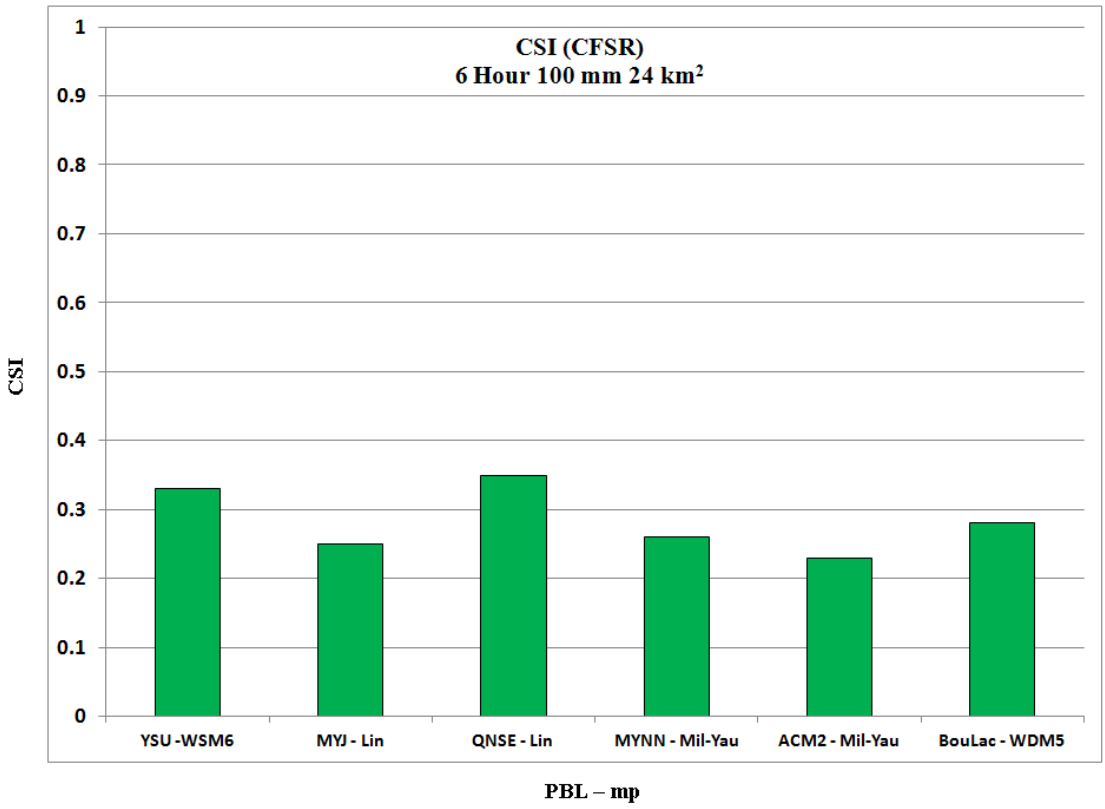

Figure 21: Maximum 6 Hr 100 mm 24 km^2 PBL - mp CSI scores

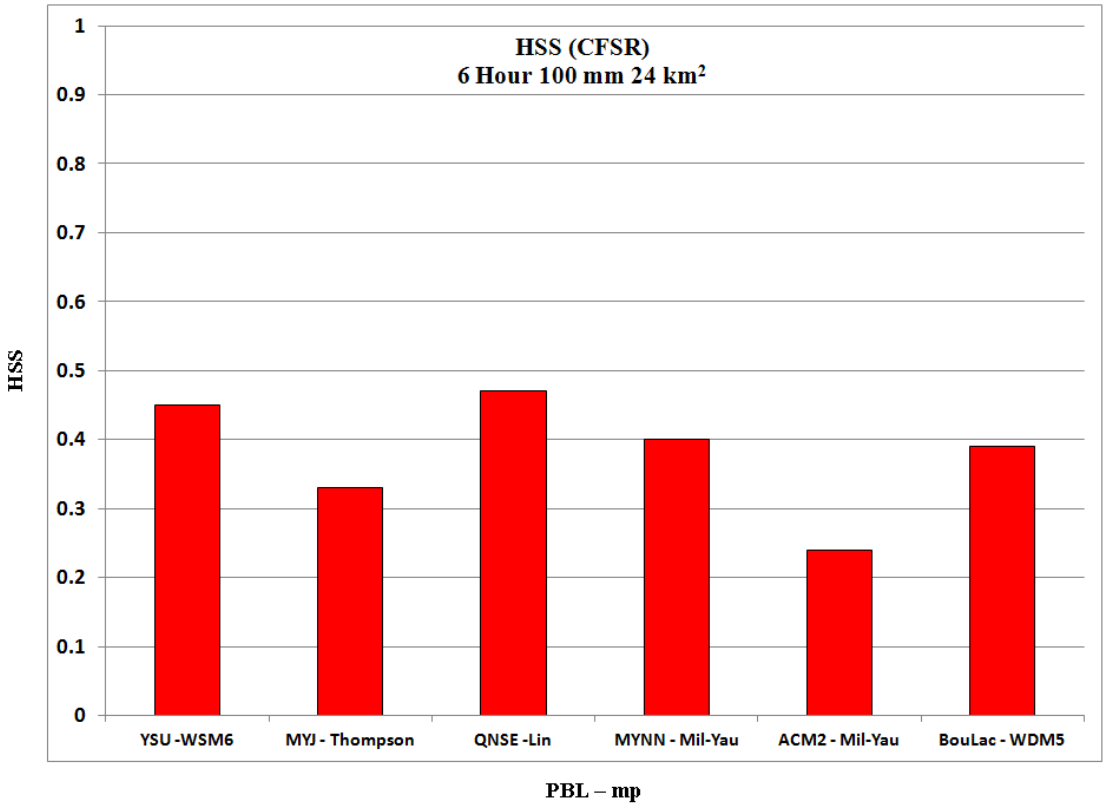

Figure 22: Maximum 6 Hr 100 mm 24 km^2 PBL - mp HSS

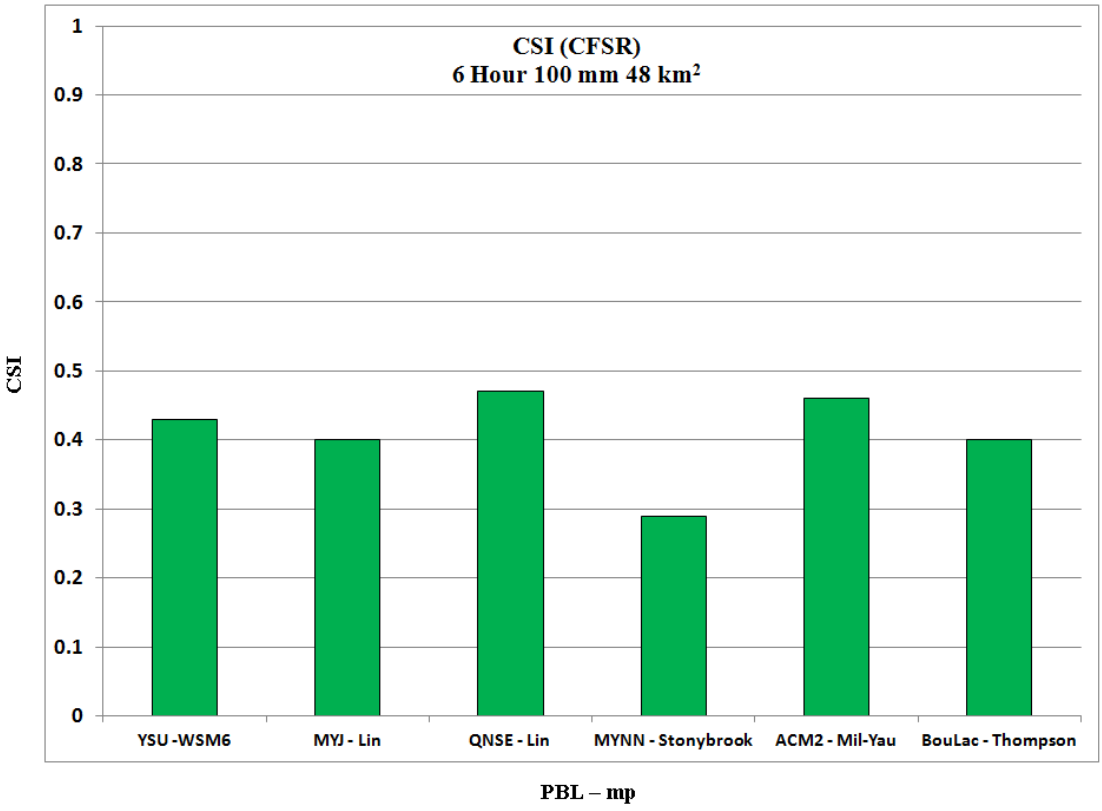

Figure 23: Maximum 6 Hr 100mm 48 km^2 PBL - mp CSI scores

The parameterized verification domain category of six-hour 100 mm rain accumulation over 48 km^2, or a geographic county scale, displayed better bias with the Lin microphysical scheme (i.e., 47% highest score occurrence). Strong performers were the WRF's 6 - class microphysical schemes; the WDM6 and WSM6. The Lin microphysics scheme consistently performed the best through the entire 6 hour period between 1800 - 2400 UTC. CSI best microphysical scheme performers were the Lin (i.e., 25% number one occurrence across all PBLs), with the WDM5 and Thompson schemes a near second (i.e., both 22% number one occurrences across all PBLs). There was correlation between the better microphysical performers and maximum CSI scoring; particularly with the Lin

scheme (Fig. 23). Early period notable performers were the Lin and Thompson schemes with the late period favoring the WDM5 microphysical scheme. Within the HSS statistics, the WDM5 microphysical scheme displayed a number one occurrence 26% of the time with the Mil - Yau and Thompson microphysical schemes following up second (i.e., 20%) and third (i.e., 14%), respectively. The best early period HSS performers were the Mil - Yau and Thompson microphysical schemes with the WDM5 scheme being the best late period performer. The best microphysical scheme correlation between the top performers and the maximum accuracy (i.e., skill) scores were the Lin and WDM6 microphysical schemes and the Mil - Yau and Thompson microphysical schemes (Fig. 23, 24). In doubling the areal coverage, overall six-hour 100 mm rainfall accumulation skill was much improved with 86% of the PBL - microphysical schemes displaying skill (i.e., positive HSS statistics). The favored PBL - microphysical relationship best performers were the MYJ - Lin (e.g., 75% number one occurrence) with a second-place tie occurring with the ACM2 - Mil-Yau and MYNN - WDM5 combination schemes (e.g., 50% number one occurrence). The ACM2 - Mil-Yau and the BouLac - WDM5 PBL - microphysical scheme combinations achieved the maximum accuracy scores (Table 1).

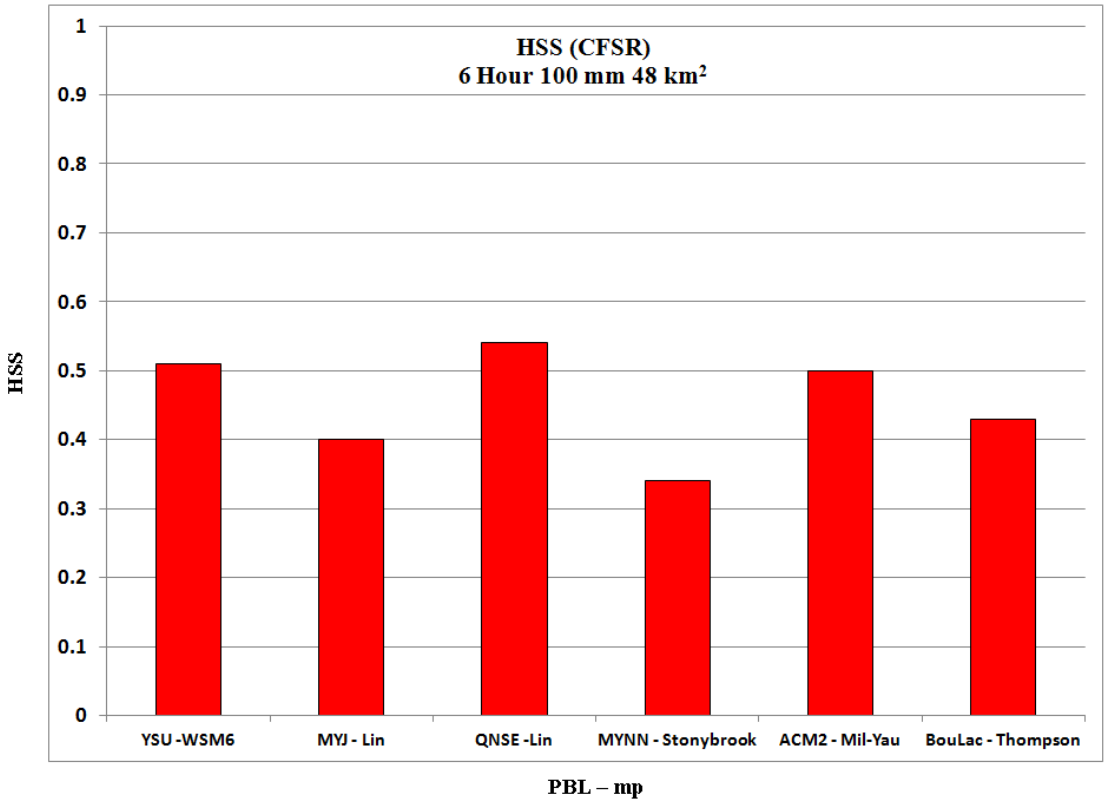

Figure 24: Maximum 6 Hr 100mm 48 km^2 PBL - mp HSS

Within the CFSR dataset, the best overall skill pattern (i.e., best performers) amongst the eight microphysical schemes was the WDM5, followed by the Thompson and the Lin. The reasoning for this success was that the WDM5 and Thompson microphysical schemes employed double moments while the Lin and Thompson forecasted the existence of graupel.

The better PBL - microphysical combination performers, across the five temporal/quantitative rainfall accumulation/spatial parameterized verification domain categories, were the ACM2 - Mil - Yau with a 67.2% number one ranking occurrence

rate. It should be noted that the ACM2 - Mil - Yau relationship also displayed the highest occurrence of obtaining a top three score ranking within all five of the verification domain categories. The MYNN - WDM 5 combination came in with a mean number one ranking 69.3% of the time while having a 60% occurrence top three placement rate. Although the BouLac - WDM5 PBL - microphysical combination ranked within the top three overall rankings 40% of the time, its average number one placement rankings were the highest; a 81.5 % occurrence rate.

11.2 **European Re-Analysis (ERA - Interim) initialization**

The ERA - Interim re-analysis data set was used to initialize a third of the WRF - EMS output data. One interesting observation was that this dataset differed in how it handled bias (i.e., FB). Typically, during the first hour of 1800 - 1900 UTC, there was gross over-forecasting across all five temporal/quantitative/spatial parameterized verification domain categories followed by an under-forecasting trend through the remainder of the six-hour period (Fig. 25). Overall skill was lacking with negative HSS statistics recorded for the majority of the PBL - microphysical scheme combinations. A climate-based, or pure chance forecast, would prove to be just as accurate as many of these ERA-Interim - initialized WRF - EMS output data. In a relative sense, there were various PBLs or microphysical schemes that performed better than others amongst the five parameterized verification domain categories.

ERA - Interim											
		1 hr / 50 mm / 24 km^2		3 hr / 25 mm / 6 km^2		3 hr / 100 mm / 24 km^2		6 hr / 100 mm / 24 km^2		6 hr / 100 mm /48 km^2	
PBL	mp	CSI	HSS	CSI	HSS	CSI	HSS	CSI	HSS	CSI	HSS
ACM2	Lin	**0.094**	**0.069**	0.294	**0.295**	**0.201**	**0.268**	**0.194**	**0.152**	**0.369**	0.209
	WDM5	0.000	-0.043	0.188	0.159	0.000	-0.017	0.026	-0.043	0.146	0.016
	WDM6	0.058	-0.006	**0.313**	0.272	0.044	-0.008	0.163	0.137	0.313	**0.236**
Bou - Lac	Lin	**0.089**	**0.052**	0.360	0.340	**0.052**	**0.010**	0.077	-0.045	0.242	0.083
	WDM5	0.033	-0.009	0.298	0.286	0.000	-0.019	0.035	0.011	0.167	**0.187**
	WDM6	0.054	0.000	**0.385**	**0.399**	0.000	-0.018	**0.080**	**0.014**	**0.265**	0.180
MYNN	Lin	**0.231**	**0.297**	0.388	0.375	**0.194**	**0.257**	**0.239**	**0.271**	**0.433**	**0.445**
	WDM5	0.070	0.057	0.296	0.261	0.000	0.000	0.017	-0.043	0.138	0.055
	WDM6	0.182	0.229	**0.393**	**0.391**	0.108	0.126	0.150	0.136	0.332	0.322

Table 2: Maximum accuracy scores over the five verification domains (ERA - Interim)

The parameterized hourly 50 mm rain accumulation over a geographic city scale verification domain category's bias exhibited extreme over-forecasting within the first hour, then a subsequent hourly decline in the various scheme combinations' ability to accurately gauge the forecast occurrence of the temporal/quantitative rainfall accumulation/spatial thresholds (i.e., large variance about 1) (Fig. 25). Typically, the WDM5 microphysical scheme performed the best, or recorded scores nearest to 1, in time. Within FB, the best microphysical performer was the Thompson microphysical scheme across all PBLs (i.e., 22% number one ranking occurrence). Two strong microphysical scheme performers were the WDM5 and WDM6 schemes. The Thompson, WDM5 and WDM6 microphysical schemes made the top three score rankings for all PBL - microphysical combinations in the latter half of the period (i.e., 2200 – 2400 UTC); 17 out of the total 18 ranking matrices. This success can be attributed to all three of these schemes employing double moment mathematics that include rain droplet concentration number. Within the first four hours, the Mil - Yau microphysical scheme repeatedly ranked within various PBL's top three rankings; a relatively high 14% top

three occurrence rate. Skill was very low, or non-existent, as nearly all of CSI scores were between 0 and 0.1. The best microphysical scheme performer was the Lin scheme where it ranked number one 69% of the time across all PBLs. The WSM6 was another scheme that registered relatively higher CSI scores, albeit low, with a 17% occurrence within the top three rankings. There were many fails in the first (1800 - 1900 UTC) and last (2300 - 2400 UTC) periods with only three out of 36 possibles, all Lin microphysical schemes, registering an actual (non-zero) score during the last 2300 - 2400 UTC hour. All HSS values were negative for every scheme during every hour except between 2100 - 2200 UTC. Any low positive values were produced either by the Lin or WDM6 microphysical schemes. The relatively highest scoring PBL - microphysical combination schemes were MYNN - Lin and the YSU - Lin combinations (Fig. 26). The favored PBL - microphysical scheme combination that ranked number one in FB and CSI scoring was the MYNN - Lin (i.e., 56% occurrence) with the ACM2 - Mil-Yau and MYNN or BouLac - Thompson microphysical scheme relationships displaying the highest top ranking occurrences. The maximum accuracy scores aligned with the ACM2 and the MYNN PBLs in association with the Lin microphysical scheme (Table 2). Higher-order PBL schemes, in association with the Lin microphysics, statistically performed better over time and produced the highest statistical scores. This success can be attributed to the Lin being a 6-Class microphysical scheme that can prognosticate the development and existence of graupel within cumulonimbus clouds.

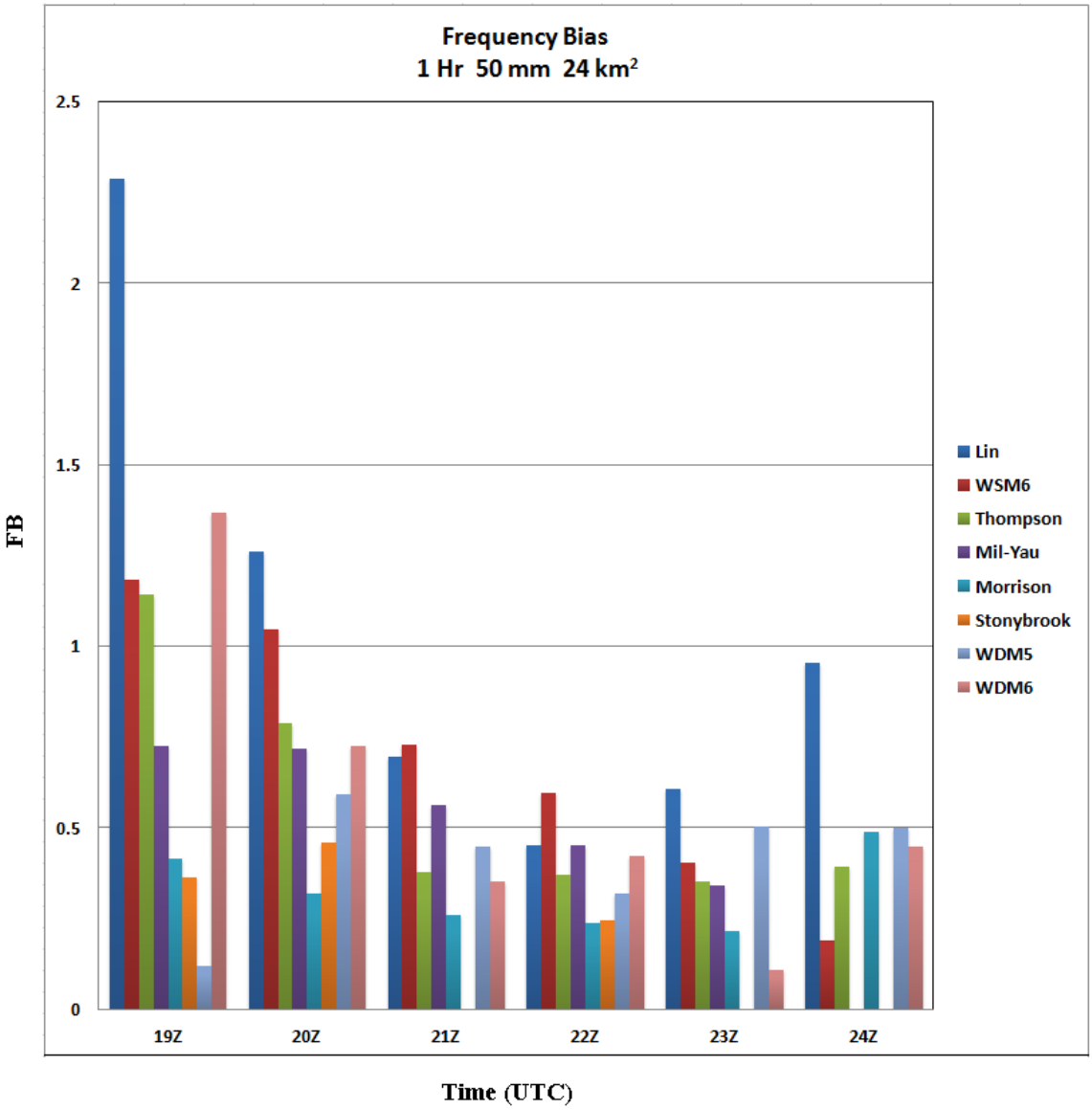

Figure 25: QNSE PBL - mp FB

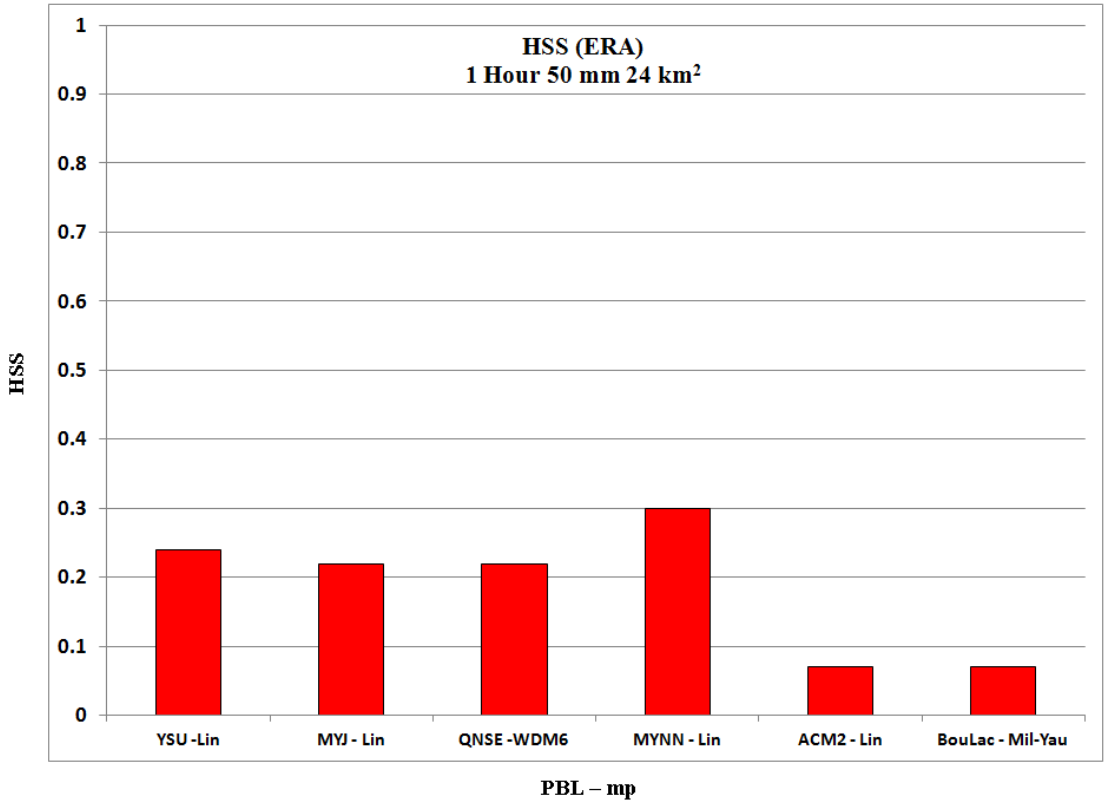

Figure 26: Maximum 1 Hr 50 mm 24 km^2 PBL - mp HSS

The parameterized three-hour 25 mm town/suburb scale verification domain category was unique in that it was the only category that actually depicted better bias statistics with time (Fig. 27, 28). The advanced 2.5 closure MYNN PBL scheme's microphysics bias improved through the first half of the period (Fig. 28). The top rated Thompson scheme (i.e., 28% number one occurrence rate) improved with time across all PBL schemes. Of note, the WSM6 microphysical scheme recorded a perfect bias score at 2000 UTC within both the MYNN and ACM2 PBL schemes (Fig. 27, 28). Another perfect bias score was registered by the MYNN - Morrison PBL - microphysical scheme combination at 2100 UTC (Fig. 28). CSI scoring was dominated by the four microphysical schemes of

the WDM6, WSM6, Lin, and the Morrison. The WDM6 scheme recorded a number one ranking 64% of the time while the WSM6 performed strong with a number one occurrence of 19%. The WDM6 was ranked number one 67% of the time and, during 2200 UTC, ranked number one across every PBL scheme. The WSM6 and Lin microphysics were again top bias and skill performers (Fig. 27 - 29). The favored top ranking PBL and microphysical relationships within the CSI and HSS statistical categories were the WDM6 across four PBLs; the YSU, MYJ, MYNN, and the BouLac (Fig. 29). The MYNN / ACM2 - Lin and the BouLac - WSM6 PBL - microphysical scheme relationships ranked number one 50% of the time. The reoccurrence of these regularly higher scoring combinations is in correlation with more advanced PBL schemes being in association with more complex microphysical schemes.

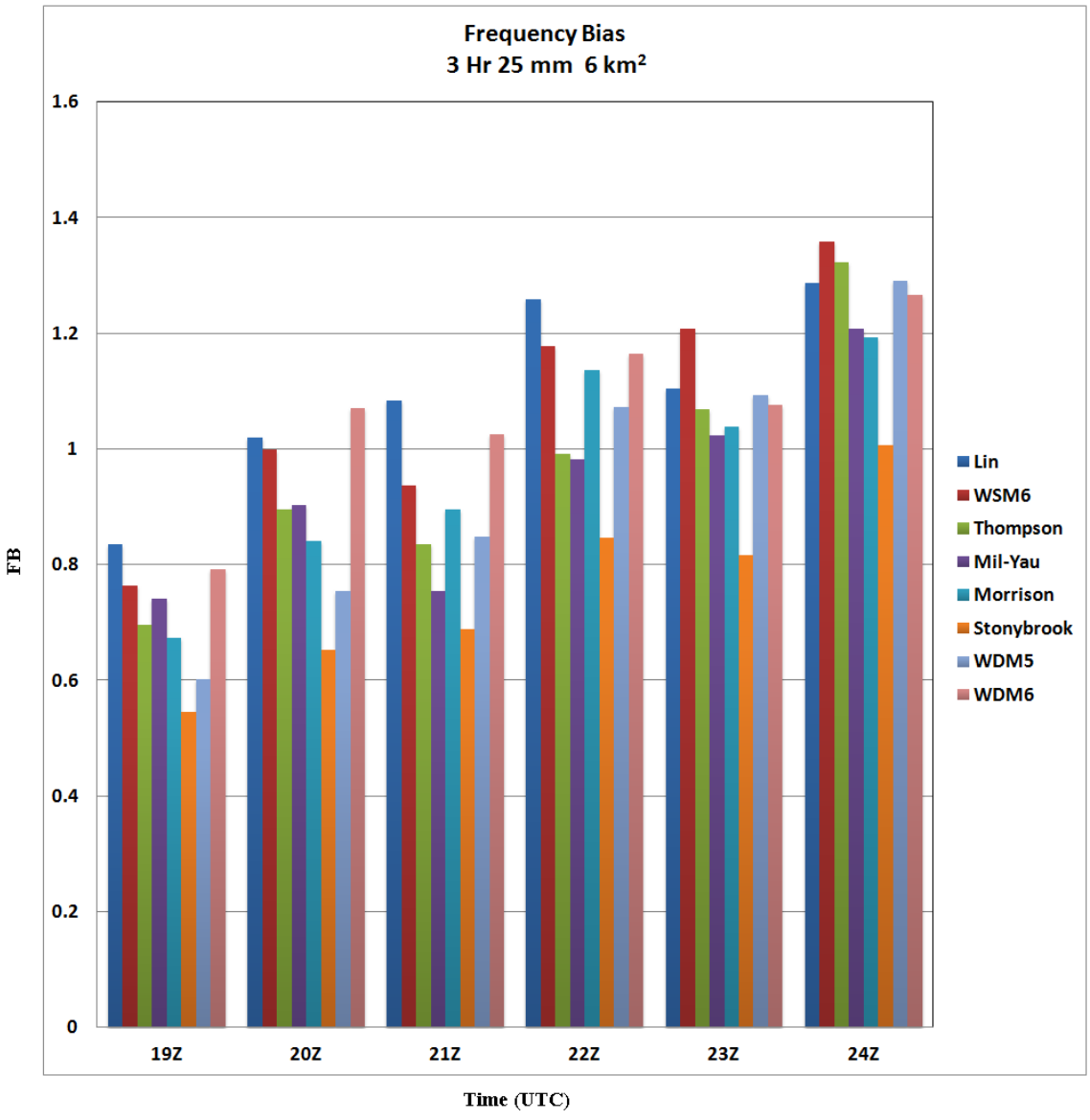

Figure 27: ACM2 PBL - mp FB

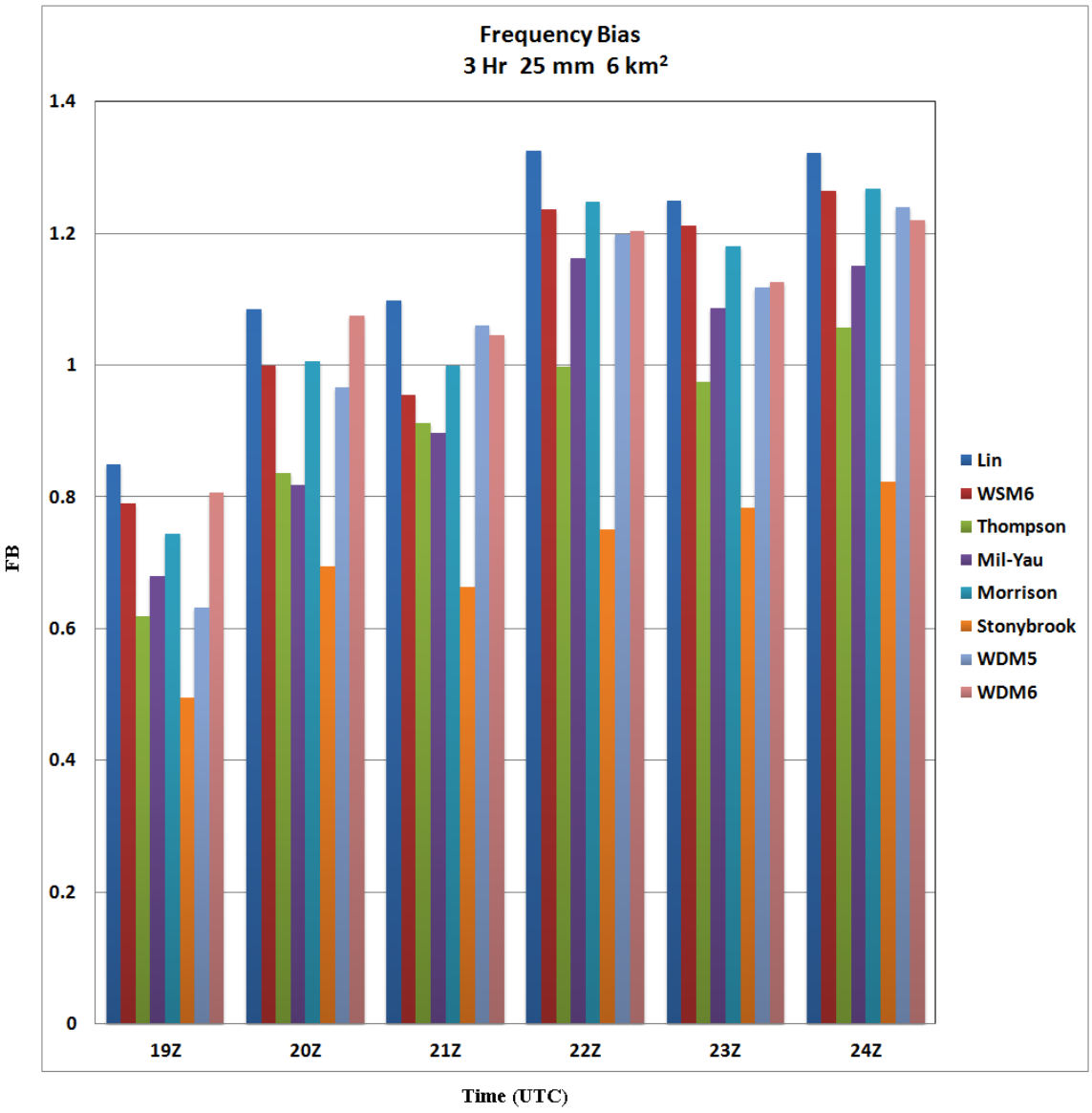

Figure 28: MYNN PBL - mp FB

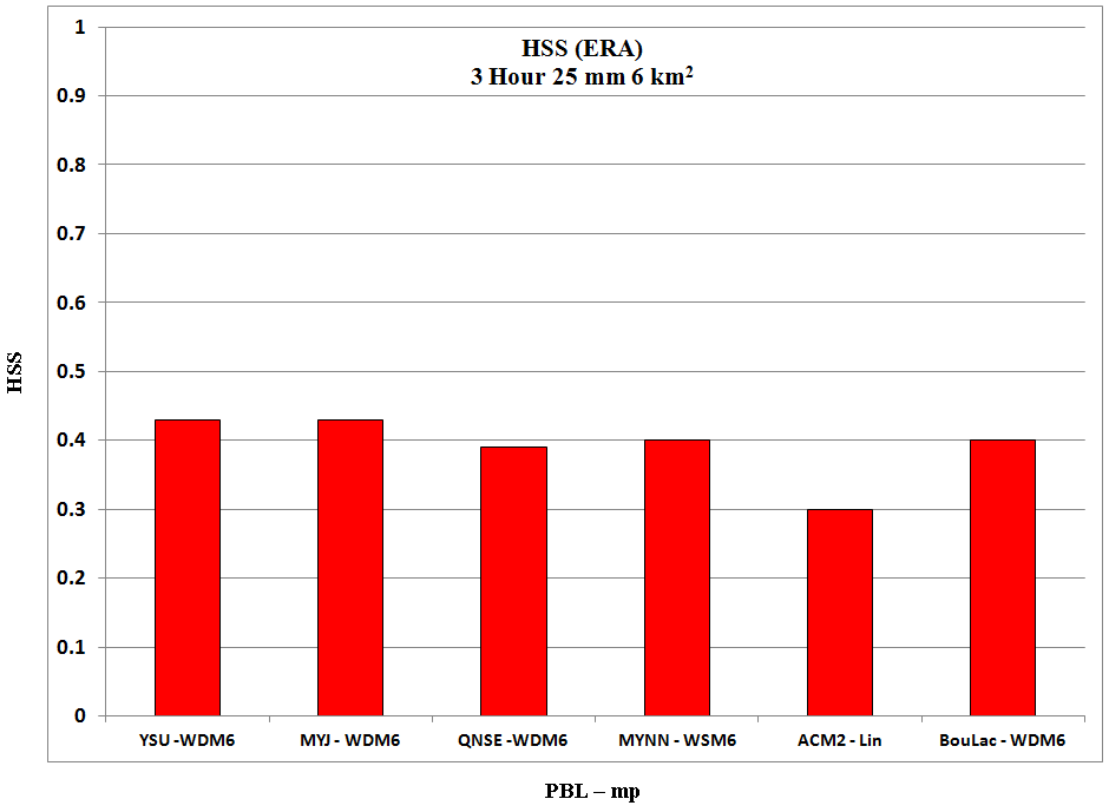

Figure 29: Maximum 3 Hr 25 mm 6 km^2 PBL - mp HSS

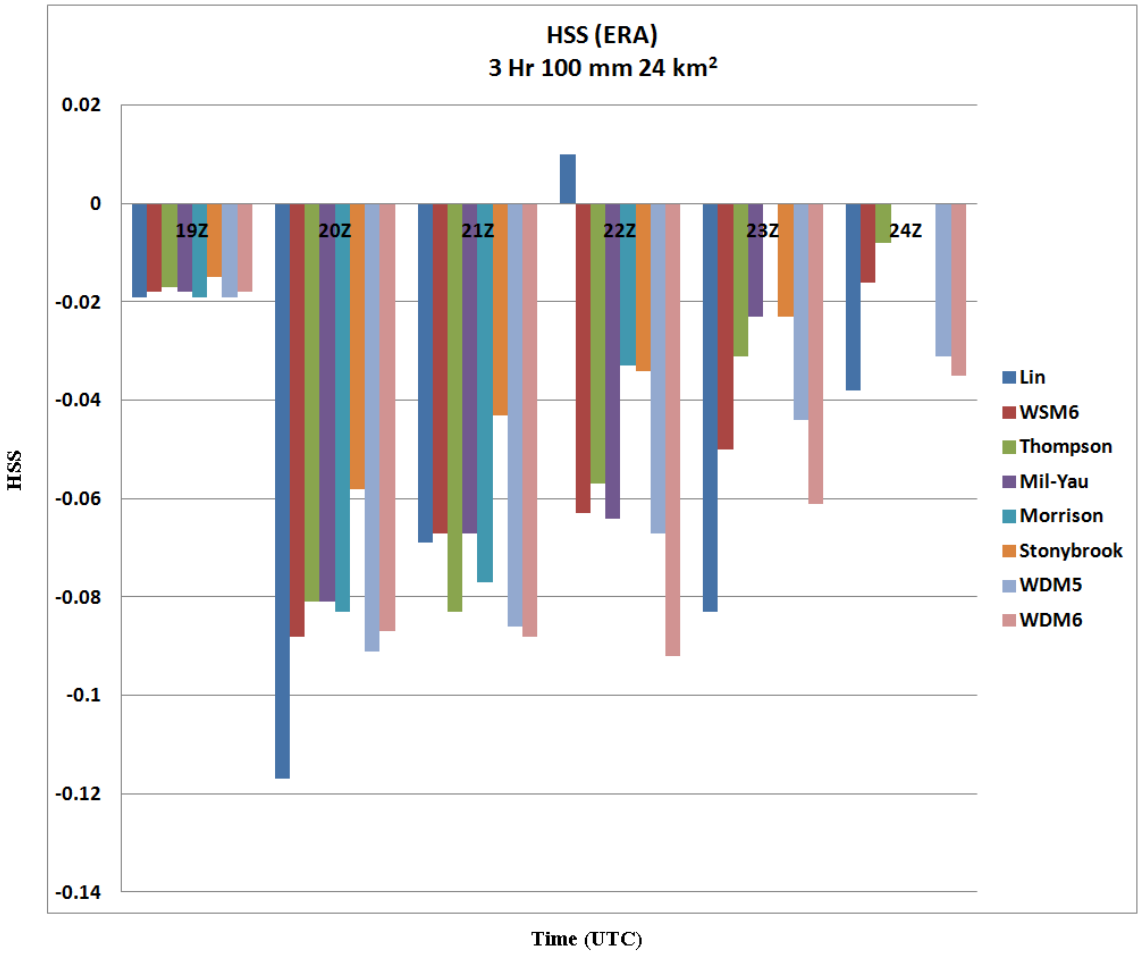

Figure 30: BouLac PBL - mp HSS

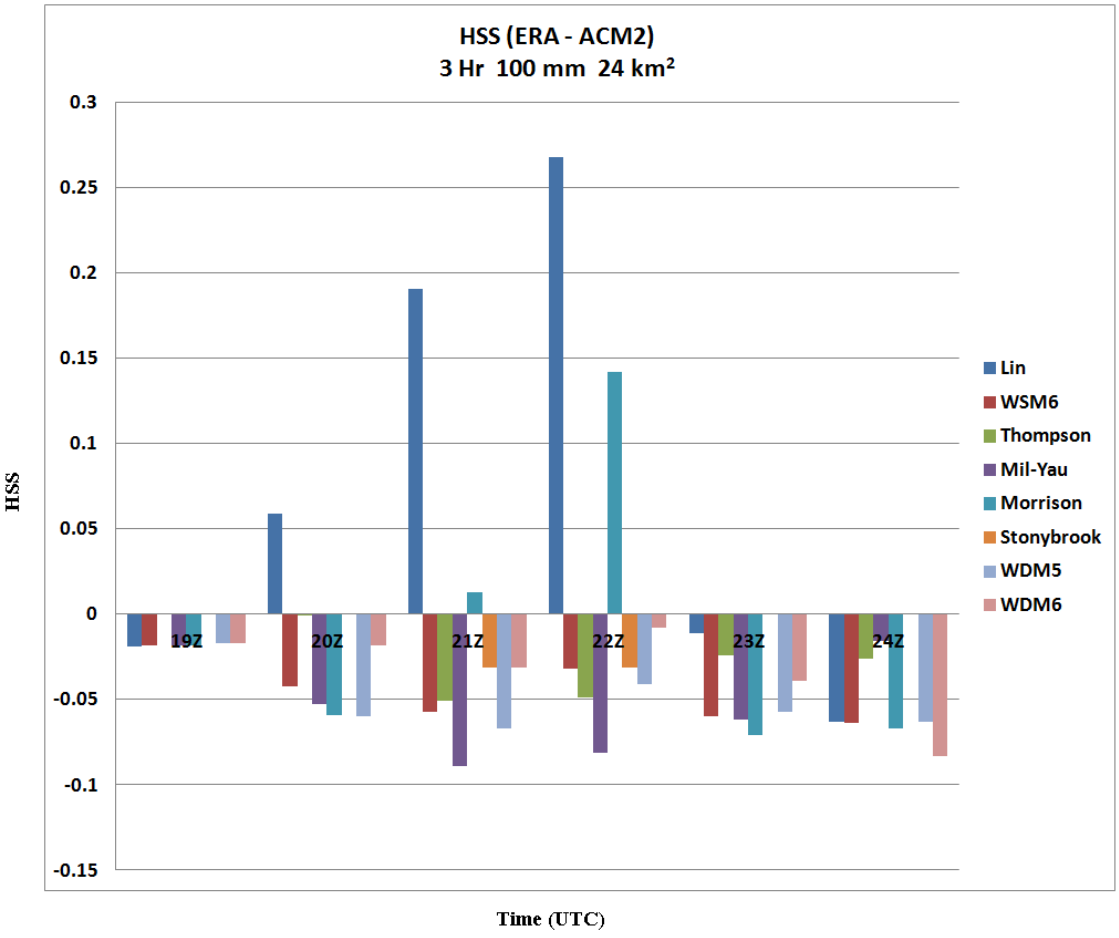

Figure 31: ACM2 PBL - mp HSS

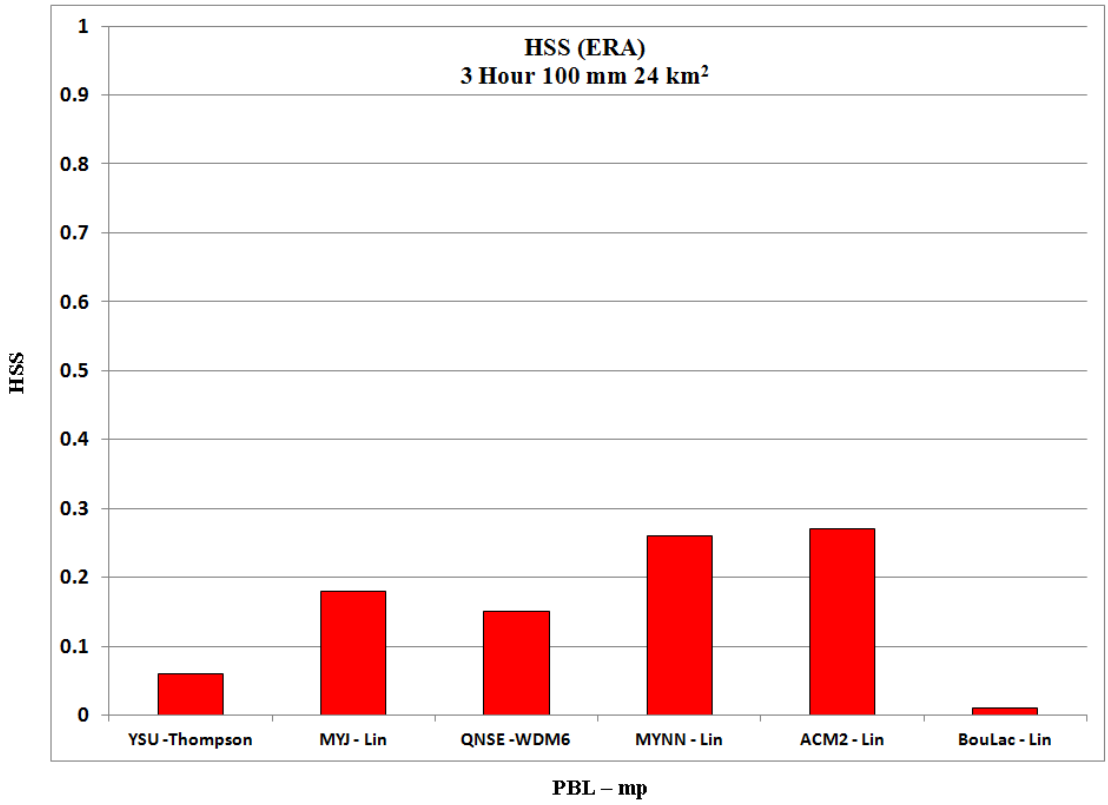

Figure 32: Maximum 3 Hr 100 mm 24 km^2 PBL - mp HSS

The three-hour 100 mm rain accumulation over the 24 km^2 (i.e., city scale) domain's more accurate bias scores favored the Lin microphysical scheme; registering top rankings with a 36% occurrence. The WDM6 microphysical scheme was a strong scheme with a 17% number one occurrence rate. The first 1800 - 1900 UTC hour was significantly over-forecast while the last hour was severely under-forecast. It should be noted that the ACM2 - WDM6 PBL - microphysical scheme combination scored a near-perfect 0.999 score at 2200 UTC. The CSI showed no skill with not a single PBL - microphysical scheme combination registered a score (i.e., 0) during the first hour of 1800 - 1900 UTC. An example of this was the one positive BouLac - Lin PBL - microphysical scheme score

within the 2100 - 2200 UTC hour (Fig. 30). When there were non-zero scores, the Lin microphysical scheme ranked the highest 83% of the time with the second highest-skilled scheme being the WDM6 at a 19% number one occurrence. HSSs were very poor with the majority of these scores being negative (Fig. 30, 31). The relatively best microphysical schemes, or those schemes that recorded the maximum accuracy values, were the Lin and WDM6 schemes across most PBLs (Fig. 32).

The 6-hour 100 mm 24 km^2 domain skill scores were very low with no dominant scheme noted within the bias statistics. The relatively best microphysical scheme was the Lin with the WSM6 and WDM6 being notable performers. The Lin microphysical scheme dominated the CSI category by ranking number one with a 72% occurrence rate. The Lin microphysical scheme scored highest across every PBL between 2000 and 2100 UTC. Early in the period, the Mil - Yau microphysical scheme performed admirably while, latter in the period, the WDM6 and WSM6 microphysical schemes consistently achieved top rankings. The HSS values were very low and were all negative between 2000 - 2100 UTC. The favored number one ranked (i.e., maximum score producing) PBL - microphysical scheme relationships belonged to either the Lin or the WDM6 microphysical schemes across numerous PBLs (Fig. 33).

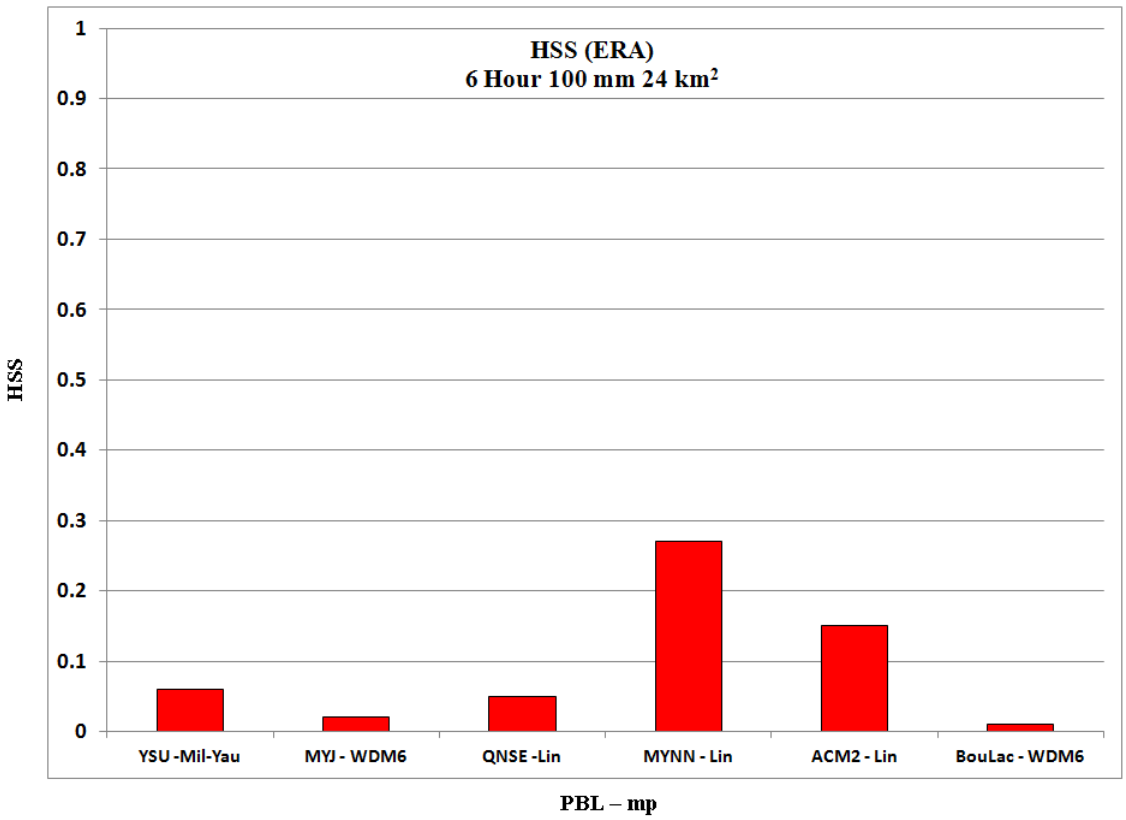

Figure 33: Maximum 6 Hr 100 mm 24 km^2 PBL - mp HSS

The Lin microphysical scheme displayed the most accurate bias within the 6-hour 100 mm 48 km^2 domain; a 25% occurrence of a maximum score. The WDM6, WSM6, and the Lin microphysics were again consistent top ranking schemes. A near perfect bias score of 0.999 was recorded by the MYJ - WDM5 PBL - microphysical scheme relationship between 2200 - 2300 UTC. The Lin microphysical scheme ranked number one over 50% of the model runs. The WRF microphysical schemes of the WSM6, WDM5 and the WDM6 frequently ranked high early in the period. The WDM5/6 and Lin microphysical schemes consistently scored the maximum skill (Fig. 34, 35). The one

favored PBL - microphysical scheme combination, in relation to top ranking, was the Lin microphysical scheme across many PBLs (Fig. 35).

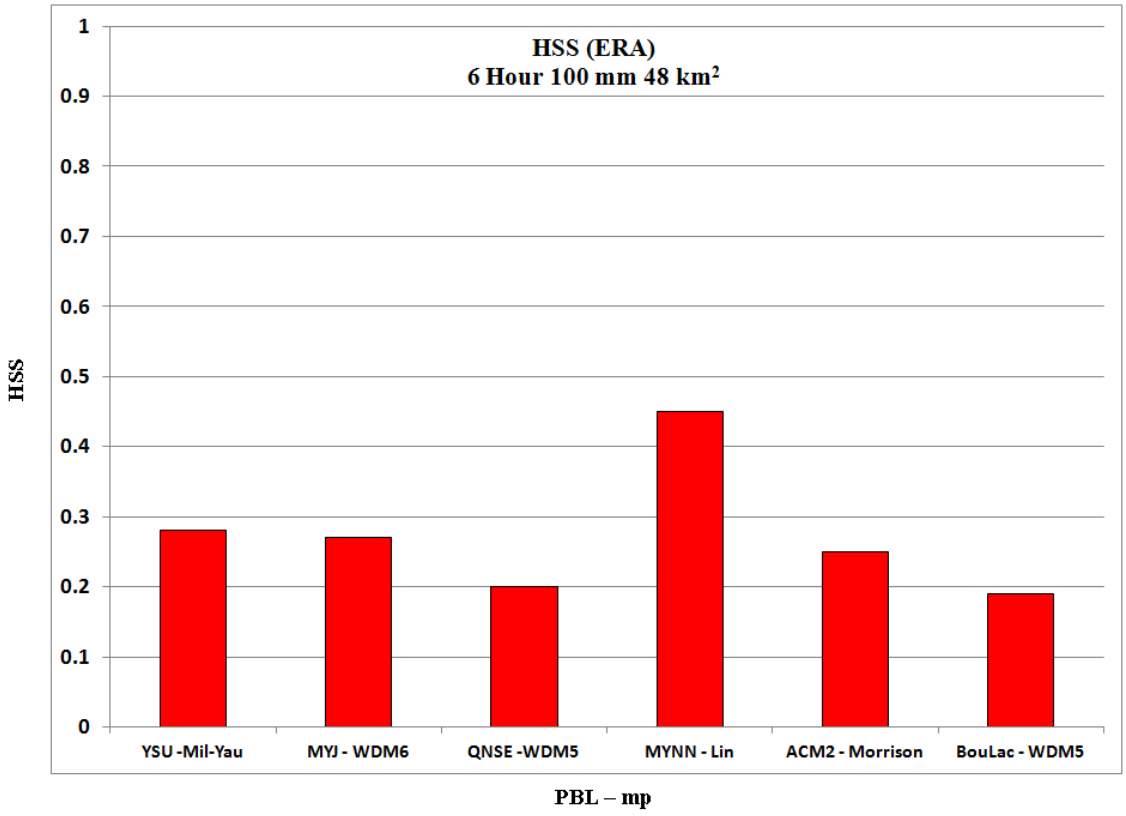

Figure 34: Maximum 6 Hr 100 mm 48 km^2 PBL - mp HSS

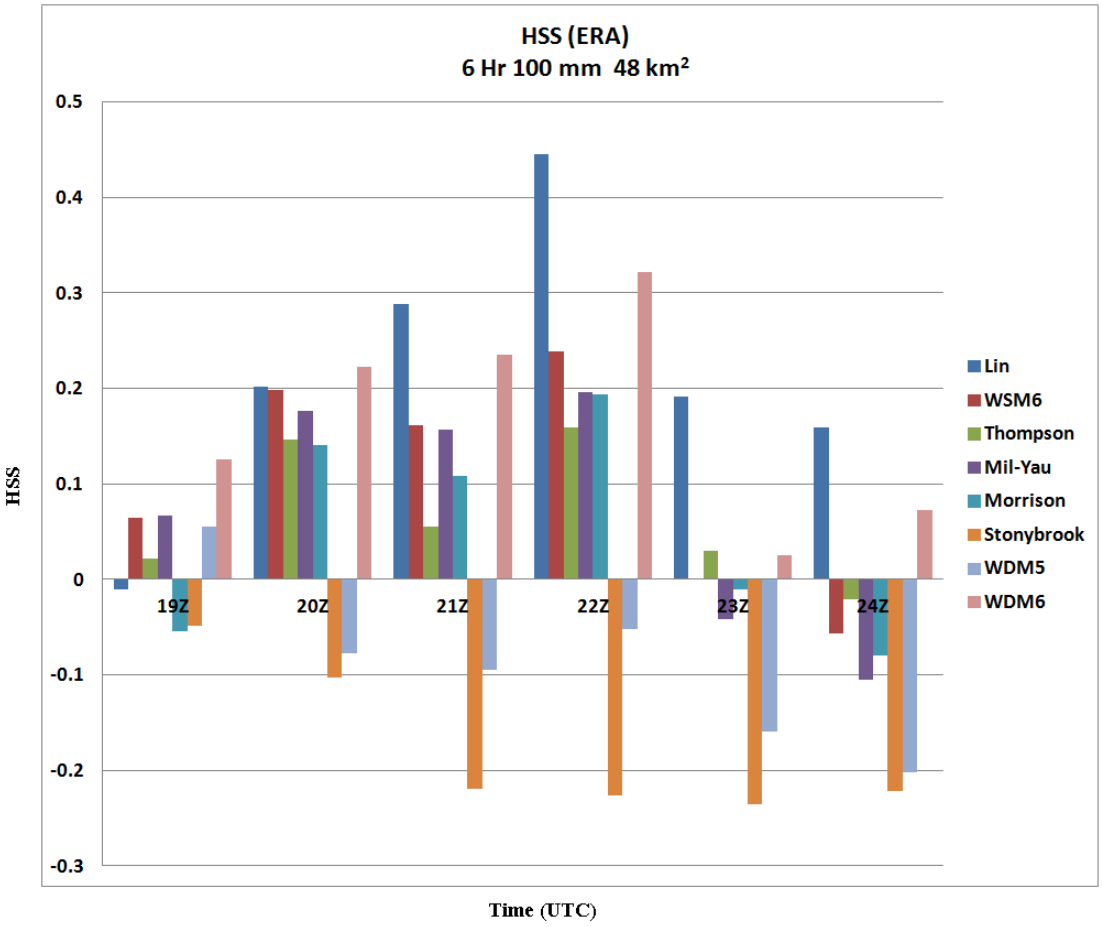

Figure 35: MYNN PBL - mp HSS

Amongst all parameterized verification domain categories, the best overall skill displayed by any microphysical scheme was the Lin, followed by the WDM6. Although the WDM6 scheme achieved the highest number of top three rankings at over 300, it only ranked number one 33% of the time. The Lin microphysical scheme was in the top three nearly 300 times, but boasted a maximum ranking score 61% of the time. The Lin and WDM6 microphysics are schemes that inherently include the existence of graupel. Prior research has indicated that accurately forecasting the existence of graupel within a cumulonimbus'

cloud rain-ice precipitation microphysical processes may improve NWP precipitation forecasts. Statistically, these two microphysical schemes frequently scored higher than the remainder of the six schemes used in this particular case study.

The overall best PBL - microphysical scheme combination performers (e.g., maximum CSI/HSS statistics), or those relationships that ranked number one with the highest frequency, were the MYNN - Lin at a 74% occurrence, the ACM2 - Lin with a 59% occurrence and the BouLac - Lin with a 37% occurrence. The research has shown that, when associating these more complex microphysical schemes with higher order PBL schemes, there is good correlation with maximum skill scores.

11.3 **12 km^2 North American Model (NAM12) initialization**

The third set of WRF - EMS output were initialized with the NAM at a 12 km^2 resolution, updated on three-hour cycles commencing on April 18th, 2009 at 0000 UTC through April 19th, 2009 at 0000 UTC. Of the three main initialization data sets, the NAM12 model initialization resulted in the poorest scores. The poor results were attributed to the fact that the NAM12 model did not initialize well while not having the benefit of subsequent meteorological parameter updates. Three-hour updates from 0300 UTC onward were initialized with the prior three-hour prognosis. Since the NAM12 did not initialize well on April, 18th at 0000 UTC, subsequent updates were only compounding initialization error downstream. Many hourly PBL - microphysical output within all rain rate/accumulation, temporal, and spatial domain categories resulted in very

low, or simply no, skill. In fact, when analyzing all the 4,320 WRF - EMS output PBL - microphysical combination files, the majority displayed little to no data. Thus, statistical thresholds were fixed as to what was deemed relative to a project that had two previous large reanalysis datasets. FB was set between 0.80 and 1.20, CSI greater than 0.20 and HSS greater than 0.15. FB results were scarce, but it was discovered that the scores that fell within the +/- 0.20 range around 1.0 typically occurred during the first 1800 – 1900 UTC hour or the within the last hour of 2300 - 2400 UTC. In perspective, out of the 4,320 possible bias candidates, only 27 met the +/- 0.20 range centered on 1.0, or 0.625 % of all runs. The majority of the frequency bias sets were significantly over, or under, forecast. Favored PBLs were the ACM2 and YSU with the favored microphysical scheme being the Mil - Yau. It is logical then that the two best PBL - microphysical relationships favored the ACM2 - Mil - Yau and the YSU - WSM6 relationships where both combinations had the best scores within their respective rain domain categories. It was noted that two ACM2 - Mil - Yau runs scored a perfect 1.0 in the 6 hour / 100 mm / 48 km^2 domain category and a 0.99 in the 3 hour / 100 mm / 24 km^2 domain category. The YSU - WSM6 PBL - microphysical scheme combination performed well; only slightly over-forecasting three out of the five parameterized verification domain categories. CSI scoring is where the NAM12 truly displayed how poor it performed as only 8 of 4,320 possible scores were registered, a meager 0.19% success rate of achieving a 0.20 CSI value or higher. A 0.26 from the BouLac - WSM6 was the highest CSI score and it was the favored PBL - microphysical relationship. This is significant marker as this relationship recorded a top three ranking in three of only eight scores greater than 0.20, or a 38% occurrence. This BouLac - WSM6 combination also did well in the CFSR and

ERA - Interim datasets, scoring a 30% and 47% top three rankings occurrence, respectively.

11.4 **CSI / HSS statistical (accuracy score) results and discussion**

The WRF - EMS output was statistically scored for accuracy by using two indices, the Critical Success Index (CSI) and the Heidke Skill Score (HSS). The CSI and HSS were used in the verification of five rainfall accumulation categories defined over specific parameterized temporal and areal verification domains.

CFSR / ERA - Interim											
		1 hr / 50 mm / 24 km^2		3 hr / 25 mm / 6 km^2		3 hr / 100 mm / 24 km^2		6 hr / 100 mm / 24 km^2		6 hr / 100 mm / 48 km^2	
PBL	mp	CSI	HSS	CSI	HSS	CSI	HSS	CSI	HSS	CSI	HSS
ACM2	Lin	0.094	0.069	0.339	0.357	**0.201**	**0.268**	0.217	0.152	0.386	0.283
	Mil - Yau	**0.265**	**0.405**	**0.397**	**0.452**	0.155	0.236	**0.227**	-0.032	**0.457**	**0.501**
	Thompson	0.028	-0.014	0.247	0.253	0.035	0.000	0.173	0.111	0.297	0.390
	WDM5	0.088	0.129	0.315	0.347	0.000	-0.013	0.143	**0.211**	0.237	0.296
	WDM6	0.110	0.149	0.313	0.296	0.091	0.013	0.163	0.147	0.313	0.262
Bou - Lac	Lin	0.090	0.115	0.360	0.340	0.073	0.063	0.164	0.245	0.242	0.174
	Mil - Yau	0.077	0.069	0.265	0.202	0.022	0.000	0.236	0.358	0.230	0.274
	Thompson	0.136	0.192	0.311	0.296	0.057	0.057	0.273	0.361	**0.395**	**0.426**
	WDM5	0.131	0.161	**0.410**	**0.434**	**0.118**	**0.147**	**0.279**	**0.386**	0.308	0.353
	WDM6	**0.155**	**0.201**	0.385	0.399	0.006	-0.011	0.113	0.167	0.265	0.194
MYJ	Lin	0.179	0.221	0.284	0.270	**0.148**	**0.181**	**0.247**	0.319	**0.398**	**0.406**
	Mil - Yau	0.074	0.056	0.221	0.235	0.034	0.029	0.179	0.275	0.285	0.334
	Thompson	**0.230**	**0.351**	0.299	0.291	0.006	0.066	0.245	**0.330**	0.291	0.320
	WDM5	0.081	0.122	**0.448**	**0.491**	0.113	0.151	0.219	0.293	0.277	0.305
	WDM6	0.106	0.105	0.399	0.426	0.058	0.038	0.212	0.323	0.313	0.265
MYNN	Lin	**0.231**	**0.297**	0.388	0.375	**0.194**	**0.257**	0.239	0.271	**0.433**	**0.445**
	Mil - Yau	0.141	0.181	0.327	0.299	0.008	0.000	**0.255**	**0.395**	0.253	0.292
	Thompson	0.104	0.108	0.287	0.312	0.123	0.153	0.234	0.315	0.285	0.312
	WDM5	0.088	0.129	**0.431**	**0.456**	0.099	0.166	0.201	0.257	0.284	0.281
	WDM6	0.182	0.229	0.393	0.391	0.108	0.126	0.212	0.321	0.332	0.322
QNSE	Lin	0.115	0.122	0.326	0.310	**0.110**	0.119	**0.351**	**0.471**	**0.465**	**0.541**
	Mil - Yau	0.063	0.055	0.234	0.245	0.000	0.000	0.221	0.319	0.273	0.335
	Thompson	0.073	0.076	0.286	0.272	0.033	0.040	0.231	0.334	0.236	0.272
	WDM5	0.086	0.102	**0.419**	**0.447**	0.076	0.106	0.276	0.386	0.274	0.326
	WDM6	**0.176**	**0.217**	0.363	0.391	0.107	**0.153**	0.184	0.284	0.243	0.229

Table 3: Maximum accuracy scores over the five verification domains (CFSR / ERA - Interim)

The highest CSI scores, or those scores over 0.50, were rare, but those scores did occur within the three hour duration of both low rainfall over a small area and high rainfall over a more moderate area. The CFSR initialized YSU - Thompson combination scored the highest CSI score in the study with a 0.68 at 2300 UTC for the three hour 100 mm 24 km^2 category. The second highest score of a 0.65 was from the 2200 UTC CFSR initialized MYNN - Stonybrook combination over the three hour 25 mm 6 km^2 category. This study's higher CSI scores were associated with the model output that was initialized by the CFSR reanalysis data set. All of the highest CSI scores, within the five parameterized verification domain categories, resided in the CFSR data set (Table 1, 2). Across all PBL - microphysical scheme combinations, the highest mean categorical CFSR CSI score was 0.31 with the ERA - Interim average being a 0.23. The NAM12's mean was also 0.23 but, only over a much smaller sample size (e.g., eight data points), versus a 30 sample size in the CFSR and ERA - Interim data sets. As previously discussed, this study's statistical data was analyzed by using a two-prong approach; marking those notable PBL - microphysical scheme combinations that consistently performed well across all verification domains (i.e., best performers) as well as those PBL - microphysical scheme combinations that recorded the highest, or maximum, quantitative scores.

Within the CFSR initialization data set, the best performing PBL was the YSU; the MYNN was the best performing PBL within the ERA - Interim data set. The best performing microphysical scheme was the Lin; recording the highest score in 20 out of 30 possible parameterized verification domains (i.e., a 67% occurrence). There was noted

correlation between higher CSI scores and particular PBL and microphysical scheme relationships. The ACM2 - Mil - Yau within the CFSR dataset scored the highest accuracy scores across all parameterized verification domain categories (Table 1). The ERA - Interim data set produced two PBL - microphysical combinations that displayed the attribute of achieving the highest accuracy scores in nearly all five parameterized verification domain categories; the ACM2 - Lin and MYNN - Lin (Table 2).

The maximum accuracy scores across both the CFSR and ERA - Interim reanalysis initialization datasets revealed that the two PBL - microphysical scheme combinations that consistently scored the highest were the MYNN - Lin and the BouLac - WDM5 (Table 3). The overall best performing PBL - microphysical scheme relationships, across both initialization datasets, were the MYJ - Lin and the BouLac - WSM6 combinations. These combinations registered the highest CSI scores in 5 of the possible 15 scenarios (i.e., a 33% occurrence). The PBL and microphysical scheme that continually show up within this research, or display the most consistency in terms of overall performance or when registering maximum skill scores, are the BouLac PBL and the Lin microphysical scheme, respectively. Deductive reasoning can fortify the theory that there is a viable connection between higher order PBLs that, when placed in tandem with microphysical schemes that inherently resolve the graupel species, lead to a higher skill success rate (i.e., more accurate bias and skill scores). The more successful BouLac is a PBL scheme that is related to another fairly successful MYJ scheme within this research in terms of sharing the same surface layer scheme; the Monin - Obukhov similarity theory surface layer scheme. Along with the Noah LSM, the BouLac and MYJ also ingest the Urban

Canopy Model (UCM) into their algorithmic structure. Logically, these PBLs ingested and utilized more high resolution land surface data. The additional LSM/UCM data would aid in better differentiating TKE-related physical processes that arise from modeling over an urban landscape versus that of agricultural or forest land coverage (e.g. crop fields, groves of trees). The physics of heat, moisture, and momentum advection over an urban landscape, when radiation reflectivity and shadowing created by man-made surfaces are parameterized, may give the BouLac PBL scheme an advantage in the development of a suitable PBL in which to create and maintain strong high-precipitation thunderstorms.

The highest HSS statistics across all PBL and microphysical scheme combinations, or scores over 0.50, were just as rare as the CSI. Four of the five highest HSS values in the parameterized verification domain categories occurred within the CFSR data set. Intuitively, the maximum HSS values occurred in the six hour 100 mm 48 km^2 category during the last 2300 - 2400 UTC hour; a 0.54 for the QNSE - Lin and a 0.51 for the YSU - WSM6 PBL - microphysical scheme combinations. Generally, maximum HSS, in relation to the overall better performers, belonged to model output that was initialized by the CFSR reanalysis data set. The highest mean categorical CFSR HSS score was 0.34, while the ERA - Interim HSS average was 0.22. The NAM12's mean was also 0.20 but only out of a sample of six data points, versus 30 in the CFSR and ERA-Interim data sets. The highest accuracy scores generally occurred in three verification domain categories; the three hour 25 mm over town/suburb geographic scale and over the two six hour domains (Table 3). Logical reasoning for these higher scores being grouped within this

three hour domain is that, even though it was the smallest areal coverage domain, 25 mm of rain was easier achieved within a grid-based verification method. A promising aspect of this research was with the six hour domain statistical success. The research focused on simulating an extreme rainfall event, defined as an event that produced at least 100 mm of rain during a relatively short period of time (e.g., six hours), and the higher accuracy scores fell within these two six hour domains (Table 3). This domain's highest skill scores were varied amongst five better performing microphysics across all PBLs, but consistent scores greater than 0.25, with many in the .30 to .50 range (Table 3). This increases confidence that progress is being made in improving the forecast of a high rainfall event, within a six hour precipitation forecast window used by the U.S. National Weather Service over a typical United States city or county geographic scale, 24 hours out. The highest six hour 100 mm county scale accuracy scores (i.e., greater than 0.40) aligned themselves with the more complex Lin or Mil - Yau microphysical schemes in association with the higher order closure, LSM/UCM data-fed MYNN or BouLac PBL schemes (Table 3).

When forming 3 x 6 matrices of the statistical data in a more qualitative-sense (i.e., simply ranking bias and skill scores), the overall better performing PBLs were the ACM2 and YSU when initialized with the CFSR dataset. The MYNN consistently performed the best when initialized with the ERA - Interim dataset. The best performing microphysical scheme was the Lin scheme; achieving the highest ranking 16 out of the 30 possible outcomes (i.e., 53% occurrence). There was correlation between higher HSS and particular PBL and microphysical schemes. The CFSR initialized ACM2 - Mil - Yau

relationship scored maximum HSS in four-out-of-five rainfall accumulation, over varying temporal and spatial categories. The PBL - microphysical scheme combinations in the ERA - Interim dataset that matched the same four-out-of-five maximum HSS rainfall accumulation categorical scores were the Lin across both the MYNN and ACM2 PBLs. The best performing PBL - microphysical scheme combinations across all three initialization data sets were the ACM2 - Mil - Yau and the BouLac - WDM5 combinations; scoring maximum HSS in 4 of the possible 15 scenarios (i.e., 27% occurrence). The highest scoring PBL - microphysical scheme combinations across the CFSR and ERA-Interim datasets were the ACM2 - Mil - Yau and the MYNN - Lin combinations (Table 3).

11.5 **Final results and discussion**

This research gathered all three statistical score results on Frequency Bias, Critical Success Index, and Heidke Skill Score across the three initialization data sets (e.g., CFSR, ERA - Interim, and NAM12) and discovered there were correlations between higher statistical scores (i.e., maximum scores) and particular PBL and/or microphysical schemes. Although the NAM12 was a poor performer within this research, it was still important to include this initialization data. In real world forecasting, this model may be the "model of choice" for initialization. This is a popular initialization model as it is a higher resolution model, compared to a spectral model (e.g., GFS), and updates more frequently (i.e., every three hours) than would the 12 hour-updated ECMWF. The study's

results are categorized as *best performers* or *maximum scorers* within the five parameterized verification domain categories that may, or may not, have correlation.

The 1 hour / 50 mm / 24 km^2 category's best microphysical scheme performers were the Lin, WDM5, Thompson, and Mil - Yau. The most accurate PBL - microphysical combinations were the ACM2 - Mil - Yau, QNSE - Thompson, and the YSU - WDM6. The maximum scoring PBL - microphysical scheme combination was the ACM2 - Mil - Yau (Table 3).

The 3 hour / 25 mm / 6 km^2 category's best microphysical scheme performers were the WDM6, Lin, Thompson, and WDM5. The most consistently accurate PBL - microphysical combination was the ACM2 - Mil - Yau. The maximum scoring PBL - microphysical scheme combination was the MYJ - WDM5 (Table 3).

The 3 hour / 100 mm / 24 km^2 category's best microphysical scheme performers were the WDM5, Lin, Mil-Yau, and WDM6. The most consistently accurate PBL - microphysical scheme relationships were the ACM2 - Mil - Yau and the BouLac - WDM5. The YSU - Thompson scheme combination scored the highest accuracy (CSI) score within this study of a 0.68 at 2300 UTC. The maximum scoring PBL - microphysical scheme combination within this relatively-lower scored verification domain was the ACM2 - Lin (Table 3). The reason this category received lower scores is because it is generally more difficult, with current high-resolution modeling, to accurately simulate extreme rainfall rates of

100 mm within a relatively-short three hour duration over a geographic area approximately the size of a large U.S. city (e.g., 24 km^2).

The 6 hour / 100 mm / 24 km^2 category's best microphysical scheme performers were the Lin, WDM5, Thompson, and the Stonybrook. The most accurate PBL - microphysical combinations were the MYJ - Lin, QNSE - Lin, and ACM2 - Lin. The maximum scoring PBL - microphysical scheme combination was the QNSE - Lin (Table 3). Within this verification domain, there was good correlation between the best performer and the maximum scoring combination; the QNSE - Lin relationship. Logically, when more advanced QNSE PBL theory was coupled with the historically strong performing six-class Lin microphysical scheme, higher accuracy was achieved.

The 6 hour / 100 mm / 48 km^2 category's best performers were the Lin, WDM5, Thompson, and WSM6. The most consistently accurate PBL - microphysical combinations were the QNSE - Lin and ACM2 - Mil - Yau relationships. The maximum scoring PBL - microphysical scheme combination within this six-hour 100 mm county-size domain was the QNSE - Lin (Table 3). This QNSE - Lin relationship proved again that there was a strong correlation between the more qualitative *best performer* and the most quantitative *maximum scorer* across this important event-capturing domain.

The majority of these PBL - microphysical scheme combinations, although performing statistically well (i.e., occasionally achieving high skill scores), still suffered from improper timing and poor spatial placement of the highest hourly rain accumulation.

When the modeled output data was visually-analyzed through IDV, there were a few PBL and microphysical scheme combinations that best simulated the placement of highest rainfall that occurred within a couple of hours of the (actual) observed occurrence. Thus, success in this research is defined in a relative-sense. The majority of the numerous PBL - microphysical scheme combinations failed to adequately resolve the temporal and spatial nature of the observed, or remotely-sensed, rainfall accumulation with any mentionable degree of accuracy.

The three initialization data sets provided varied results amongst the 48 PBL - microphysical scheme combinations. The CFSR reanalysis was the best performer between both reanalysis datasets and this reasoning is discussed within Chapter 5's Initialization Data. CFSR-initialized output outscored the ERA - Interim initialized output in 44 out of the possible 60 highest accuracy/skill scores (i.e., CSI, HSS) across all five parameterized verification domain categories. It should be noted that the CFSR initialized output accounted for the highest maximum accuracy/skill scores across all six PBLs in the 3 hour/ 25 mm/ 6 km^2 and the 6 hour / 100 mm / 24 km^2 parameterized verification domain categories. The NAM12 model output results were extremely poor as the majority of its CSI and HSS results across all five parameterized verification domain categories were of low skill. Generally, the NAM12 initialized CSI and HSS accuracy values were under 0.20 with the majority of the combined scores being either zero or negative (i.e., no HSS skill). The NAM12 initialization dataset proved to have little, to no, skill within this research and, therefore, may not be considered in future studies.

When comparing the graphical output data against Stage IV radar verification data (Fig. 36), WRF- EMS output would tend to over-forecast early in the six hour time period. Generally, output data would trend to an under-forecast during the latter hours of the event across all five parameterized verification domains; during the time of the extreme rainfall over southern Harris and northern Galveston counties. In determining how the simulations handled the downstream nature of the event, three better performing PBL - microphysical scheme relationships were chosen for graphical representation. The CFSR ACM2 - Mil - Yau simulation was the one scheme combination that best handled the timing and location of the most extreme rainfall. Although the heaviest rainfall of approximately 175 mm fell over the Clear Creek channel from 1800 - 2000 UTC, the ACM2 - Mil - Yau simulated one or two heavy rain core 80 - 90 mm per hour rates between 2000 - 2200 UTC. The two hour-simulated rain accumulations measured between 160 - 180 mm accumulations that match up well with observed storm (rain) totals of between 150 - 200 mm across this same geographic region from southern Fort Bend County into northern Brazoria County (Fig. 37, 38). A two hour lag in the timing of the simulation's core rain, compared to that observed over Clear Creek, may be an inaccurate perception; an assumption that the simulation's extreme rainfall accumulations were an attempt to resolve the highest core rainfall over Clear Creek. If one does not make this assumption, than the ACM2 - Mil-Yau accurately simulated the quantitative hourly rainfall rates of greater than 80 mm approximately over the same geographic location (e.g., southern Fort Bend and northern Brazoria counties) that received the region's highest training-in-nature core rain. The ERA - Interim MYJ - Lin relationship simulation advected the core rain in from the northwest, versus from the

observed south and west direction. Hence, this PBL - microphysical combination's core hour rainfall rates of 103 mm were displaced further north, over the western side of Houston during 2000 - 2100 UTC (Fig. 39, 40). This PBL - microphysical scheme combination displayed the greatest skill with its ability to accurately simulate, albeit delayed by an hour, greater than 100 mm per hour rainfall rates. Very few simulations could simulate hourly rainfall rates of greater than 75 mm, much less 100 mm per hour. The QNSE - Thompson PBL - microphysical scheme did well with forecasting the timing and spatial nature of the event (Fig. 41, 42). Although significantly under-forecasting hourly rainfall rates (e.g., 50 mm/hr), this combination displayed skill with its ability to properly place its core rain accumulation within 40 km (i.e., southwestern Harris County) of the highest observed rain swath extending east from southern Fort Bend County into northern Galveston County. If these simulations were used in a real-world National Weather Service operational forecasting scenario, many forecasters would be delighted to resolve an event with the accuracy displayed with these particular PBL - microphysical scheme combinations.

The better performing PBL - microphysical schemes exhibited the creation and downstream evolution of a meso-low within the modeled surface mass (i.e., pressure) field. The highest precipitation during the afternoon of April 18th, 2009 occurred just north and east of an observed meso-low within the surface pressure field. There was a correlation made between the more accurate precipitation-forecasting PBL - microphysical schemes (e.g., ACM2 - Mil - Yau) and the existence of a vicinity meso-low. The enhanced moist inflow into the cluster of thunderstorms from this mesoscale

low likely contributed to the higher core rain accumulation observed along the west-to-east path from southern Fort Bend County into northern Galveston Counties' Clear Creek channel. Therefore, it is a logical assumption that, if a PBL - microphysical scheme combination can accurately create (i.e., simulate) a mesoscale low within the surface pressure field, then there will be a higher probability of that particular PBL - microphysical relationship producing extreme rainfall rates within the vicinity of the modeled meso-low. The ACM2 - Mil - Yau PBL - microphysical scheme combination simulated a meso-low between 1004 – 1006 mb just south and/or west of its simulated maximum (core) rainfall (Fig. 43, 44). Surrounding Automated Surface Observing System (ASOS) observations of surface pressure during the event were between 1007 - 1008 mb, although un-measurable mesoscale surface pressures were likely lower closer to the cumulonimbus updrafts. The MYJ - Lin and QNSE - Thompson PBL - microphysical schemes were also able to resolve a meso-low in the vicinity of their core rains. Albeit slightly early, the MYJ - Lin PBL - microphysical schemes combination did simulate a tight 1008 mb meso-low within the pressure field just west of its highest simulated rainfall over west Houston (Fig. 45). The QNSE - Thompson PBL - microphysical scheme combination was also successful at creating, developing, and evolving a vicinity 1010 mb meso-low within a few kilometers of its simulated highest core rain (Fig. 47, 48).

12. Conclusions

Thesis Prediction*: If this research's WRF simulations are structured in the aforementioned manner, then will this output have the ability to forecast the magnitude, or scope, of a high rainfall event's temporal and spatial behavior?*

Thesis (Working) Hypothesis: *There were favorable PBL - microphysical scheme combinations that more accurately forecast the magnitude and scope of this particular case study's extreme rainfall event in both time and space. These scheme combinations all exhibited higher order mathematical derivations within their PBL structures as well as double moment and higher specie numbers within the microphysical scheme algorithms. The PBL - microphysical schemes that achieved higher skill, through statistical scoring methods across various parameterized verification domains, were those tandem relationships that inherently owned higher order, or more advanced, mathematical and physical characteristics.*

This research discovered that generally half of the chosen eight microphysical schemes consistently came up with relatively higher scores when compared across this work's parameterized verification domains. The better performing microphysical schemes that achieved these highest statistical results in frequency bias, CSI, and HSS were the Lin, Mil - Yau, Thompson, and the WDM6 schemes. All four of these microphysical schemes include the presence of graupel within their cloud physics. The definition of graupel is precipitation that forms when supercooled water droplets freeze upon contact with a

falling ice crystal or snowflake. Cumulonimbus clouds that exhibit strong updraft and downdraft structure through higher altitudes will have a greater probability of more efficiently initiating this ice accretion process within the hail growth zone (e.g., between -10 °C and -20 °C) that is typically required in the creation of graupel. The introduction of graupel within a cumulonimbus is typically a marker of a high precipitation supercell. If graupel is properly simulated within a towering, high echo top cumulonimbus cloud then the assumption is that the Wegener-Bergeron-Findeisen processes of effective ice crystal growth within a mixed phase deep convective cloud will be sufficient to produce a super-saturated environment for supercooled liquid droplets and a sub-saturated environment for ice. A higher saturation vapor pressure over the supercooled droplets, in relation to the ice crystals, would ultimately result in rapid evaporation of supercooled droplets in favor of rapid ice crystal growth through vapor deposition (i.e., ice crystal growth at the expense of the evaporating supercooled droplet field). Efficient ice crystal development will allow a high flux of ice crystal, hail, or even graupel to fall into the lower, warm layers and melt. The additional downward fluxes of mid-layer ice into the sub-freezing lower layers (e.g., lower 3 km) would only increase rain production, or create a high rainfall rate scenario. Thus, if graupel is more accurately simulated within the evolution of strong convective environments then it can deduced that a more accurate gauge, or measure, of the graupel species would be beneficial to more accurate high rainfall rate forecasts.

This study concluded those microphysical schemes that included double moments, or the ability to calculate the number concentration along with the mass (mixing ratio)

concentration of the various species, had a positive impact upon achieving higher accuracy. Those schemes that included both the species' mixing ratios and their number concentration had a higher probability of achieving maximum statistical scores within their respective PBLs. The research showed that, concerning this particular spring season southeastern Texas high rainfall event, the better performing microphysical schemes were the Thompson, Mil - Yau, and WDM6 schemes. These schemes either have the ability to simulate the concentration number of ice and rain nuclei (e.g., Thompson), cloud, rain, and CCN nuclei number concentration (e.g., WDM6) or can differentiate the number concentration for six different species (e.g., cloud, rain, ice, snow, graupel, and hail) such as within the highly complex Mil - Yau microphysical scheme. Within the Mil - Yau scheme, water vapor is included with the 12 mixing ratio and number concentration variables of cloud, rain, ice, snow, graupel, and hail; 13 total variables. The importance of including the number concentration variables, in tandem with the mixing ratio variables, cannot be understated as three of this study's four best performers (e.g., Thompson, Mil - Yau, and WDM6) all contain these particular double moment attributes.

High rainfall events are those climatologically rare events that are typically difficult to resolve even with the tool of high-resolution NWP modeling. The model's ability to create and properly develop mesoscale features within the mass field algorithms (e.g., surface pressure) in both time and space will significantly improve that system's capability of accurately simulating locally high rainfall. It is difficult to determine if a particular PBL received a high score, or performed better in relation to the other schemes, because it was influenced by its associated microphysical scheme, land use modeling,

and/or surface layer physics. Deductive reasoning states that, since the ACM2 was the more successful PBL within this research, that there was correlation between this scheme's ability to more accurately reproduce cumulonimbus updraft / downdraft structure (i.e., narrow and fast / wide and diffusive, respectively) to that of better resolving the temporal and spatial nature of the highest rainfall. Logically, the MYNN PBL scheme was another successful scheme as it was more mathematically advanced in its higher 2.5 order closure methodology. There was correlation between the MYNN's ability to better resolve sub-grid diffusivity and this study's higher accuracy scores. Other successful PBL schemes, in relation to this work's higher rainfall forecast statistics, were the QNSE and the BouLac. A correlation can be made between this case study's higher statistical scores and the QNSE's advanced theory on simulating diffusive sub-grid eddy flow behavior within vicious environments. The BouLac PBL's scheme relationship with the Noah LSM, coupled with the UCM, may have positive feedback on improving rainfall forecast statistics. The BouLac's ability to assimilate more land surface and urban landscape data may be beneficial in better resolving smaller scale high rainfall-leading-to-flooding events over urbanized areas. In summary, when comparing all PBLs within this research, there are more advanced algorithms within the more modern PBLs that can handle such complexities as upward or downward flux (e.g., ACM2) or that can better close off sub-scale/grid eddy behavior within viscous flow (e.g., QNSE) or even those more closely related to surface layer schemes or LSM/UCMs (e.g., BouLac). As was discovered within this research, it may be advantageous to pair these more advanced PBLs with more complex microphysical schemes in better resolving extreme rainfall. Because of the numerous tangential influences inherent within these PBL - microphysical

scheme relationships, the scope of this study did not have the breadth required in making truly definitive "end-all" conclusions.

13. Future Work

This research has opened up many more avenues of future study. Although this study thoroughly examined many physical schemes within various initialization modes, significantly more work needs to be accomplished on similar high rainfall events. This research has laid the foundation for using this study's stronger initialization PBL - microphysical scheme combinations with the WRF - EMS (version 3.x) in attempting to accurately simulate similar synoptically-forced high rainfall events. Fortunately, this research has the benefit of having two more high rainfall events to explore within a 10-day period of the April 18th, 2009 event; the April 24th and April 28th, 2009 greater Houston, Texas area high rainfall events. Even though this case study was the most extreme in terms of localized extreme rainfall production, it is highly unusual to have three high rainfall events occur within a 10-day period of one another. This is advantageous for future research as the other two events occurred within a similar synoptic environment and in close proximity of one another. The seasonal timing of these three events is not the only unique quality driving future exploration. The commonality of each event's historical significance alone will continue an interest to continue research. All three events had 3 hour rain rates of a 100 year return period or better. All three events were rather short in duration (e.g. 6 hours or less) as rainfall totals did not increase

much during 12 and 24 hour periods. The example was this case study where 252 mm of its total 279 mm (9.9 of its total 11 inches) of rain fell within 6 hours; 175 mm (6.9 inches) in one hour! The motivation to continue future work exists based upon a couple of interesting facts about the other two high rainfall events. The April 24th, 2009 event was only a 6 hour event with over half of its total rainfall of 97 mm (3.8 inches) being measured within just one hour. The April 28th, 2009 event had a slightly longer duration with 107 mm (4.2 inches) of rain that fell within the first 6 hours.

Computer program scripts need to be written to more efficiently handle the automatic execution of numerous NWP modeling runs. Automatic run scripts could be scheduled to run at specific times while varying the PBL - microphysical schemes. Future research could better determine the idiosyncrasies of each successfully performing physical scheme. Collaboration with the model developers could provide the necessary feedback required in furthering PBL and microphysical evolution. Questions have arisen during this research, such as do certain PBL - microphysical scheme combinations complement one another and, if so, why the correlation? Future research and collaboration with the modeling developers may provide some insight into the questions that have arisen within the scope of this study. Lastly, future research and continued interest in this area of high resolution regional NWP modeling will only strengthen confidence on what particular PBL - microphysical scheme(s) an operational forecasting unit employs within their local WRF - EMS model in better resolving (i.e., forecasting) the future evolution of an approaching, potentially dangerous, high rainfall-producing storm system.

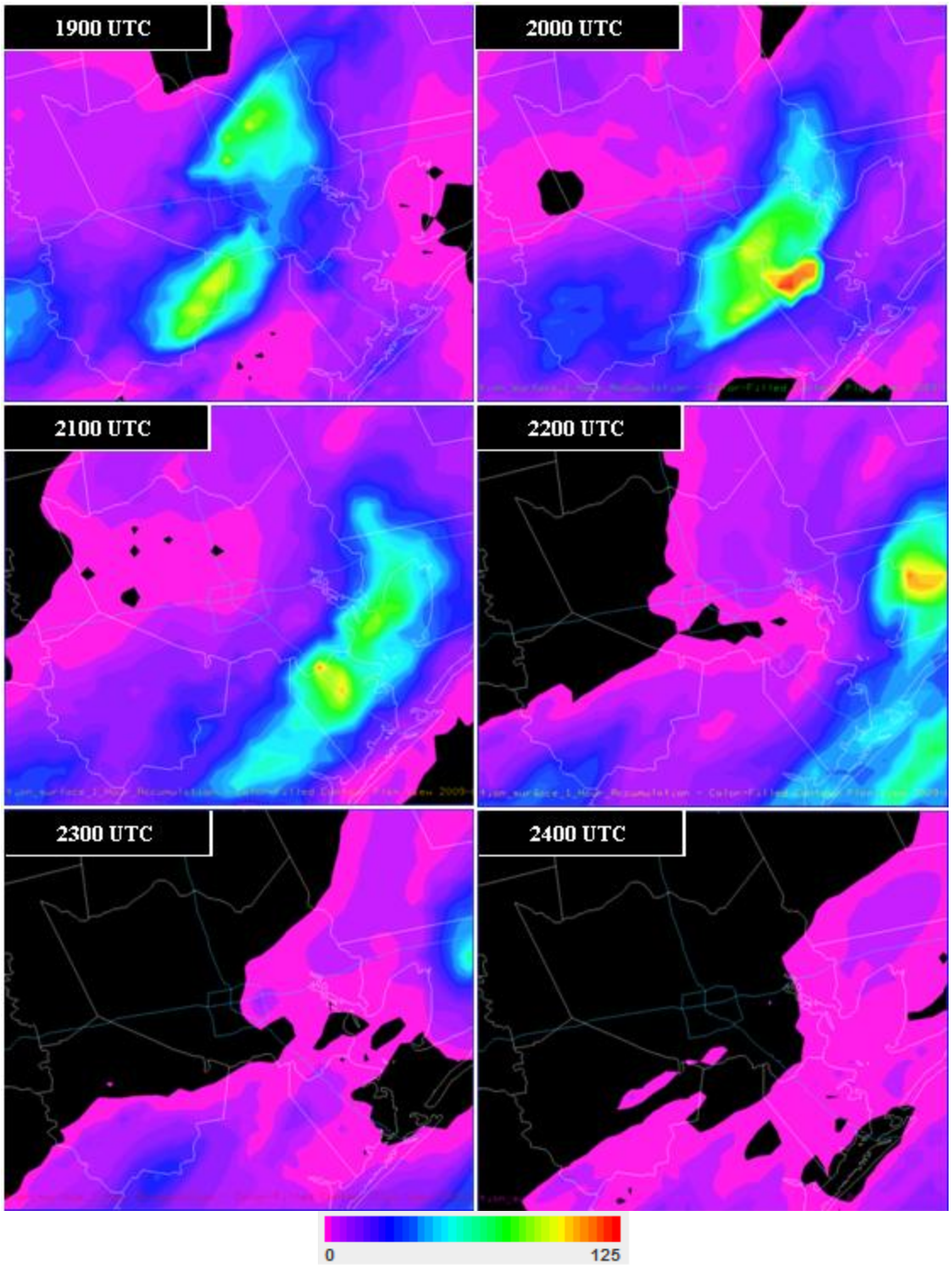

Figure 36: Stage IV radar verification data for rain accumulation (mm) (1800 – 2400 UTC)

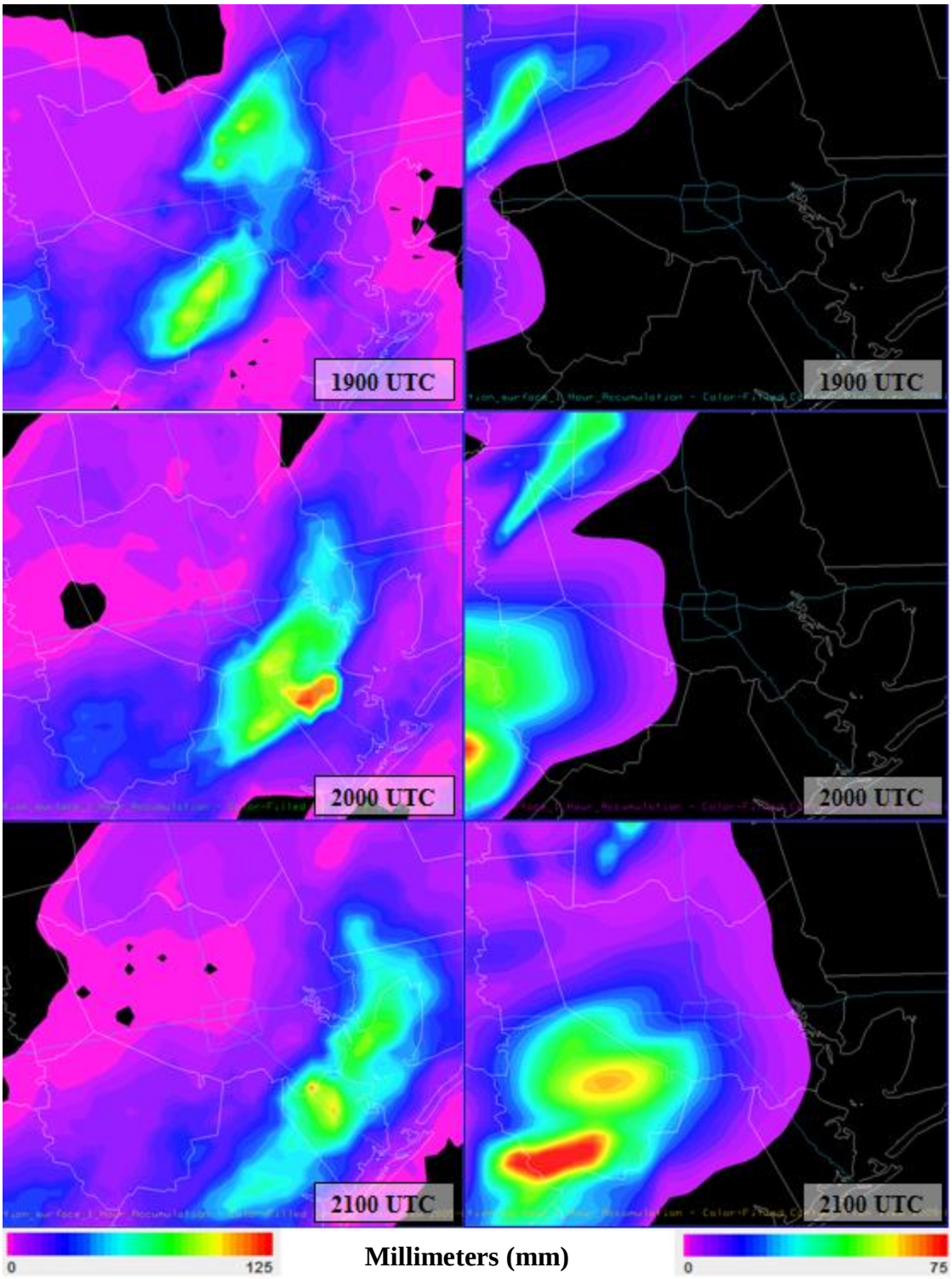

Figure 37: Stage IV (left column) / ACM2 - Mil - Yau (right column) Verification / PBL - mp rain accumulation (mm)

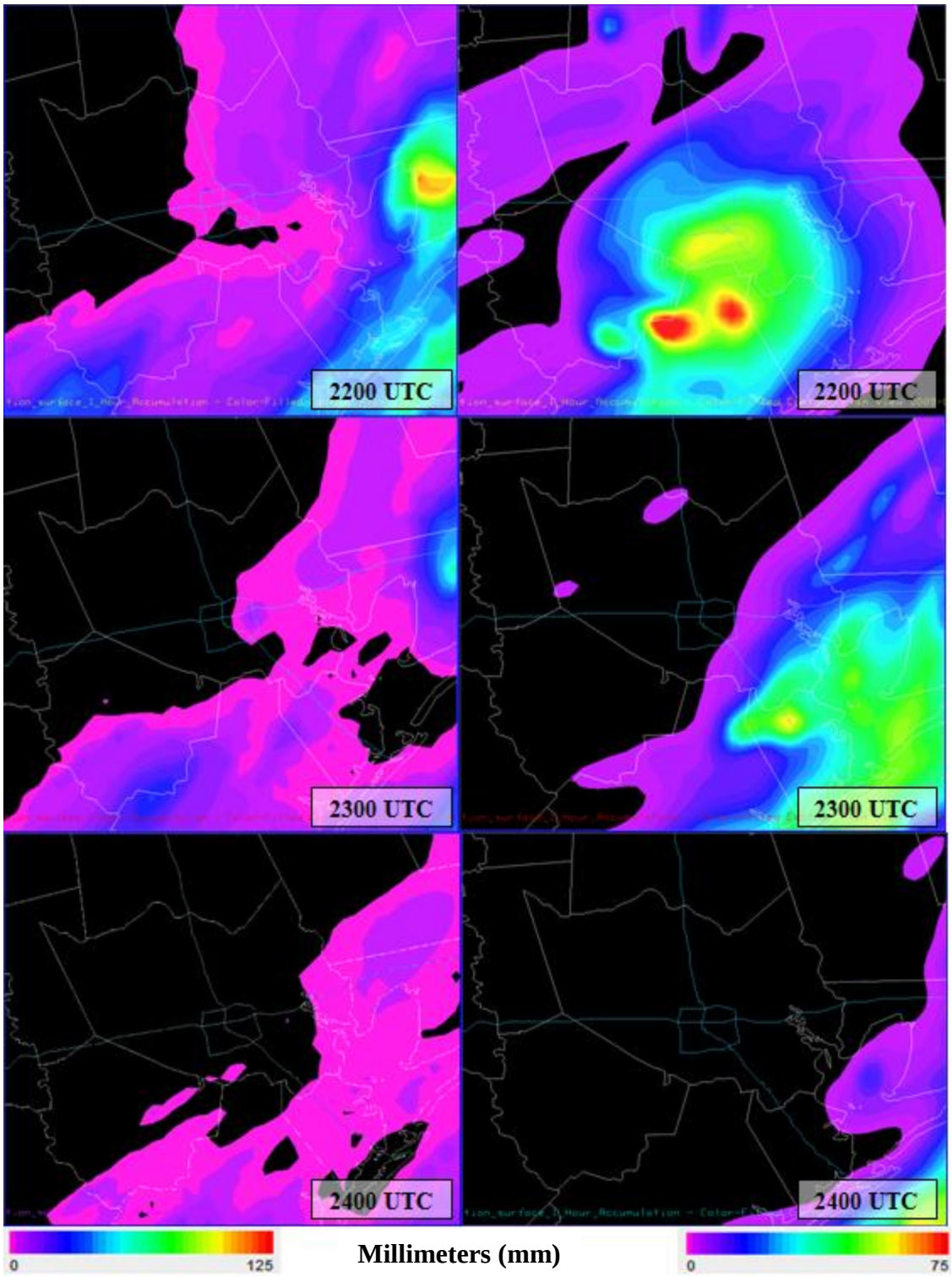

Figure 38: Stage IV (left column) / ACM2 - Mil - Yau (right column) Verification / PBL - mp rain accumulation (mm)

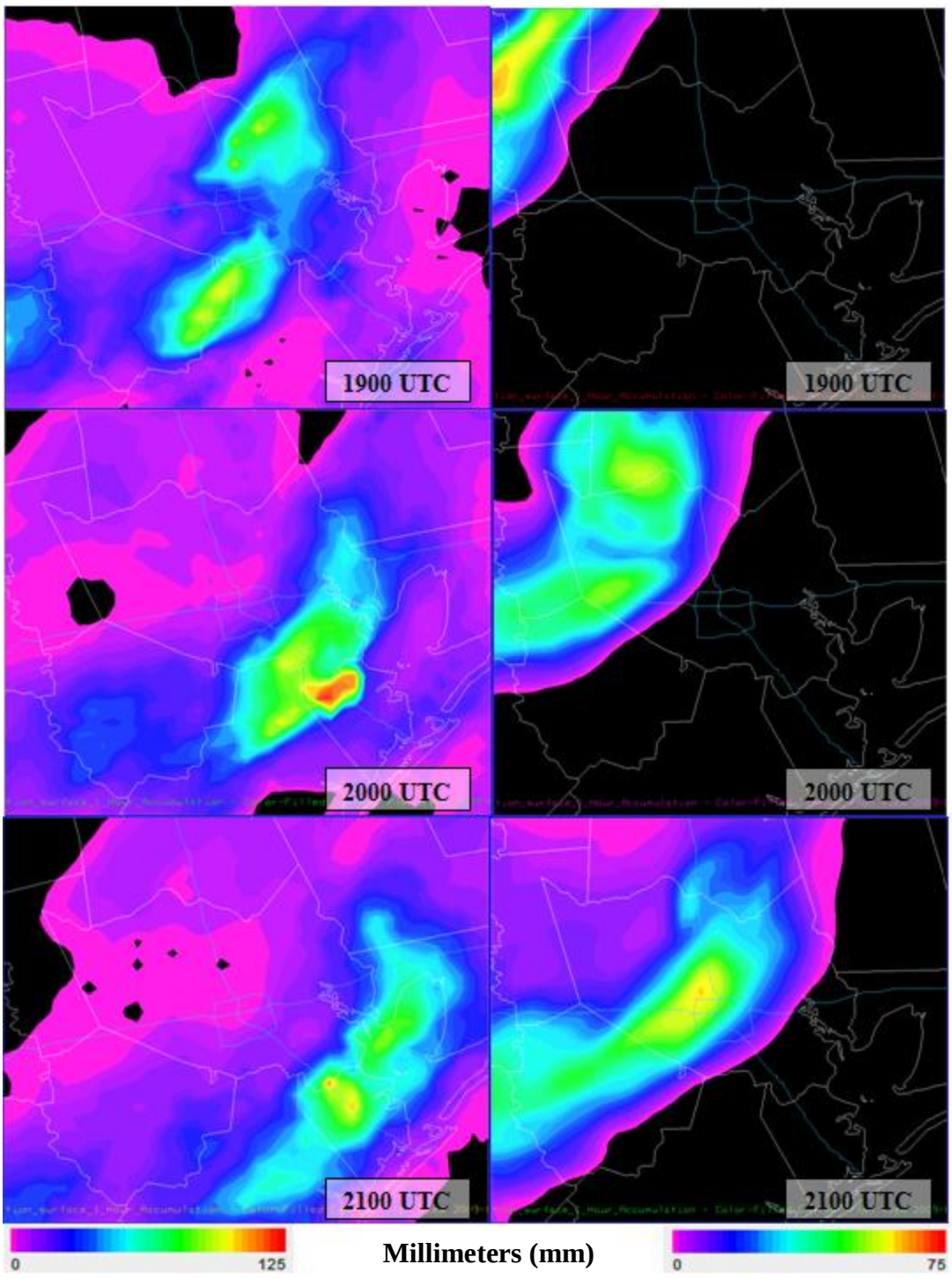

Figure 39: Stage IV (left column) / MYJ - Lin (right column) Verification / PBL - mp rain accumulation (mm)

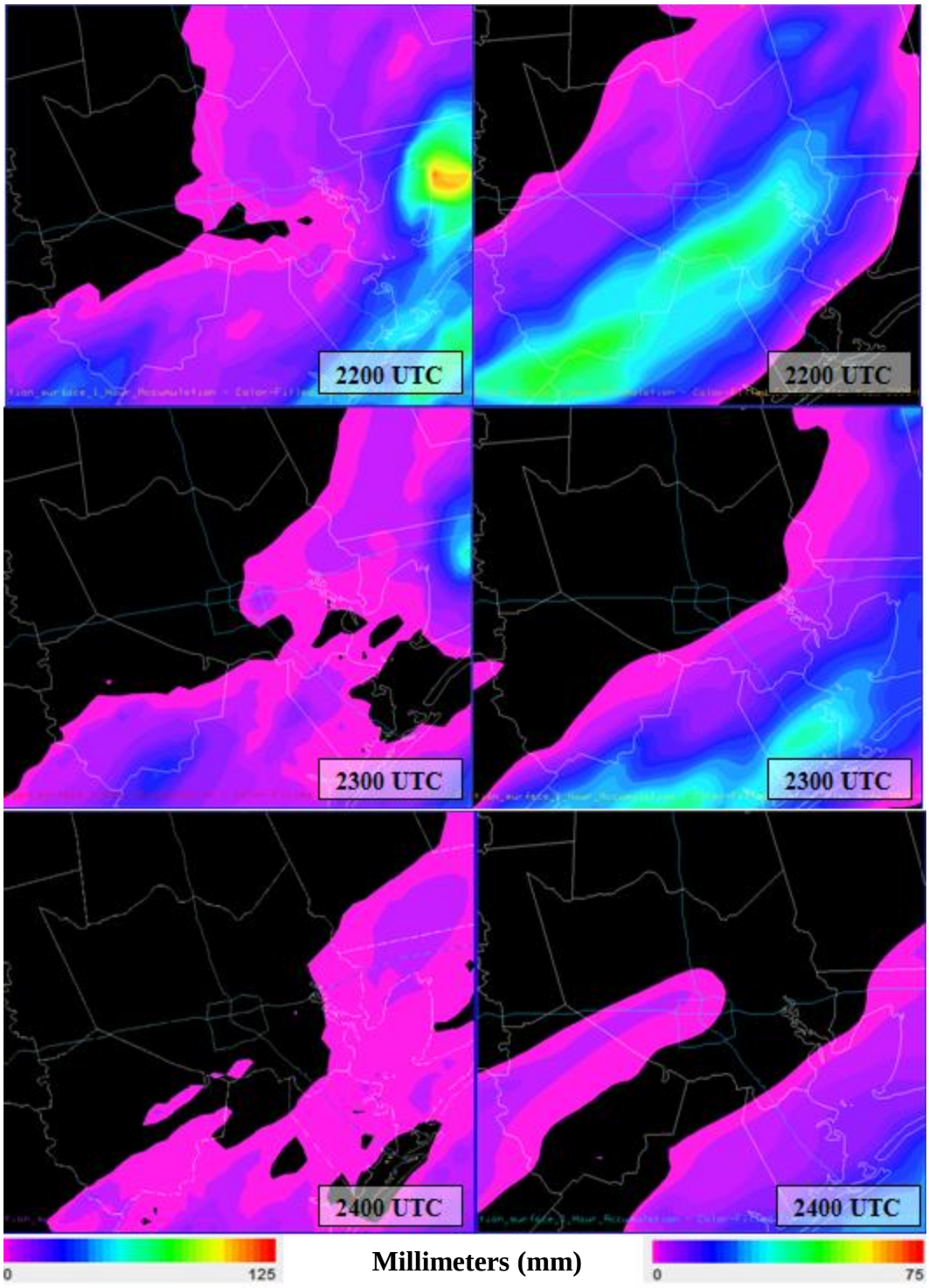

Figure 40: Stage IV (left column) / MYJ - Lin (right column) Verification / PBL - mp rain accumulation (mm)

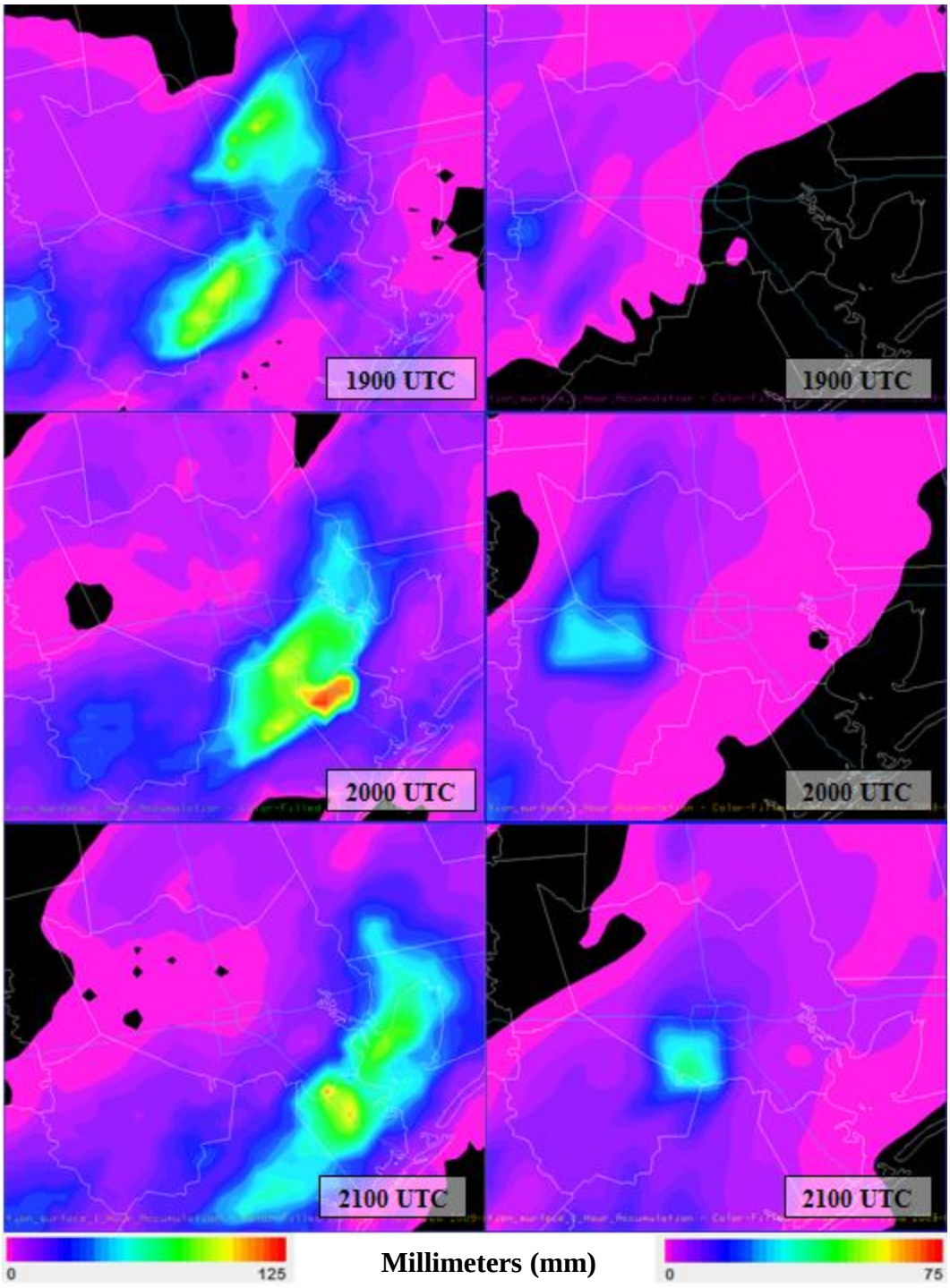

Figure 41: Stage IV (left column) / QNSE - Thompson (right column) Verification / PBL - mp rain accumulation (mm)

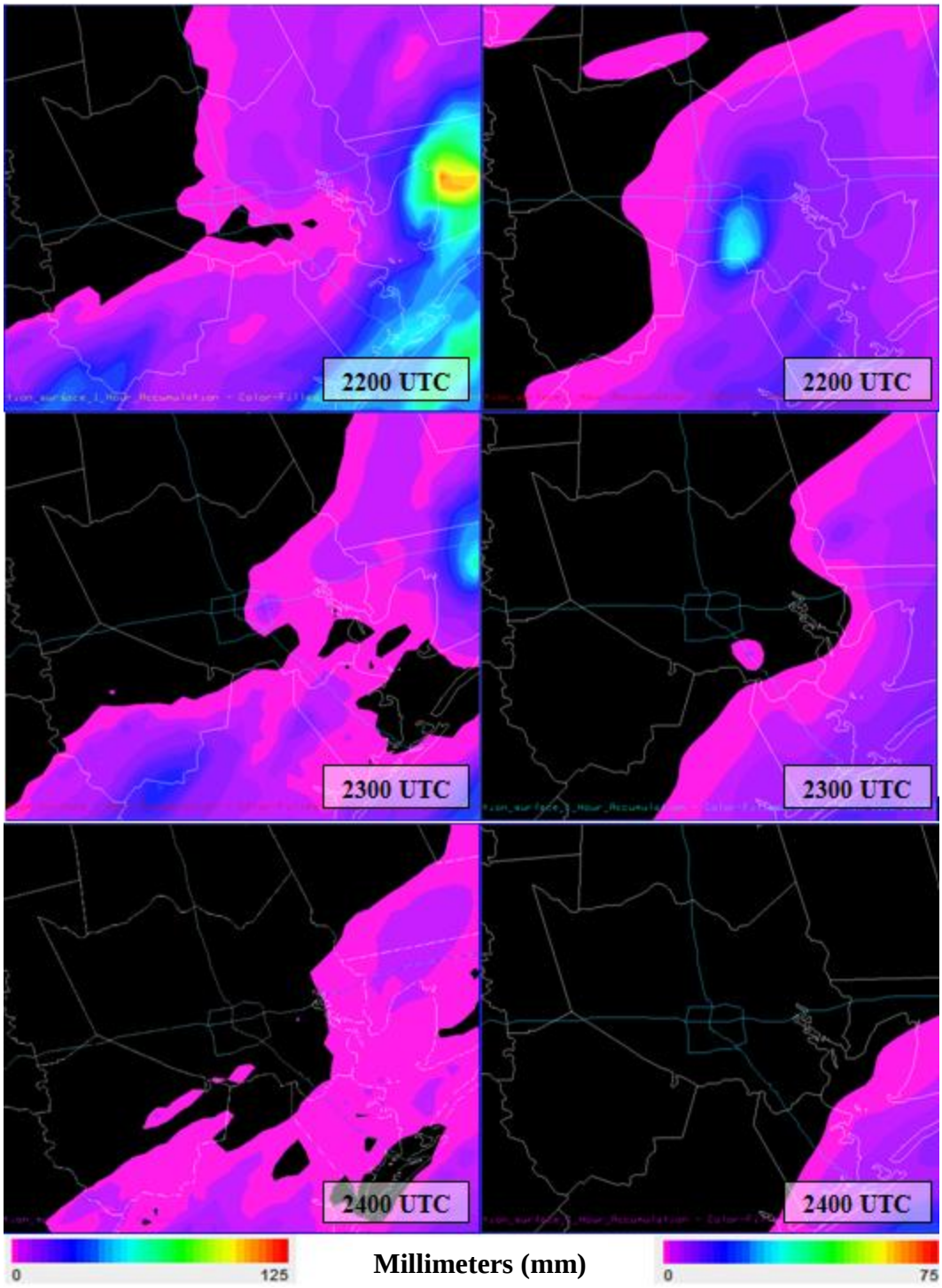

Figure 42: Stage IV (left column) / QNSE - Thompson (right column) Verification / PBL - mp rain accumulation (mm)

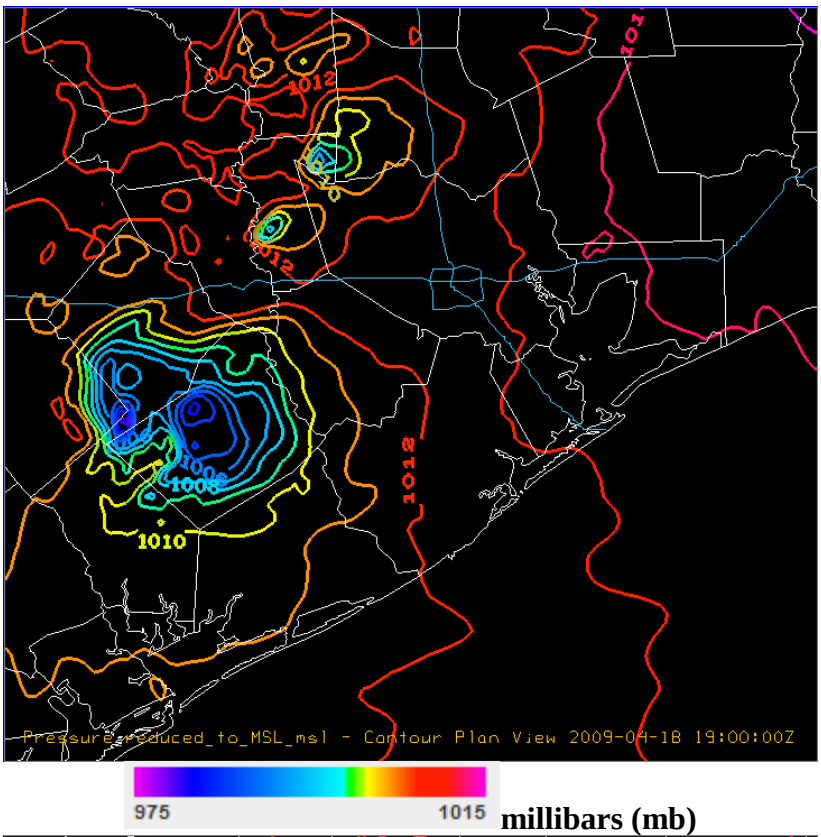

Figure 43: 1900 – 2000 UTC meso-low (blue) within the ACM2 – Mil - Yau PBL - mp relationship

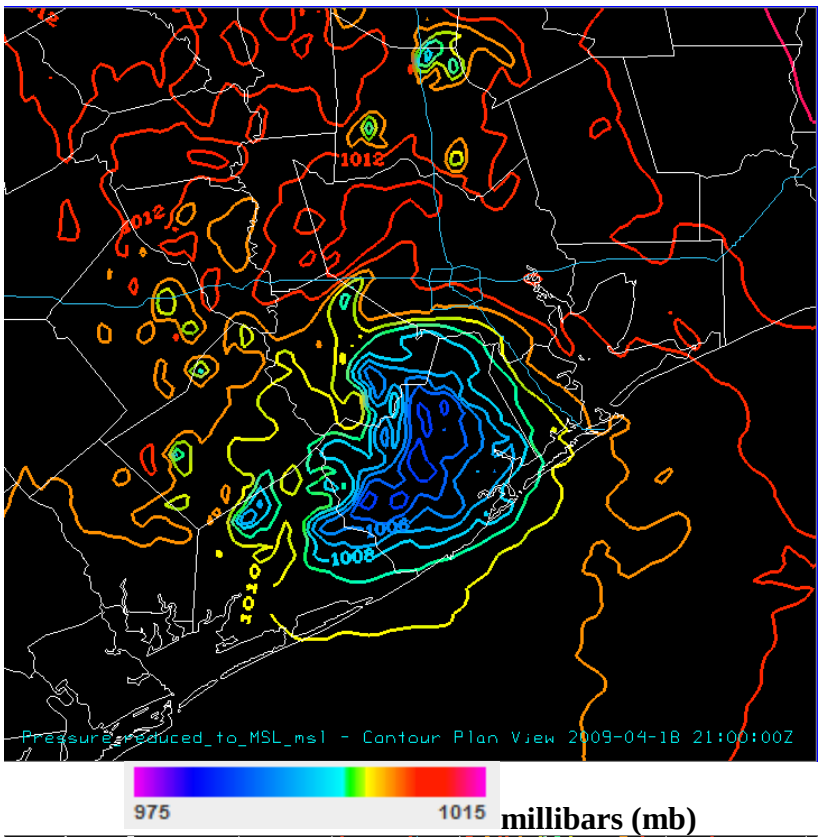

millibars (mb)

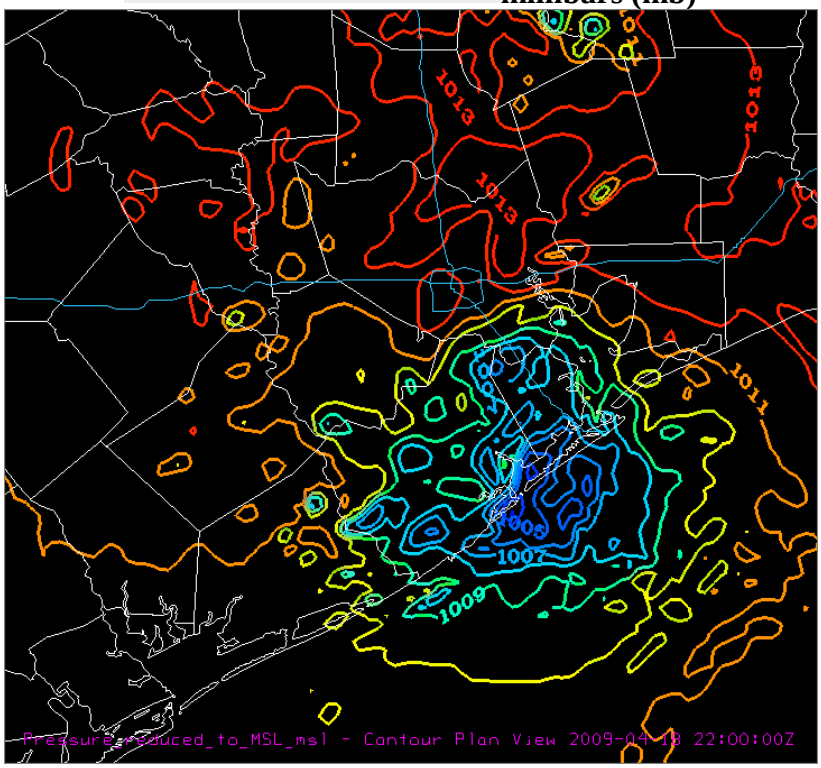

Figure 44: 2100 – 2200 UTC meso-low (blue) within the ACM2 – Mil - Yau PBL - mp relationship

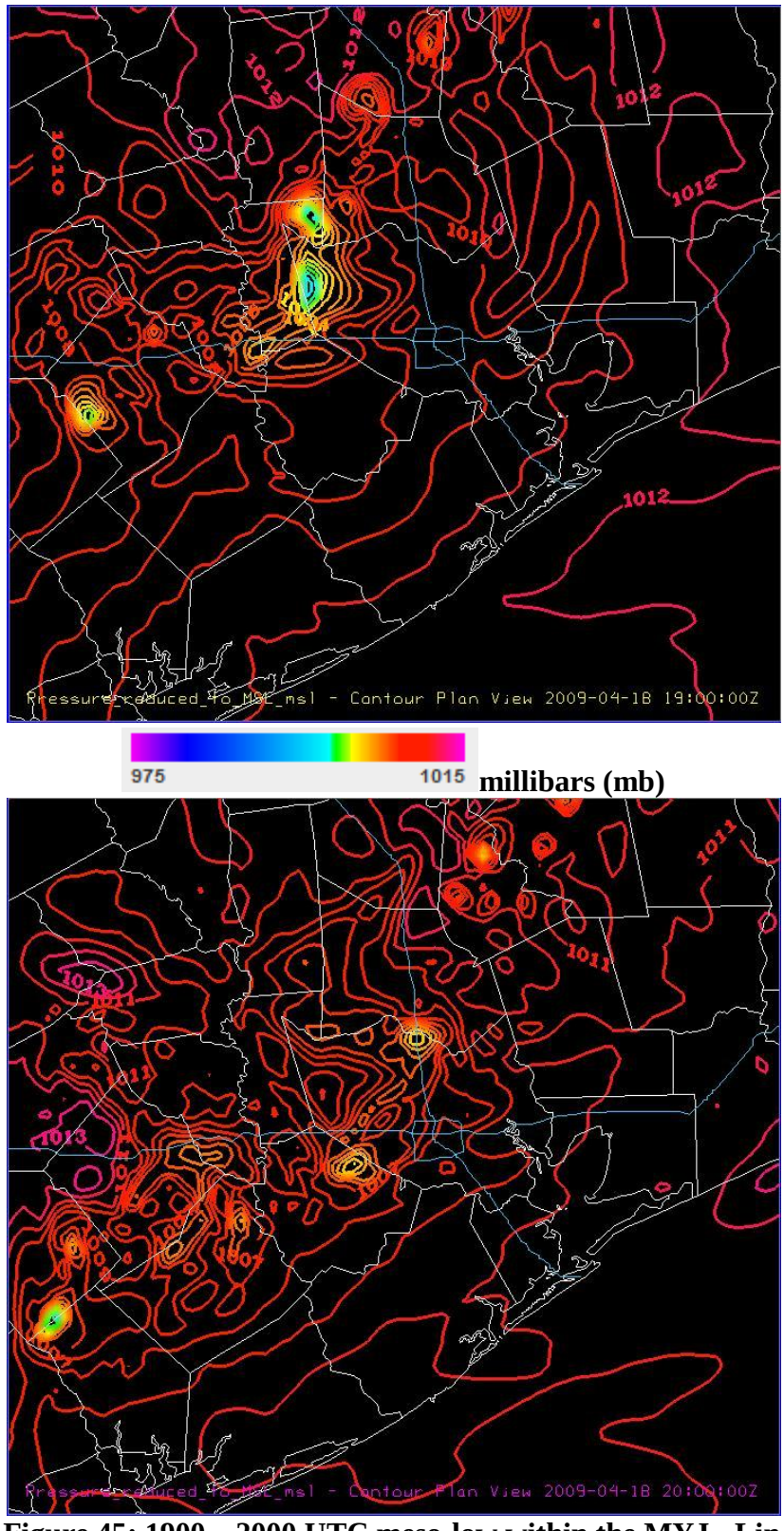

Figure 45: 1900 – 2000 UTC meso-low within the MYJ - Lin PBL - mp relationship

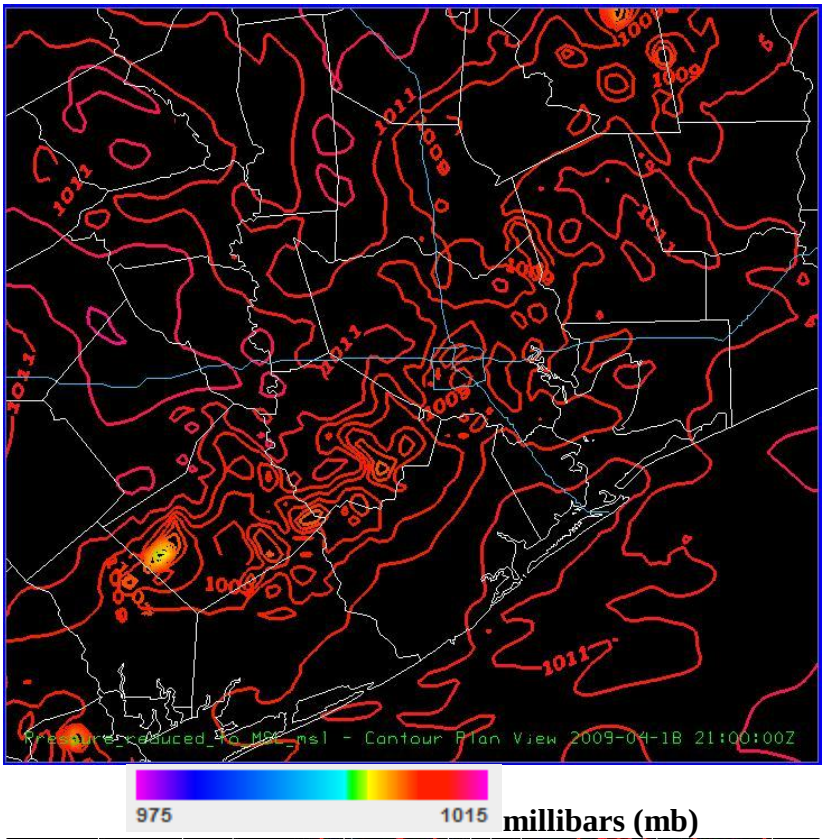

Figure 46: 2100 – 2200 UTC meso-low within the MYJ - Lin PBL - mp relationship

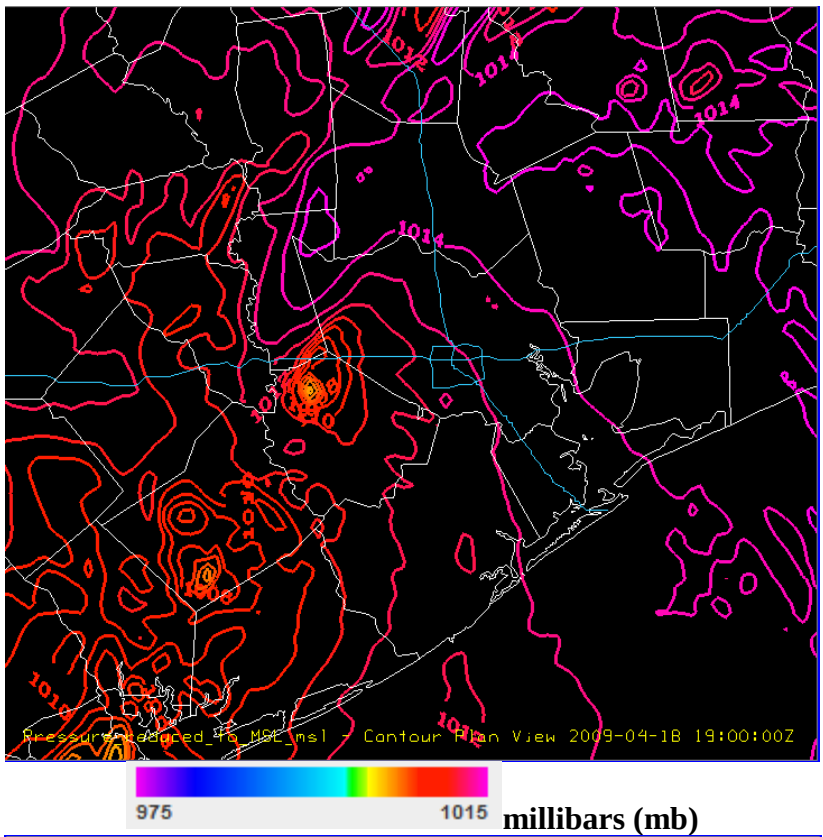

Figure 47: 1900 – 2000 UTC meso-low within the QNSE - Thompson PBL - mp relationship

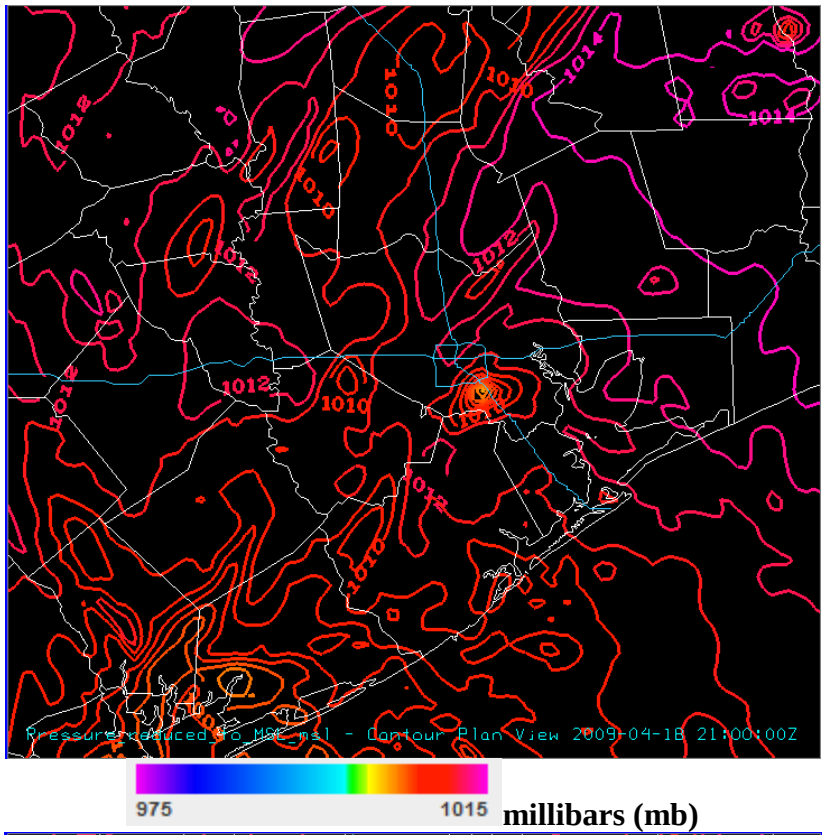

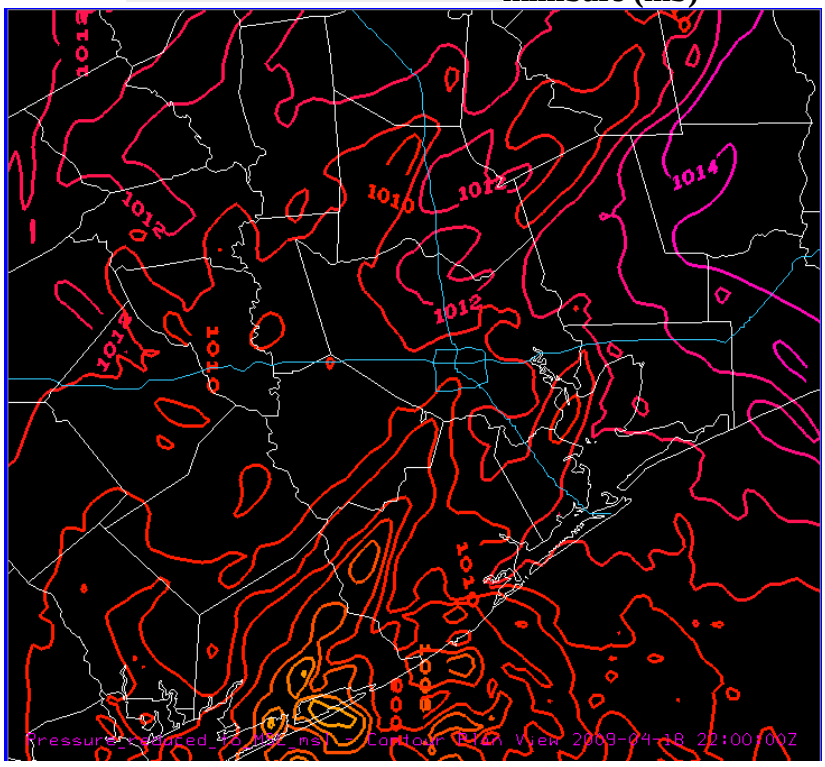

Figure 48: 2000 – 2100 UTC meso-low within the QNSE - Thompson PBL - mp relationship

Bibliography

Air Pollution Training Institute. *Monin-Obukhov Length.* 2000. http://www.shodor.org/os411/courses/411c/module06/unit01/page08.html (accessed February 4, 2013).

Aligo, E. A., W. A. Gallus, and M. Segal. "On the Impact of WRF Model Vertical Grid Resolution on Midwest Summer Rainfall Forecasts." *Weather and Forecasting (AMS),* 2008: 575 - 594.

Arakawa, A., and V.R. Lamb. *Computational design of the basic dynamical process of the UCLA general circulation model.* New York: Academic Press, 1977.

Barcelona Supercomputing Center . *NMMB/BSC Project.* 2013. http://www.bsc.es/earth-sciences/nmmbbsc-project (accessed February 4, 2013).

Blackadar, A. K. "Modeling the noctural bondary layer." *Proceedings of 4th Symposium of Atmospheric Turbulence, Diffusion and Air Quality.* Boston: American Meteorological Society, 1976. 46 - 49.

Bougeault, P., and Lacarrere P. "Parameterization of Orography–Induced Turbulence in a Mesobeta—Scale Model." *Monthly Weather Review, Vol. 117,* 1989: 1872 – 1890.

Carbone, R. E., J. D. Tuttle, D. A. Ahijevych, and S. B. Trier. "Inferences of predictability associated with warm season precipitation episodes." *Journal of Atmospheric Science,* 2002: 2033-2056.

Case, J., S. V. Kumar, J. Srikishen, and G. J. Jedlovec. "Impoving Numerical Weather Predictions of Summertime Precipitation over the Southeastern United States through a High-Resolution Initialization of the Surface State." *Weather and Forecasting,* 2011: 785 - 807.

Chen, F. "The Noah Land Surface Model in WRF." Boulder: Research Applications Laboratory, The Institute for Integrative and Multidisciplinary Earth Studies, NCAR.

Chen, F., and J. Dudhia. "Coupling an Advanced Land Surface-Hydrology Model with the Penn State-NCAR MM5 Modeling System." *Monthly Weather Review, Vol. 129,* 2001: 569 - 585.

Chen, Fei. "The Noah Land Surface Model in WRF ." *ATMS 597R: Advanced Mesoscale Modeling with WRF - University of Illinois.* April 17, 2007.

http://www.atmos.illinois.edu/~snesbitt/ATMS597R/notes/noahLSM-tutorial.pdf (accessed February 2, 2013).

Climate Forecast System Reanalysis (CFSR). October 01, 2013. https://climatedataguide.ucar.edu/climate-data/climate-forecast-system-reanalysis-cfsr.

Colle, B. A., C. F. Mass, and K. J. Westrick. "MM5 precipitation verification over the Pacific Northwest during the 1997–99 Cool seasons." *Weather and Forecasting*, 2000: 730–744.

Dee, D. P. et al. "The ERA-Interim reanalysis: Configuration and Performance of the Data Assimlation System." *Quarterly Journal of the Royal Meteorological Society, Vol. 137*, 2011: 553 - 597.

Developmental Testbed Center (DTC). *MET Users Page.* 2013. http://www.dtcenter.org/met/users/index.php (accessed December 20, 2012).

Dudhia, J. "Numerical Study of Convection Observed during the Winter Monsoon Experiment Using a Mesoscale Two-Dimensional Model." *Journal of the Atmospheric Sciences*, 1989: 3077 - 3107.

Dudhia, Jimy. "WRF Modeling System Overview." *WRF Users Page.* July 23, 2012. http://www.mmm.ucar.edu/wrf/users/tutorial/201207/WRF_Overview_Dudhia.pdf (accessed February 2, 2013).

ERA-Interim. January 23, 2008. http://www.ecmwf.int/research/era/do/get/era-interim.

Fu, Q., and K. N. Liou. "On The Correlated-k Distribution Method for Radiative Transfer in Nonhomogeneous Atmospheres." *Journal of Atmospheric Sciences*, 1992: 2139 - 2156.

Gallus, W. A., and J. F. Bresch. "Comparison of Impacts of WRF Dynamic Core, Physics Package, and Initial Conditions on Warm Season Rainfall Forecasts." *Monthly Weather Review*, 2005: 2632 - 2641.

Gaudet, B., and W., R. Cotton. "Statistical Characteristics of a Real-Time Precipitation Forecasting Model." *Weather and Forecasting*, 1998: 966 - 982.

Gilliam, R., J. Pliem, and A. Xiu. "Implementation of the Pleim-Xiu Land Surface Model and Asymmetric Convective Model in the WRF Model." *UCAR Workshop.* Boulder, 2007.

Hamill, T. M. "Hypothesis test for evaluating numerical precipitation forecasts." *Weather and Forecasting (A.M.S.)*, 1999: 155 - 167.

HCFCD. *Harris County Flood Control District.* 2010. http://www.hcfcd.org/index.asp (accessed November 22, 2012).

—. *Harris County Flood Warning System.* April 19, 2009. http://www.harriscountyfws.org/GageDetail/Index/130?R=1&From=4/18/2009%203:00%20PM (accessed November 22, 2012).

Hong, S. Y., and J. W. Lee. "Assessment of the WRF model in reproducing a flash-flood heavy rainfall." *Atmospheric Research*, 2009: 818-831.

Hong, S. Y., and S. W. Kim. "Stable boundary layer mixing in a vertical diffusion scheme." *Proc. Ninth Annual WRF User's Workshop.* Boulder, 2008.

Hong, S. Y., J. Dudhia, and S. H. Chen. "A revised approach to ice microphysical processes for the bulk parameterization of clouds and precipitation." *Mon. Wea. Rev., Vol. 132.*, 2004: 103 – 120.

Hong, S. Y., Y. Noh, and J. Dudhia. "A New Vertical Diffusion Package with an Explicit Treatment of Entrainment Processes." *Monthly Weather Review*, 2006: 2318 - 2341.

Hu, X.M., J. W. Nielsen-Gammon, and F. Zhang. "Evaluation of Three Planetary Boundary Layer Schemes in the WRF Model." *Journal of Applied Meteorology and Climatology*, 2010: 1831 - 1844.

Hu, Xiao-Ming, J. W. Nielsen-Gammon, and F. Zhang. "Evaluation of Three Planetary Boundary Layer Schemes in the WRF Model." *Journal of Applied Meteorology and Climatology, Vol. 49*, 2010: 1831-1844.

Instituto Nacional de Pesquisas Espaciais / Centro de Previsão de Tempo e Estudos Climáticos (INPE/CPTEC). *Eta Model.* 2006. http://etamodel.cptec.inpe.br/ (accessed February 20, 2013).

Janjić, Z. I. *Nonsingular Implementation of the Mellor-Yamada Level 2.5 Scheme in the NCEP Meso model.* Silver Spring: NCEP, 2002.

Jankov, I., W., A. Gallus, M. Segal, B. Shaw, and S. E. Koch. "The Impact of Different WRF Model Physical Parameterizations and Their Interactions on Warm Season MCS Rainfall." *Weather and Forecasting (A.M.S.)*, 2005: 1048 - 1060.

Jian, G. J., S. L. Shieh, and J. A. McGinley. "Precipitation simulation associated with Typhoon Sinlaku (2002) in Taiwan area using the LAPS diabatic initialization for MM5." *Terrestrial, Atmospheric and Oceanic Sciences*, 2003: 261 - 288.

Kain, J. S., and J. M. Fritsch. "Convective parameterization for mesoscale models: The Kain- Fritsch scheme. The representation of cumulus convection in numerical models." *American Meteorology Society*, 1993: 165 - 170.

Kalnay, E., et al. "The NCEP/NCAR 40-Year Reanalysis Project." *American Meteorological Society, Vol. 77*, 1996: 437 - 471.

Kusaka, H., and F. Kimura. "Thermal effects of urban canyon structure on the nocturnal heat island." *Journal of Applied Meteorology, Vol. 43*, 2004: 1899 - 1910.

Lacis, A. A., and J. E. Hansen. *N.A.S.A. Goddard Institute for Space Studies.* 1974 a. http://pubs.giss.nasa.gov/abs/la05000n.html (accessed December 20, 2012).

Lacis, A. A., and J. E. Hansen. "A Parameterization for the Absorption of Solar Radiation in the Earth's Atmosphere." *Journal of Atmospheric Sciences*, 1974 b: 118 - 133.

Lim, K. S., and S. Y. Hong. "Development of an effective double–moment cloud microphysics scheme with prognostic cloud condensation nuclei (CCN) for weather and climate models." *Monthly Weather Review, Vol.138*, 2010: 1587 – 1612.

Lin, Y. L., R. D. Farley, and H. D. Orville. "Bulk parameterization of the snow field in a cloud model." *J. Climate Appl. Met, Vol. 22*, 1983: 1065–1092.

Lin, Y., and B. Colle. "A new bulk microphysical scheme that includes riming intensity and temperature–dependent ice characteristics." *Monthly Weather Review, Vol. 139*, 2011: 1013 – 1035.

Mellor, G., L., and T. Yamada. "A Hierarchy of Turbulence Closure Models for Planterary Boundary Layers." *Journal of Atmospheric Sciences*, 1974: 1791 - 1806.

MetEd - UCAR. *NAM NMM-B Turbulence.* October 2011. http://www.meted.ucar.edu/nwp/pcu2/nambturb1.htm (accessed December 20, 2012).

—. *Understanding Assimilation Systems: How Models CreateTheir Own Initial Conditions.* 2009 a. http://www.meted.ucar.edu/nwp/model_dataassimilation/ (accessed February 20, 2013).

MetEd. *ARW/EM-WRF Radiation Scheme.* 2012 a. http://www.meted.ucar.edu/nwp/pcu2/ens_matrix/sref_arwrad.htm (accessed December 20, 2012).

Milbrandt, J. A., and M. K. Yau. "A Multimoment Bulk Microphysics Parameterization. Part I Analysis of the Role of the Spectral Shape Parameter." *Journal of the Atmopsheric Sciences, Vol. 62*, 2005: 3051 - 3064.

Mlawer, E. J., S. J. Taubman, P. D. Brown, M. J. Iacono, and S. A. Clough. "Radiative transfer for inhomogeneous atmosphere." *Journal of Geophysical Research Atmospheres*, 1997: 663 - 682.

Monin, A.S., and A.M. Obukhov. "Basic laws of turbulent mixing in the surface layer of the atmosphere." *Tr. Akad. Nauk SSSR Geofiz. Inst 24*, 1954: 163–187.

Morrison, H. "On the Numerical Treatment of Hydrometeor Sedimentation in Bulk and Hybrid Bulk-Bin Microphysics Schemes." *Monthly Weather Review, Vol. 140*, 2011: 1572 - 1588.

Morrison, H., G. Thompson, and V. Tatarskii. "Impact of Cloud Microphysics on the Development of Trailing Stratiform Precipitation in a Simulated Squall Line, Comparison of One and Two Moment Schemes." *Monthly Weather Review, Vol. 137*, 2009: 991 – 1007.

Nakanishi, M., and H. Niino. "An improved Mellor–Yamada level 3 model: its numerical stability and application to a regional prediction of advecting fog." *Bound. Layer Meteor., Vol 119*, 2006: 397 – 407.

Nakanishi, M., and H. Niino. "Development of an improved turbulence closure model for the atmospheric boundary layer." *J. Meteor. Soc. Japan, Vol. 87*, 2009: 895–912.

NOAA. *Rapid Refresh.* December 28, 2012. http://rapidrefresh.noaa.gov/ (accessed Febraury 2, 2013).

NOAA/SPC. *SPC SREF Page.* October 30, 2012. http://www.spc.noaa.gov/exper/sref/index_old.html (accessed February 2, 2013).

NWS. "Natural Hazard Statistics 1995-2011." *National Weather Service Office of Climate, Water, and Weather Services Natural Hazard Statistics.* September 25, 2012. http://www.nws.noaa.gov/om/hazstats.shtml (accessed January 23, 2013).

—. *NWS.* January 1, 2013 b. www.weather.gov (accessed December 20, 2012).

—. *NWS, Houston - Galveston, Texas Weather Forecast Office.* January 23, 2013 a. http://www.srh.noaa.gov/hgx/?n=severe_weather_awareness_flashflood (accessed January 25, 2013).

—. "Southeast Texas Hazardous Weather Information." *Houston-Galveston National Weather Service.* April 09, 2009. www.srh.noaa.gov/images/hgx/stormdata/apr09hgx.pdf.

Olson, J., and J. M. Brown. "Modifications to the MYNN PBL and Surface Layer Scheme for WRF-ARW." *WRF Users Workshop.* Boulder, CO, 2012. 2-7.

Overview of current atmopsheric anaylses. February 14, 2014. http://reanalyses.org/atmosphere/overview-current-reanalyses.

Overview of current atmospheric reanalyses. Feb 14, 2014. http://reanalyses.org/atmosphere/overview-current-reanalyses.

Pagowski, M. "Some Comments On PBL Parameterizations in WRF." *UCAR.* 2004. http://www.mmm.ucar.edu/mm5/workshop/ws04/Session1/Pagowski.Mariusz_web.pdf (accessed February 10, 2013).

Pleim, J. E. "A Combined Local and Nonlocal Closure Model for the Atmospheric Boundary Layer. Part I: Model Description and Testing." *J. Appl. Meteor. Climatol., Vol. 46*, 2007: 1383 – 1395.

Research Applications Laboratory (RAL). *Land-Surface Atmosphere Interactions.* 2013. http://www.rap.ucar.edu/research/land/ (accessed February 2, 2013).

Schlatter, T. W. "Variational assimilation of meteorological observations in the lower atmosphere: A tutorial on how it works." *Journal of Atmospheric and Solar-Terrestrial Physics,* 2000: 1057 - 1070.

Shin, H., and S. Hong. "Intercomparison of Planetary Boundary-Layer Parametrizations in the WRF Model for a Single Day from CASES-99." *Boundary-Layer Meterorology, Vol. 139*, 2011: 261 - 281.

Stein, U., and P. Alpert. "Factor separation in numerical simulations." *Journal of Atmospheric Science* , 1993: 2107 - 2115.

Strensrud, D. J., and M. S. Wandishin. "The correspondence ratios in forecast evaluation." *AMS - Weather & Forecasting*, 2000: 593 - 602.

Stull, R. B. *An Introduction to Boundary Layer Meteorology.* Springer, 1988.

Sukoriansky, S., B. Galperin, and V. Perov. "A quasi-normal scale elimination model of turbulence and its application to stably stratified flows." *Nonlinear Processes in Geophysics, Vol. 13*, 2006: 9 - 22.

Thépaut, J. N., P. Courtier, G. Belaud, and G. Lemaître. "Dynamical structure functions in a four-dimensional variational assimilation." *Q. J. R. Meteorol. Soc. 122*, 1996: 535–561.

Thompson, G., P. R. Field, M. R. Rasmussen, and W. D. Hall. "Explicit Forecasts of Winter Precipitation Using an Improved Bulk Microphysics Scheme. Part II

Implementation of a New Snow Parameterizatio." *Monthly Weather Review, Vol.136*, 2008: 5095 – 5115.

Tonnesen, et al. "Air quality models." 1998.

U. S. Dept. of Energy. *U. S. Dept. of Energy - Office of Science.* 2013. http://www.arm.gov/about/glossary#W (accessed February 6, 2013).

UCAR. *Advanced-research WRF Dynamics and Numerics.* February 28, 2007 a. http://www.mmm.ucar.edu/wrf/users/docs/wrf-dyn.html (accessed December 20, 2012).

(UCAR), University Corporation for Atmospheric Research. *WRF Users Page - Modeling System Overview.* April 2, 2010. http://www.mmm.ucar.edu/wrf/users/docs/user_guide_V3/users_guide_chap1.htm (accessed November 22, 2012).

—. *The Weather Research and Forecasting Model.* 2013 a. http://www.wrf-model.org/index.php (accessed December 20, 2012).

—. *User's Guide for Advanced Research WRF (ARW) Modeling System Version 2: Chapter 5* . February 1, 2012. http://www.mmm.ucar.edu/wrf/users/docs/user_guide/users_guide_chap5.html#Phys (accessed November 22, 2012).

—. *WRF ARW Online Tutorial.* December 20, 2011 a. http://www.mmm.ucar.edu/wrf/OnLineTutorial/index.htm (accessed December 20, 2012).

—. "WRF-ARW User's Guide Ver.3." *WRF User's Page.* April 2012 . http://www.mmm.ucar.edu/wrf/users/docs/user_guide_V3/ARWUsersGuideV3.pdf (accessed December 20, 2012).

—. *WRF-NMM Online Tutorial.* Febraury 2, 2013 b. http://www.dtcenter.org/wrf-nmm/users/OnLineTutorial/NMM/index.php (accessed December 20, 2012).

—. "WRF-NMM User's Guide Ver.3." *WRF-NMM Online Tutorial.* January 2013 c. http://www.dtcenter.org/wrf-nmm/users/docs/user_guide/V3/users_guide_nmm_chap1-7.pdf (accessed December 20, 2012).

Wanqiu, W., X. Pingping, Y. Soo-Hyun, Y. Xue, A. Kumar, and X. Wu. "An assessment of the surface climate in the NCEP climate forecast system reanalysis." *Climate Dynamics, Vol. 37*, 2011: 1601 - 1620.

Wanqui, W., X. Pingping, and Y. Soo-Hyun. "An Assessment of the Surface Climate in the NCEP Climate Forecast System Reanalysis." *Climate Dynamics*, 2010.

Weisman, M. L., C. Davis, W. Wang, K. W. Manning, and J. B. Kelmp. "Experiences with 0–36-h Explicit Convective Forecasts with the WRF-ARW Model." *Weather And Forecasting*, 2007: 407-437.

Whitaker, J. S., G. P. Compo, and J. N. Thépaut. "A comparison of variational and ensemble-based data assimilation systems for reanalysis of sparse observations." *Mon. Weather Rev. 137*, 2009: 1991-1999.

Wilson, J. W., and R. D. Roberts. "Summary of convective storm initiation and during IHOP: observational and modeling perspective." *Monthly Weather Review*, 2002: 23-47.

Wyngaard, J. C., and R.A. Brost. "Top-down and bottom-up diffusion of a scalar in the convective boundary layer." *Journal of the Atmospheric Sciences, Vol. 41*, 1984: 102-112.

Xie, B., J. C. H. Fung, A. Chan, and A. Lau. "Evaluation of nonlocal and local planetary boundary layer schemes in the WRF model." *Journal of Geophysical Research, Vol. 117*, 2012: D12103.

Xue, M., and W. J. Martin. "A high-resolution modeling study of the 24 May 2002 dryline case during IHOP. Part I: numerical simulation and general evolution of the dryline and convection." *Monthly Weather Review*, 2006: 149-171.

Zhang, D. L., K. Gao, and D. B. Parsons. "Numerical simulation of an intense squall line during 10–11 June 1985." *Monthly Weather Review*, 1988: 960-994.